

AD-A056 812

HONEYWELL INC MINNEAPOLIS MINN SYSTEMS AND RESEARCH --ETC F/G 17/7
INDEPENDENT STABILITY AND CONTROL ANALYSIS OF NAVIGATION DEVELO--ETC(U)
JAN 78 R E POPE, M D WARD, M F BARRETT F04701-75-C-0135
78SRC10-VOL-2 SAMSO-TR-78-74-VOL-2 NL

UNCLASSIFIED

1 OF 3
AD
A056812



Air Force Report SAMSO TR 78-74

LEVEL III

Volume II

A056811

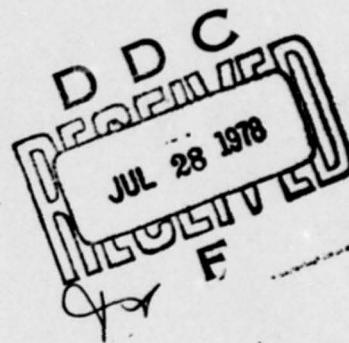
AD A056812

**INDEPENDENT STABILITY AND CONTROL ANALYSIS
OF NAVIGATION DEVELOPMENT SATELLITES
FOR THE GLOBAL POSITIONING SYSTEM**

FINAL REPORT

VOLUME II: APPENDIXES

**R. E. POPE
M. D. WARD
M. F. BARRETT
J. G. RUPERT
S. P. KAU**



AD No. **DDC FILE COPY**

January 1978

For Period February 1975 to September 1977

**Prepared for
SAMSO (YEZ)
P. O. Box 92960
Worldway Postal Center
Los Angeles, California 90009**

**Honeywell
SYSTEMS & RESEARCH CENTER
2600 RIDGWAY PARKWAY
MINNEAPOLIS, MINNESOTA 55413**

This document has been approved
for public release and sale; its
distribution is unlimited.

78 07 24 03 4

UNCLASSIFIED

SECURITY CLASSIFICATION OF THIS PAGE (WHEN DATA ENTERED)

REPORT DOCUMENTATION PAGE		READ INSTRUCTIONS BEFORE COMPLETING FORM
1. REPORT NUMBER SAMSO TR-78-74-VOL. H	2. GOV'T ACCESSION NUMBER	3. RECIPIENT'S CATALOG NUMBER
4. TITLE (AND SUBTITLE) Independent Stability and Control Analysis of Navigation Development Satellites for the Global Positioning System - Volume II. Appendixes	5. TYPE OF REPORT/PERIOD COVERED Final Report 3 Feb. 1975 to 9 Sept. 1977	6. PERFORMING ORG. REPORT NUMBER 78SRC10-VOL-2
7. AUTHOR(S) R. E./Pope, J. G./Rupert M. D./Ward, S. P./Kau M. F./Barrett	8. CONTRACT OR GRANT NUMBER(S) F04701-75-C-0135	10. PROGRAM ELEMENT, PROJECT, TASK AREA & WORK UNIT NUMBERS
9. PERFORMING ORGANIZATION NAME/ADDRESS Honeywell Systems and Research Center 2600 Ridgway Parkway Minneapolis, Minnesota 55413	12. REPORT DATE January 1978	13. NUMBER OF PAGES 198
11. CONTROLLING OFFICE NAME/ADDRESS SAMSO (YEZ) P.O. Box 92960, Worldway Postal Center Los Angeles, California 90009	14. MONITORING AGENCY NAME/ADDRESS (IF DIFFERENT FROM CONT. OFF.)	15. SECURITY CLASSIFICATION (OF THIS REPORT) Unclassified
15a. DECLASSIFICATION DOWNGRADING SCHEDULE		
16. DISTRIBUTION STATEMENT (OF THIS REPORT) Approved for public release; distribution unlimited.		
17. DISTRIBUTION STATEMENT (OF THE ABSTRACT ENTERED IN BLOCK 20, IF DIFFERENT FROM REPORT)		
18. SUPPLEMENTARY NOTES		
19. KEY WORDS (CONTINUE ON REVERSE SIDE IF NECESSARY AND IDENTIFY BY BLOCK NUMBER) GPS Satellite attitude control Satellite simulation and modeling Control and stability analysis		
20. ABSTRACT (CONTINUE ON REVERSE SIDE IF NECESSARY AND IDENTIFY BY BLOCK NUMBER) This report documents the results of an independent stability and control analysis of the control systems and procedures of the navigation development satellite (NDS) for the global positioning system (GPS). The analysis consisted of detailed analytical investigation substantiated with sophisticated satellite system modeling and simulation of the following GPS mission events: (continued on reverse)		

DD FORM
1 JAN 73

1473

EDITION OF 1 NOV 55 IS OBSOLETE

UNCLASSIFIED

SECURITY CLASSIFICATION OF THIS PAGE (WHEN DATA ENTERED)

HD-168 REV 11/74

UNCLASSIFIED

SECURITY CLASSIFICATION OF THIS PAGE (WHEN DATA ENTERED)

20. ABSTRACT (concluded)

- Spin phase
- Despin
- Earth acquisition
- Panel deployment
- Sun acquisition
- On-orbit operations

The results of the analysis indicated satisfactory performance in all mission phases analyzed. A redesign of the jet control system was recommended to facilitate earth acquisition operations.

UNCLASSIFIED

SECURITY CLASSIFICATION OF THIS PAGE (WHEN DATA ENTERED)

CONTENTS

Appendix	Page
(A) - - DATA BASELINE DEFINITION, 15 JULY 1977,	1
(B) - - ONE-BODY MODEL EQUATIONS,	7
(C) - - THREE-BODY DYNAMIC MODEL,	15
(D) - - NUTATION DAMPER MODEL,	23
(E) - - MODEL FOR GPS DIGITAL SPIN SUN SENSOR (SSS),	45
(F) - - REACTION JET MODEL FOR GPS INDEPENDENT ANALYSIS,	63
(G) - - GPS DEPLOYMENT MODEL,	77
(H) - - SOLAR PRESSURE TORQUE AND FORCE MODEL,	81
(I) - - SOLAR ARRAY FLEXIBILITY MODEL,	109
(J) - - COMBINED EARTH SENSOR MODEL, and	147
(K) - - WHEEL-MOMENTUM COUPLING,	191

ACCESSION for	
NTIS	Whole Section <input checked="" type="checkbox"/>
DDC	Diff Section <input type="checkbox"/>
UNANNOUNCED	<input type="checkbox"/>
JUSTIFICATION	
BY	
DISTRIBUTION/AVAILABILITY CODES	
or and/or SPECIAL	
A	

APPENDIX A

DATA BASELINE DEFINITION, 15 JULY 1977

APPENDIX A

DATA BASELINE DEFINITION, 15 JULY 1977

DATA ITEM	SOURCE	DATE
1. Mass Properties	Computer Listing PR #19	27 January 1977
2. Jet Control System	Rockwell Block Diagram MC476-0146, Rev. F, Seq. 4	Received 29 March 1977
3. Wheel Control System	Rockwell Block Diagram MC476-0146, Rev. F, Seq. 4	Received 29 March 1977
4. Earth Sensor	Performance Analysis of Static Earth Sensor, Barnes Engineering Company	5 August 1975
5. Yaw Sun Sensor	Yaw Sun Sensor Output Characteristics, Rev. B and Rev. C, MCR G0569	11 February 1977
a. Thermal Variation-- <u>±</u> 0.6 percent	(See Solar Array Drive)	
6. Thruster Locations	Scaled from Rockwell Drawing V505-900003, Rev. C	27 January 1975
7. Thruster Characteristics		
a. 0.1 lb	GPS 0.1 lbF REA, Qualification Test Report CDRL, Item A005, Contract F04701-74-C-0527	31 March 1976
b. 5.0 lb	GPS 5.0 lbF REA, Qualification Test Report CDRL, Item A005, Contract F040701-74-C-0527	31 March 1976

DATA ITEM	SOURCE	DATE
7. c. RCS Tank Blowdown Profile, 5.0 lb and 0.1 lb Thruster Performance	GPS Propellant Budget	Received from SAMSO, June 1977
8. Wheel Dynamics	Motor Torque Speed, Curve Plot No. 5, Design Review Data, Item R-005 Bendix to Rockwell	14 January 1975
9. Solar Array Drive		
a. Pulse Width Normal 50 \pm 5 milliseconds	Solar Array Drive and Power Transfer System, Rockwell	6 June 1976
b. Pulse Width Extended 85 \pm 8.5 milliseconds	Document No. MC476-0143, Rev. B and C, Seq. 05 and 05	
c. Slew Command 64 pulses	and Global Positioning System	
d. Expected Slew Normal 11.85° \pm 6°	Operations Handbook, Volume 1 Section 2.3: EPS Description, CDRL Item A00G, Contract No.	
e. Expected Slew Extended 38.4° \pm 18°	F04701-74-C-0527	
f. Max Pulse Rate 1 to 1.85		
g. Deadband, 1 to 1.7°		
h. Driving Torque 145 oz-in min		
i. Coulomb Friction 65 oz-in max		
j. Solar Array Drive Torques	Ball Brothers Memo	5 February 1976
k. Minimum Pulse Rate	Phil Talley Memo	22 October 1975

DATA ITEM	SOURCE	DATE
10. Nutation Damper		
a. Radius of Curvature 158.25" + 10" to 18"	Blue Print Damper Assembly Nutation GPS Rockwell Drawing No. V505-520016	15 January 1976
b. Length of tube 15.75"		
c. Mass of Ball .018 slugs	Rockwell Viewgraph	CDR
d. Dissipation Coefficient $c_D = 0.017 \pm 30\%$	Honeywell Memo	29 September 1975
11. Pitch Sun Sensor Ball Brothers Memo	Ball Brothers Test Data	Received 15 July 1977
12. Alignment Specs		
a. CES	Global Positioning System Orbital	
b. SSS	Operations Handbook, Volume 1,	
c. YSS	Section 2.4: Control System,	
d. Reaction Wheel	Description CDRL, Item A00G,	
e. Thrusters	Contract F04701-74-C-0527, P2.4.138	
13. Precession Procedure		
a. Firing Pulse Width 93.6 msec	See Item 12	
b. Expected Precession Angle/Pulse, 0.12°		
c. Thrusters Used 17 and 18		
d. Firing Delay, 0 to 5.24 sec (increments of 10.25 msec)		
e. Minimum Number of Pulses, 4		

DATA ITEM	SOURCE	DATE
13. f. Procedure: 9 segments of 4 minutes duration; reference sss pipper pulse each revolution		
14. Despin		
a. Thrusters Used-- 11 and 13		
b. Sequence	Modified from Item 12	SAMSO Review 15 July 1977
95 to 85 rpm		
Calibrate		
85 to 75 rpm		
Recalibrate		
75 to 20 rpm		
20 to 10 rpm		
10 to 6 rpm		
6 to 1 rpm		
c. Firing Time in Increments of 5.27 sec		
15. Earth Acquisition Procedure at 1 rpm		
a. Enable roll axis control	See Item 12	
b. Wait 5.0 minutes		
c. Enable pitch axis control		
16. -y Panel Deployment	See Item 12	
Procedure with roll and pitch jet control, deploy -y panel, slew 90 deg		

DATA ITEM	SOURCE	DATE
<p>17. Sun Acquisition</p> <p>At 0.75 rpm and -y panel deployed and sun line parallel to panel normal, enable yaw jet control.</p>	See Item 12	
<p>18. +y Panel Deployment with three-axis jet control, deploy +y panel, slew 90 deg</p>	See Item 12	
<p>19. Momentum Dump Procedure</p> <p>a. Automatic dump of pitch and roll axis when momentum is greater than 0.25 ft-lb-sec</p> <p>b. Pitch axis firing times 0.1, 0.3, 0.5, or 0.7 sec (0.3 nominal)</p> <p>c. Roll axis firing times 0.8, 2.4, 4.0, or 5.6 sec (2.4 nominal)</p>	See Item 12	

APPENDIX B

ONE-BODY MODEL EQUATIONS

APPENDIX B

ONE-BODY MODEL EQUATIONS

This appendix presents the derivation of equations of motion used in the one body simulation. For Definition of Symbols, see Figure B-1.

Vector torque equations are given by

$$\begin{aligned}\int \bar{\mathbf{r}} \times d\bar{\mathbf{F}} &= \int \bar{\mathbf{r}} \times \frac{d^2 \bar{\mathbf{r}}}{dt^2} dm \\ &= \frac{d}{dt} \int \bar{\mathbf{r}} \times \left(\frac{d\bar{\mathbf{r}}}{dt} \right) dm \\ \bar{\mathbf{T}} &= \frac{d\bar{\mathbf{H}}}{dt}\end{aligned}\tag{B-1}$$

where $\bar{\mathbf{H}}$ is defined as

$$\begin{aligned}\bar{\mathbf{H}} &= \int \bar{\mathbf{r}} \times \left(\frac{d\bar{\mathbf{r}}}{dt} \right) dm \\ &= [\bar{\mathbf{J}}_0 + m_0 M(\bar{\mathbf{r}}_0, \bar{\mathbf{r}}_0) + \sum_i \bar{\mathbf{J}}_i + \sum_i m_i M(\bar{\mathbf{r}}_i, \bar{\mathbf{r}}_i)] \bar{\boldsymbol{\omega}}_0 + \sum_i \bar{\mathbf{J}}_i \bar{\boldsymbol{\omega}}_i \\ &= \bar{\mathbf{I}}_0 \bar{\boldsymbol{\omega}}_0 + \sum_i \bar{\mathbf{I}}_i \bar{\boldsymbol{\omega}}_i\end{aligned}\tag{B-2}$$

where, in body 0 coordinates,

$$M(a,b) \triangleq \begin{bmatrix} a^T & b \end{bmatrix} \mathbf{I} - a b^T$$

$$\bar{\mathbf{J}}_i \triangleq \begin{bmatrix} I_x & -I_{xy} & -I_{xz} \\ -I_{xy} & I_y & -I_{yz} \\ -I_{xz} & -I_{yz} & I_z \end{bmatrix}$$

$$\mathbf{J}_i = \mathbf{T}_{oi} \mathbf{J}_i^i \mathbf{T}_{io} \quad (\mathbf{T}_{oi} \text{ is transformation from wheel } i \text{ to body } o)$$

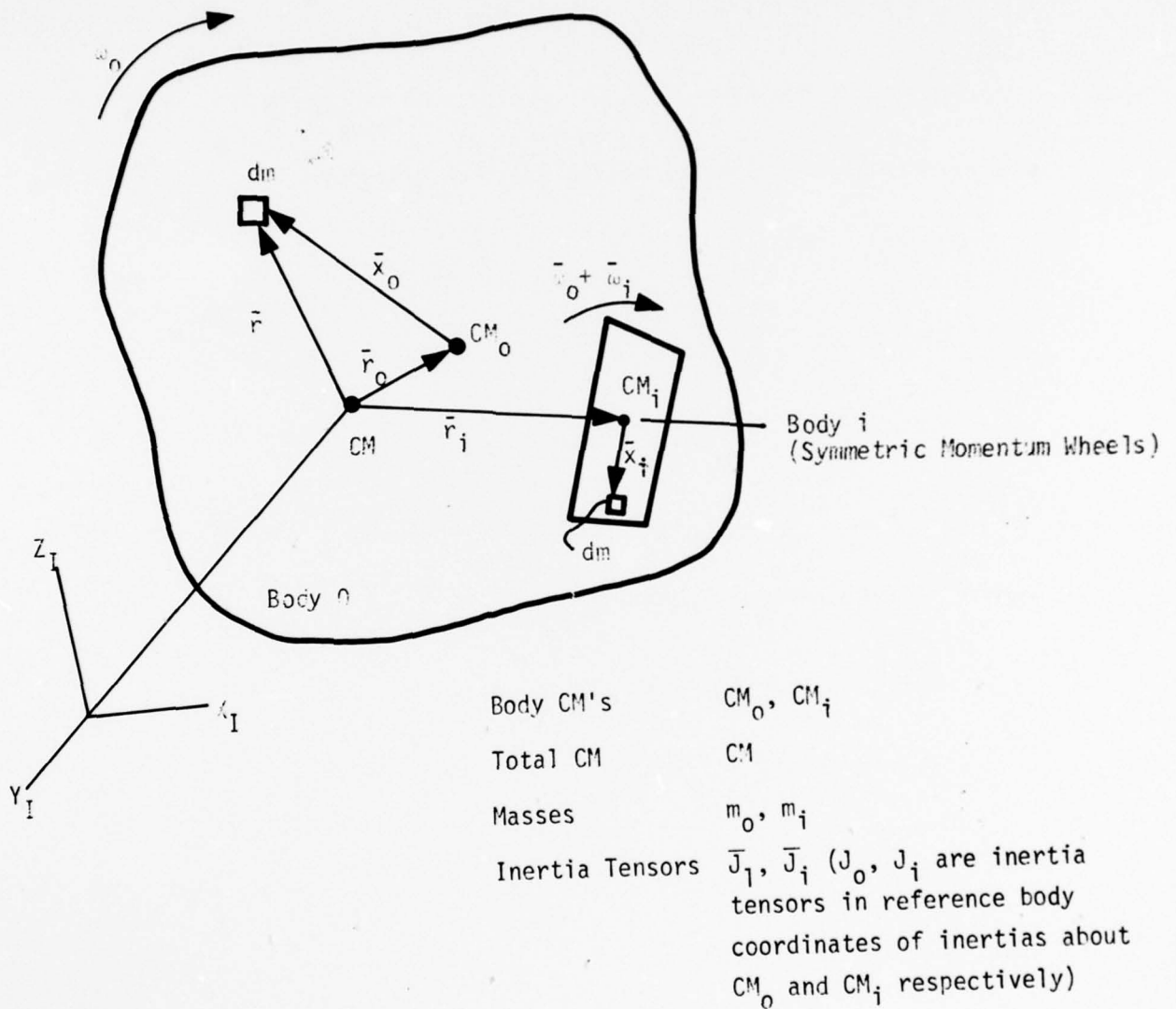


Figure B-1. Notation

$$\omega_i = T_{oi} \omega_i^i$$

$$I_x = \int (y^2 + z^2) dm = I_{yy} + I_{zz}, \text{ etc.}$$

$$I_{xy} = \int xy \, dm, \text{ etc.}$$

The rotational equations of motion are then given by

$$\begin{aligned} \bar{T} &= \frac{d\bar{H}}{dt} \\ &= \frac{d}{dt} [\bar{I}_{oo} \omega_o + \sum_i \bar{I}_{oi} \omega_i] \\ &= \frac{\delta}{\delta t} [\bar{I}_{oo} \omega_o + \sum_i \bar{I}_{oi} \omega_o] + \omega_o \times [\bar{I}_{oo} \omega_o + \sum_i \bar{I}_{oi} \omega_i] \end{aligned}$$

$$T = I_{oo} \dot{\omega}_o + \sum_i I_{oi} \dot{\omega}_i + \omega_o \times H$$

(B-3)

Wheel Torques may be described by

$$\begin{aligned} \int \bar{x}_i \times d\bar{F} &= \int \bar{x}_i \times \frac{d^2}{dt^2} \bar{x}_i \, dm \\ &= \frac{d}{dt} \int \bar{x}_i \times \frac{d\bar{x}_i}{dt} \, dm \end{aligned}$$

$$\bar{T}_i = \frac{d\bar{H}_i}{dt}$$

Wheel momentum is given by

$$\begin{aligned} \bar{H}_i &= \int \bar{x}_i \times \frac{d}{dt} \bar{x}_i \, dm \\ &= \int \bar{x}_i \times \left[\frac{\delta}{\delta t} \bar{x}_i + \omega_o \times \bar{x}_i \right] \, dm \end{aligned}$$

$$\begin{aligned}
&= \int \bar{x}_i x [\bar{\omega}_i \times \bar{x}_i + \bar{\omega}_o \times \bar{x}_i] dm \\
&= \bar{J}_i \bar{\omega}_i + \bar{J}_i \bar{\omega}_o
\end{aligned} \tag{B-4}$$

Differentiating

$$T_i = J_i \dot{\omega}_i + J_i \dot{\omega}_o + \omega_o \times J_i \omega_i + \omega_o \times J_i \omega_o \tag{B-5}$$

Torques about the wheel axis are given by

$$T_i = J_i \dot{\omega}_i + J_i \dot{\omega}_o \tag{B-6}$$

$$\sim J_i \dot{\omega}_i \tag{B-7}$$

where T_i is the sum of motor, bearing and windage torques on wheel i .
Equations B-7 and B-3 are combined to compute the body rate derivatives.

$$T = I_o \dot{\omega}_o + \sum_i T_i + \omega_o \times H \tag{B-8}$$

Kinematics

The inertial coordinate system and the Euler sequence are consistent with the Rockwell convention presented in the AVCS splinter meeting notes at the preliminary design review. Specifically, Rockwell specified a yaw pitch roll Euler sequence with the equations:

$$\begin{aligned}
\dot{\theta} &= \omega \cos \psi + q \cos \phi - r \sin \phi \\
\dot{\psi} &= (\omega \sin \psi \sin \theta + q \sin \phi + r \cos \phi) (1/\cos \theta) \\
\dot{\phi} &= p + \dot{\psi} \sin \theta + \omega \sin \psi \cos \theta
\end{aligned}$$

where

ω = orbit rate

P, Q, R = body rates

ϕ, θ, ψ = Euler angles

$\dot{\phi}, \dot{\theta}, \dot{\psi}$ = Euler rates

These equations are consistent with:

1. A local vertical system with z axis pointing toward the earth and x axis in the orbit plane and positive on the direction of motion.
2. Euler angles specifying body orientation relative to the local vertical frame.

The inertial coordinate system is the Geocentric Equatorial Frame (e.g., z axis positive North and x axis positive in the direction of the Vernal Equinox). The local vertical system is consistent with Rockwell's (e.g., z axis positive toward the earth and x axis in the orbit plane).

Two sets of Euler angles, both having a yaw pitch roll sequence, are used. The first set PSI, THETA1, PHI1 define the inertial to body transformation E. The second set, PSILV, THETA, PHI specify the orientation of the body relative to the local vertical frame and should be consistent with Rockwell's Euler angles. The inertial Euler angles are integrated in the simulation via quaternions.

Linear Motion

The simulation uses two subroutines(POSITN and RADVEC) to compute the ephemerides for the satellite and the sun. The ephemerides for the satellite and the sun are calculated using the six Kepler elements: semi major axis (a),

eccentricity (e), inclination (i), right ascension of the ascending node (Ω), argument of perigee (ω), and mean anomaly (M). The update is a simple rate term on the latter three. Table B-1 presents the six elements, their units and values for the vernal equinox condition. The rate terms are derived in the program from the fixed parameters and are given by

$$\dot{M} = \sqrt{\mu/a^3} - \frac{k\sqrt{\mu/a^3}}{[a(1-e^2)]^2} \sqrt{1-e^2} (1.5 \sin^2 i - 1)$$

$$\dot{\Omega} = \frac{k\sqrt{\mu/a^3}}{[a(1-e^2)]^2} \cos i$$

$$\dot{\omega} = \frac{k\sqrt{\mu/a^3}}{[a(1-e^2)]^2} (2.5 \sin^2 i - 2)$$

where

$$\mu = Gm = 62630.3949$$

$$k = R_E^2 J_2 \text{ (first term of perturbing force} = -19255.96124 \text{ due to Earth's oblateness)}$$

The rate terms for the sun are fixed and are included in Table B-1. The simulation updates M, Ω , ω by

$$M(t) = M(t_0) + \dot{M} \cdot (t-t_0) \quad -\pi < M \leq \pi$$

$$\Omega(t) = \Omega(t_0) + \dot{\Omega} \cdot (t-t_0) \quad -\pi < \Omega \leq \pi$$

$$\omega(t) = \omega(t_0) + \dot{\omega} \cdot (t-t_0) \quad -\pi < \omega \leq \pi$$

A seventh term, the Greenwich Hour Angle (GHA), which relates the earth-fixed coordinate system to the inertial system, given the six elements is updated via:

$$GHA(t) = GHA(t_0) + \omega_e \cdot (t-t_0)$$

$$\omega_e = \text{earth rotation rate}$$

TABLE B-1. GPS AND SOLAR EPHEMERIDES

SYMBOL	NAME	UNITS	STANDARD VALUE	
			GPS	SUN
a	Semi Major Axis	Miles	14342.	1*
e	Eccentricity	--	0.	.0167
i	Inclination	Degrees	63.	23.443
M	Mean Anomaly	Degrees	0.	88.068
Ω	Right ascension of ascending node	Degrees	0.	0.
ω	Argument of perigee	Degrees	0.	270.
\dot{M}		Degrees/sec	--	1.14074×10^{-5}
$\dot{\Omega}$		Degrees/sec	--	$.544773 \times 10^{-9}$
$\dot{\omega}$		Degrees/sec	--	0.0
GHA	Greenwich Hour Angle	Degrees		0.0

* Astronomical unit

APPENDIX C

THREE-BODY DYNAMIC MODEL

APPENDIX C

THREE-BODY DYNAMIC MODEL

This appendix contains the equations of motion for the GPS three-body model.

ROTATIONAL DYNAMICS

Let $\bar{\omega}_0 = \begin{Bmatrix} p \\ q \\ r \end{Bmatrix}$ angular velocity of reference body in reference body coordinates

Notation: \bar{x} = vector or tensor

x = components of \bar{x} in reference body coordinates

x^i = components of \bar{x} in body i coordinates

$\frac{d\bar{x}}{dt}$ = derivative of \bar{x} with respect to inertial frame

$\frac{\delta \bar{x}}{\delta t}$ = derivative of \bar{x} with respect to reference body frame

\dot{x} = componentwise differentiation of x . Note that $(\delta \bar{x} / \delta t)^0 = \dot{x}$.
(See Figure C-1.)

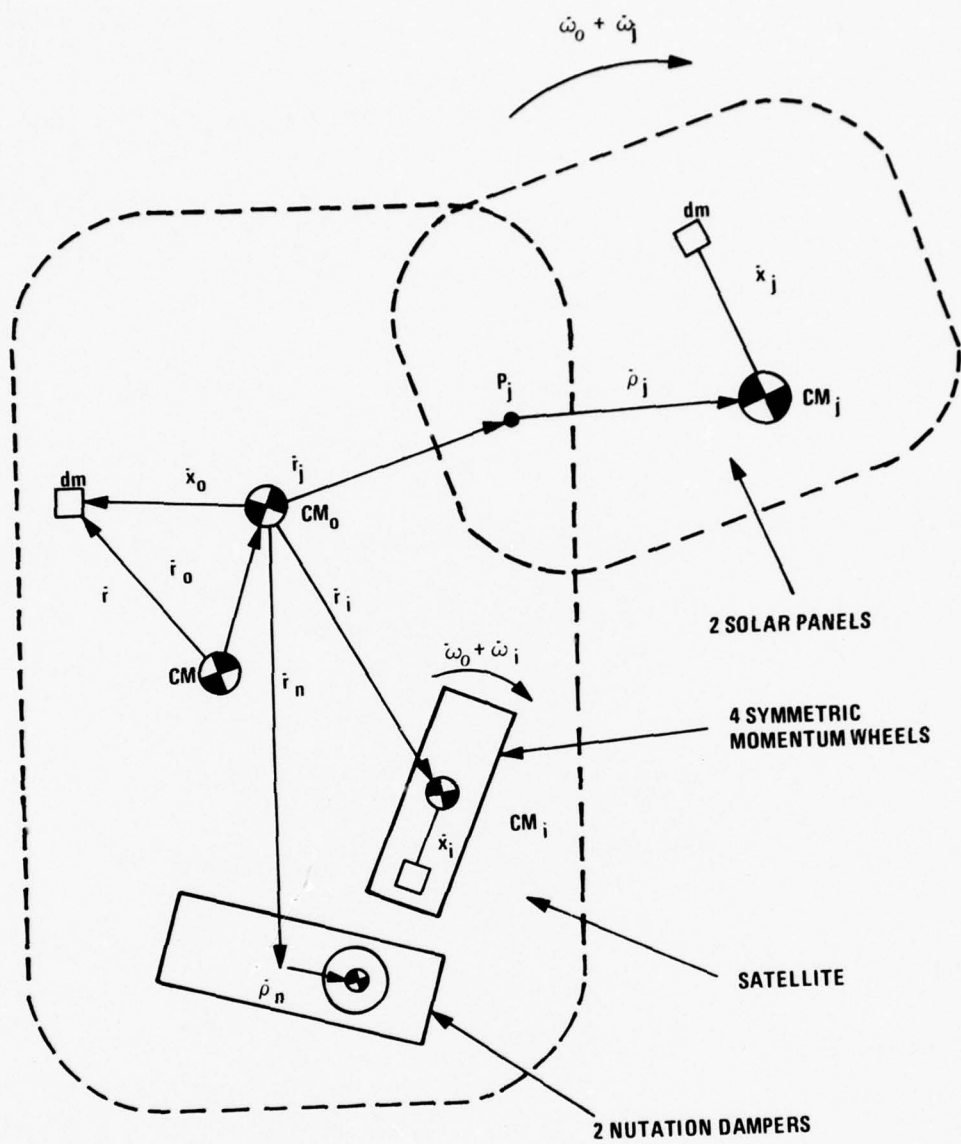
MOMENT OF NEWTON'S LAW ABOUT CM

$$\int \bar{r} \times d\bar{F} = \int \bar{r} \times \frac{d^2 \bar{r}}{dt^2} dm = \frac{d}{dt} \int \bar{r} \times \left(\frac{d\bar{r}}{dt} \right) dm$$

$$\bar{T} = \frac{d\bar{H}}{dt} \quad (C-1)$$

EVALUATION OF \bar{H}

$$\begin{aligned} \bar{H} &= \int \bar{r} \times \left(\frac{d\bar{r}}{dt} \right) dm \\ &= \int_0 (\bar{r}_0 + \bar{x}_0) \times \left(\frac{\delta \bar{r}_0}{\delta t} + \bar{\omega}_0 \times (\bar{r}_0 + \bar{x}_0) \right) dm \\ &\quad + \sum_i \int_i (\bar{r}_0 + \bar{r}_i + \bar{x}_i) \times \left(\frac{\delta \bar{r}_0}{\delta t} + \bar{\omega}_0 \times (\bar{r}_0 + \bar{r}_i + \bar{x}_i) + \bar{\omega}_i \times \bar{x}_i \right) dm \end{aligned} \quad (C-2)$$



SOLAR PANEL PIVOT POINTS P_j
 BODY CM's: CM_i, CM_j, CM_k ; CM - TOTAL CM
 MASSES: m_i, m_j, m_k, m_n ; m = TOTAL MASS
 INERTIA TENSORS (ABOUT CMs) J_0, J_i, J_j, J_k, J_n

Figure C-1. Notation

$$\begin{aligned}
& + \sum_i \int (\bar{r}_o + \bar{r}_j + \bar{\rho}_j + \bar{x}_j) \times \left(\frac{\delta \bar{r}_o}{\delta t} + \bar{\omega}_o \times (\bar{r}_o + \bar{r}_j + \bar{\rho}_j + \bar{x}_j) + \bar{\omega}_j \times (\bar{\rho}_j + \bar{x}_j) \right) dm \\
& + \sum_n \int (\bar{r}_o + \bar{r}_n + \bar{\rho}_n + \bar{x}_n) \times \left[\frac{\delta(\bar{r}_o + \bar{\rho}_n + \bar{x}_n)}{\delta t} + \bar{\omega}_o \times (\bar{r}_o + \bar{r}_n + \bar{\rho}_n + \bar{x}_n) \right] dm
\end{aligned}$$

Noting that

$$m_o \bar{r}_o + \sum_i m_i (\bar{r}_o + \bar{r}_i) + \sum_j m_j (\bar{r}_o + \bar{r}_j + \bar{\rho}_j) + \sum_n m_n (\bar{r}_o + \bar{r}_n + \bar{\rho}_n) = 0 \quad (C-3)$$

Equation (C-2) becomes

$$\bar{H} = \bar{I}_o \bar{\omega}_o + \sum_i \bar{I}_i \bar{\omega}_i + \sum_j \bar{I}_j \bar{\omega}_j + \sum_n \bar{H}_n \quad (C-4)$$

where

$$\begin{aligned}
I_o &= J_o + \sum_i J_i + \sum_j J_j + \sum_n J_n - mM(r_o, r_o) + \sum_i m_i M(r_i, r_i) \\
&+ \sum_j m_j M(r_j + \rho_j, r_j + \rho_j) + \sum_n m_n M(r_n + \rho_n, r_n + \rho_n)
\end{aligned}$$

$$I_i = J_i$$

$$I_j = J_j + m_j M(r_o + r_j + \rho_j, \rho_j)$$

$$\bar{H}_n = m_n (\bar{r}_o + \bar{r}_n + \bar{\rho}_n) \times (\delta \bar{\rho}_n / \delta t) + \int_n (\bar{r}_o + \bar{r}_n + \bar{\rho}_n + \bar{x}_n) \times (\delta \bar{x}_n / \delta t) dm$$

and

$$M(a, b) \triangleq b^T a I - b a^T$$

COMPUTATION OF H

The vectors \bar{r}_i , \bar{r}_j , \bar{r}_n , $\bar{\rho}_j^j$ are given. The vector \bar{r}_o can be computed from Equation (C-3).

Wheel Momenta

$$I_i \omega_i = T_{oi} J_i^i \omega_i^i$$

Panel Momenta

$$I_j \omega_j = T_{oj} J_j^j \omega_j^j + m_j M(r_o + r_j + \rho_j, \rho_j) \omega_j$$

where

$$\omega_j = T_{oj} \begin{Bmatrix} 0 \\ \dot{\theta}_{pj} \\ 0 \end{Bmatrix} = T_{oj} \omega_j^j$$

Nutation Dampers

Assume: $J_n = 0$ (point mass)

$$\Rightarrow H_n = m_n (\bar{r}_o + \bar{r}_n + \bar{\rho}_n) \times \frac{\delta \bar{\rho}_n}{\delta t}$$

ROTATIONAL DIFFERENTIAL EQUATION IN SATELLITE COORDINATES

$$\bar{T} = \frac{d\bar{H}}{dt} = \frac{\delta \bar{H}}{\delta t} + \bar{\omega}_o \times \bar{H}$$

$$T = I_o \dot{\omega}_o + \dot{I}_o \omega_o + \sum_i I_i \dot{\omega}_i + \sum_i I_j \dot{\omega}_j + \sum_j \dot{I}_j \omega_j + \sum_n \dot{H}_n$$

EVALUATION OF THE DERIVATIVES

Inertia Tensors

$$\begin{aligned} \dot{I}_o &= \sum_i \dot{J}_i - m[M(\dot{r}_o, r_o) + M^T(\dot{r}_o, r_o)] + \sum_j m_j[M(r_j + \rho_j, \dot{\rho}_j) + M^T(r_j + \rho_j, \dot{\rho}_j)] \\ &\quad + \sum_n m_n[M(r_n + \rho_n, \dot{\rho}_n) + M^T(r_n + \rho_n, \dot{\rho}_n)] \end{aligned}$$

$$\dot{I}_j = \dot{J}_j + m_j M(r_o + r_j + \rho_j, \dot{\rho}_j) + m_j M(r_o + \rho_j, \dot{\rho}_j)$$

where

$$\begin{aligned} \dot{\rho}_j &= \omega_j \times \rho_j \\ \dot{r}_o &= -\frac{1}{m} \left[\sum_j m_j \dot{\rho}_j + \sum_n m_n \dot{\rho}_n \right] \end{aligned}$$

WHEEL TORQUES

$$\begin{aligned} \int_i \bar{x}_i \times d\bar{F} &= \int_i \bar{x}_i \times \frac{d^2}{dt^2} \bar{x}_i \\ \Rightarrow T_i &= J_i \dot{\omega}_o + J_i \dot{\omega}_i + \omega_o \times [J_i (\omega_o + \omega_i)] \end{aligned}$$

The magnitude of the wheel torques about the axis is given by

$$T_{ia} \approx h_i \cdot T_i$$

where h_i is a unit vector along the spin axis. For example,

$$h_i = T_{oi} \begin{bmatrix} 1 \\ 0 \\ 0 \end{bmatrix}$$

PANEL TORQUES

$$\int (\bar{\rho}_j + \bar{x}_j) \times d\bar{F} = \int (\bar{\rho}_j + \bar{x}_j) \times \frac{d^2}{dt^2} (\bar{\rho}_j + \bar{x}_j + \bar{r}_{pj}) dm$$

$$\bar{T}_j = m \bar{\rho}_j \times \frac{d^2 \bar{r}_{pj}}{dt^2} + \frac{d\bar{H}}{dt} j$$

where

$$\bar{H}_j = [J_j + m_j M(\bar{\rho}_j, \bar{\rho}_j)] (\bar{\omega}_j + \bar{\omega}_o)$$

$$T_j = m_j \bar{\rho}_j \times \frac{d^2 \bar{r}_{pj}}{dt^2} + \{J_j + m_j [M(\rho_j, \dot{\rho}_j) + M^T(\rho_j, \dot{\rho}_j)]\} (\omega_j + \omega_o)$$

$$+ [J_j + m_j M(\rho_j, \rho_j)] (\dot{\omega}_j + \dot{\omega}_o) + \omega_o \times H_j$$

$$T_{ja} = h_j \cdot T_j$$

where

h_j = unit vector along panel hinge

$$= T_{oj} \begin{bmatrix} 0 \\ 1 \\ 0 \end{bmatrix}$$

and

$$\frac{d^2 \bar{r}_{pj}}{dt^2} = \rho_j \times a_{cm} + \rho_j \times \left[\frac{\delta^2 \bar{r}_o}{\delta t^2} + \omega_o \times \frac{\delta \bar{r}_o}{\delta t} \right] + [M(\dot{\rho}_j, \bar{r}_o) + M(\rho_j, \dot{\bar{r}}_o)] \omega_o$$

$$+ M(\rho_j, \bar{r}_o + \bar{r}_j) \dot{\omega}_o + \omega_o \times M(\rho_j, \bar{r}_o + \bar{r}_j) \omega_o$$

$$\frac{\delta^2 \bar{r}_o}{\delta t^2} = -\frac{1}{m} [\sum_j m_j \ddot{\rho}_j + \sum_n m_n \ddot{\rho}_n]$$

$$\ddot{\rho}_j = \dot{\omega}_j \times \rho_j + \omega_j \times \dot{\rho}_j$$

Nutation Damper Forces

$$\begin{aligned} \Sigma F &= m_n \frac{d^2}{dt^2} (r_{cm} + r_o + r_n + \rho_n) \\ &= a_{cm} + \frac{\delta^2 r_o}{\delta t^2} + \frac{\delta^2 \rho_n}{\delta t^2} + \dot{\omega}_o \times (r_o + r_n + \rho_n) \\ &\quad + \omega_o \times (\dot{r}_o + \dot{\rho}_n) \\ &\quad + \omega_o \times \left[\frac{\delta r_o}{\delta t} + \frac{\delta \rho_n}{\delta t} + \omega_o \times (r_o + r_n + \rho_n) \right] \\ \Sigma F \cdot h_n &= -k_{1n} \tilde{\rho}_n - k_{2n} \dot{\tilde{\rho}}_n \end{aligned}$$

where

$$\rho_n = \tilde{\rho}_n h_n$$

and

$$h_n = \text{unit vector along } \rho_n.$$

APPENDIX D
NUTATION DAMPER MODEL

APPENDIX D

NUTATION DAMPER MODEL

This appendix summarizes the nutation damper model implemented for the digital simulation evaluation of GPS stability and control analysis.

The nutation damper is used for passive GPS spin axis stabilization during the initial mission phases by dissipating the spacecraft precession energy. The nutation damper adopted for GPS application is of the type of ball in gas filled tube. The tube is made of aluminum and the ball of tungsten carbide. The gas is a 9 : 1 ratio mixture of nitrogen and helium at 1 atm. pressure. Physical parameters of this damper is shown in Figure D-1.

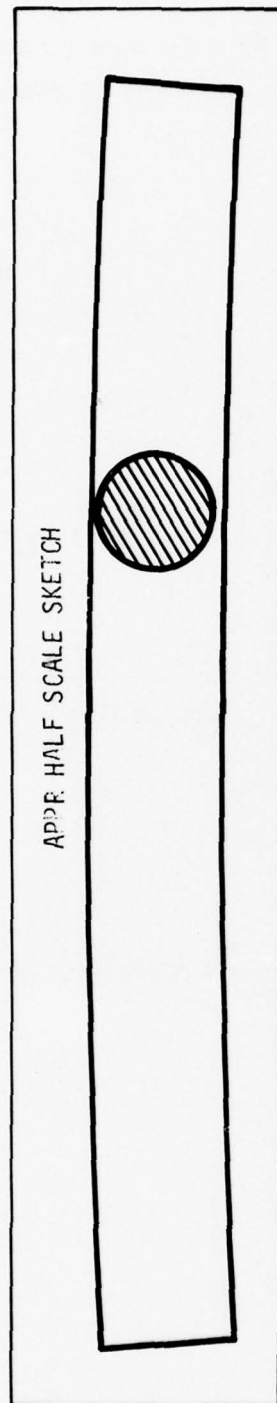
A similar damper of this type was used in the Telstar satellite, Reference D-1. Discussions on the design and analysis of ball-in-tube type nutation dampers can be found in Reference D-2.

Derivation of the torque equations presented here follows the same procedure of Reference D-2 which contains numerous typographical errors. The results, in the torque form, are compatible for integration into the three body model described in Appendix C.

DAMPER MODEL DERIVATION

To facilitate the model derivation, we shall define a vehicle fixed B-frame whose origin is at the vehicle's center of mass (excluding damper ball) with the $(\underline{X}_B - \underline{Y}_B - \underline{Z}_B)$ axes aligned with its principal axes. Also in the following consideration of vehicle rotational motions, it is assumed that the translational motion of vehicle's center of mass resulted from reactional

TYPE BALL IN GAS FILLED TUBE
TUBE CURVED TO PROVIDE CENTRIFUGAL SPRING



TUBE

I.D. 1.256 INCH

O.D. 1.566 INCH

LENGTH 16 INCHES

r = RADIUS OF CURVATURE 159 INCHES = 13.25 ft.

MATERIAL ALUMINUM

BALL

DIAMETER 1.25 INCH $r_D = 0.625$ inches

MATERIAL TUNGSTEN CARBIDE

GAS

9.7 MIXTURE NITROGEN: HELIUM

1 ATMOSPHERE

WEIGHT

1.75 LBS

Figure D-1. Nutation Damper Characteristics

forces of the damper ball can be neglected. By reference to the geometrical description of damper location in B-frame, the position of center of ball, \underline{R}_b can be written as, Figure D-2,

$$(\underline{\bar{R}}_b^B) = \begin{bmatrix} 0 \\ -a + \gamma \cos \alpha \\ b + \gamma \sin \alpha \end{bmatrix} \quad (D-1)$$

where

$$\gamma = 159 \text{ in.} = 13.25 \text{ ft.}$$

(a,b) = coordinates of tube center of curvature

Equation (1) implies that $\underline{Y}_B - \underline{Z}_B$ plane contains the damper tube.

Let the vehicle moment of inertia be such that

$$\begin{cases} I_{XX} = I_{YY} = A \\ I_{ZZ} = C \end{cases} \quad (D-2)$$

The rotational energy of the vehicle becomes,

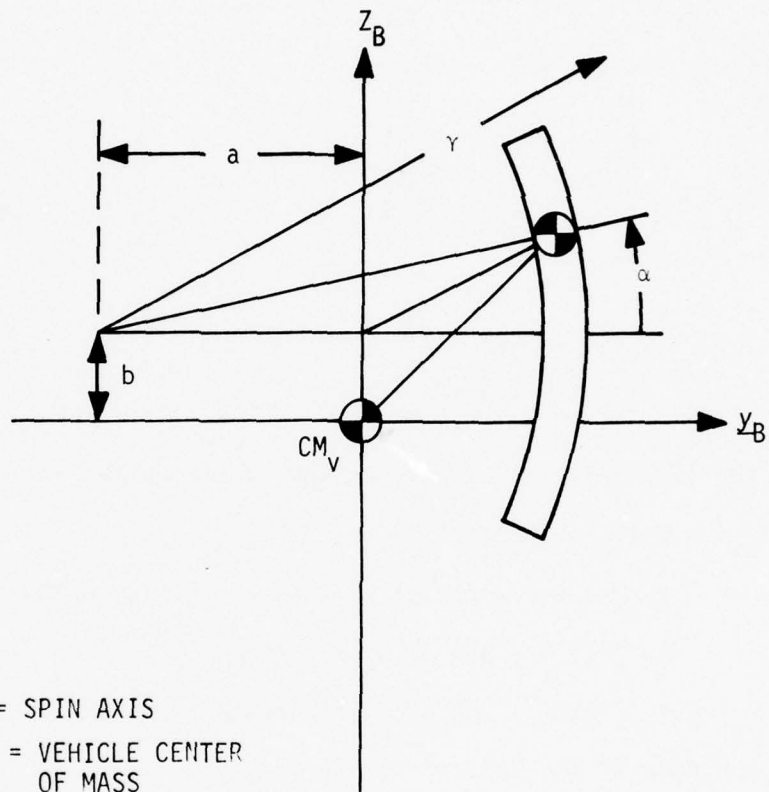
$$T_V = \frac{1}{2} A (\dot{W}_X^2 + \dot{W}_Y^2) + \frac{1}{2} C \dot{W}_Z^2 \quad (D-3)$$

The velocity of damper ball can be written through differentiation of (1) as,

$$(\underline{\dot{V}}_b^B) = T_{BI} (\underline{\dot{V}}_b^B) = T_{BI} (\underline{\dot{R}}_b^I)$$

with $(\underline{\bar{R}}_b^I) = T_{BI}^T (\underline{\bar{R}}_b^B)$, we have

$$\begin{aligned} (\underline{\dot{R}}_b^I) &= T_{BI}^T (\underline{\dot{R}}_b^B) + T_{BI}^T (\underline{\dot{R}}_b^B) \\ &= -T_{BI}^T S [\underline{\bar{W}}_B^B] (\underline{\bar{R}}_b^B) + T_{BI}^T (\underline{\dot{R}}_b^B) \end{aligned}$$



NOTE: Z_B = SPIN AXIS
 CM_V = VEHICLE CENTER
 OF MASS
 DAMPER CONTAINED IN
 PLANE ($Y_B - Z_B$)

Figure D-2. Nutation Damper in Vehicle
 Body Fixed Frame

or

$$(\dot{\underline{V}}_b^B) = -S [(\underline{W}_B^B)] (\underline{R}_b^B) + (\dot{\underline{R}}_b^B) \quad (D-4)$$

In component forms, (4) becomes,

$$\begin{bmatrix} V_X \\ V_Y \\ V_Z \end{bmatrix} = \begin{bmatrix} 0 & -W_Z & W_Y \\ W_Z & 0 & -W_X \\ -W_Y & W_X & 0 \end{bmatrix} \times \begin{bmatrix} 0 \\ -a + \gamma \cos \alpha \\ b + \gamma \sin \alpha \end{bmatrix} + \begin{bmatrix} 0 \\ -\gamma \sin \alpha \dot{\alpha} \\ \gamma \cos \alpha \dot{\alpha} \end{bmatrix} \quad (D-5)$$

Hence the translational kinetic energy of the damper ball is

$$\begin{aligned} T_b &= \frac{1}{2} M (V_X^2 + V_Y^2 + V_Z^2) \\ &= \frac{1}{2} M \{ [-(-a + \gamma \cos \alpha) W_Z + (b + \gamma \sin \alpha) W_Y]^2 \\ &\quad + [-(b + \gamma \sin \alpha) W_X - \gamma \sin \alpha \dot{\alpha}]^2 \\ &\quad + [(-a + \gamma \cos \alpha) W_X + \gamma \cos \alpha \dot{\alpha}]^2 \} \end{aligned} \quad (D-6)$$

where M = mass of the ball

$$= \frac{4}{3} \pi \gamma_b^3 \rho = 263 \text{ gm} = 0.018 \text{ slug}$$

$$\rho = \text{density of tungsten carbide (WC)} = 15.7 \text{ gm/cm}^3$$

Assuming the ball is rolling without slipping in the tube, the magnitude of the angular velocity of the ball is related to the translational velocity of the center of the ball as

$$\begin{aligned} W_b &= \frac{1}{\gamma_b} [(\dot{\underline{R}}_b^B)^T (\dot{\underline{R}}_b^B)]^{1/2} \\ &= \frac{1}{\gamma_b} [\gamma^2 \sin^2 \alpha \dot{\alpha}^2 + \gamma^2 \cos^2 \alpha \dot{\alpha}^2]^{1/2} \\ &= \frac{\gamma \dot{\alpha}}{\gamma_b} \quad \text{where } \gamma_b = \text{radius of the ball} = 0.625 \text{ in.} \end{aligned} \quad (D-7)$$

Hence, the rotational energy of the ball is

$$\begin{aligned} T &= \frac{1}{2} I_b \dot{W}_b^2 = \frac{1}{2} \left(\frac{2}{5} M \gamma_b^2 \right) \left(\frac{\gamma \dot{\alpha}}{\gamma_b} \right)^2 \\ &= \frac{1}{5} M \gamma^2 \dot{\alpha}^2 \end{aligned} \quad (D-8)$$

The drag on the ball is viscous, Reference D-3, since the tube is gas filled, the clearance between ball and tube is small and the ball moves much slower than the speed of sound. Hence, the viscous drag on the ball can be represented by Rayleigh's dissipation function as

$$\begin{aligned} F &= \frac{1}{2} C_D (\dot{\underline{R}}_b^T) (\underline{R}_b) \\ &= \frac{1}{2} C_D \gamma^2 \dot{\alpha}^2 \end{aligned} \quad (D-9)$$

where C_D is a constant to be described later.

The total energy of the system then becomes

$$\begin{aligned} T &= T_v + T_b + T_\gamma \\ &= W_X^2 \{ \frac{1}{2} A + \frac{1}{2} M (\gamma^2 + b^2 + a^2 + 2b \gamma \sin \alpha - 2a \gamma \cos \alpha) \} \\ &\quad + W_Y^2 \{ \frac{1}{2} A + \frac{1}{2} M (b^2 + 2b \gamma \sin \alpha + \gamma^2 \sin^2 \alpha) \} \\ &\quad + W_Z^2 \{ \frac{1}{2} C + \frac{1}{2} M (a^2 - 2a \gamma \cos \alpha + \gamma^2 \cos^2 \alpha) \} \\ &\quad + W_Y W_Z \{ -M (-ab - a \gamma \sin \alpha + b \gamma \cos \alpha + \gamma^2 \sin \alpha \cos \alpha) \} \\ &\quad + W_X \dot{\alpha} \{ M (\gamma^2 - a \gamma \cos \alpha + b \gamma \sin \alpha) \} \\ &\quad + \dot{\alpha}^2 \left\{ \frac{7}{10} M \gamma^2 \right\} \end{aligned} \quad (D-10)$$

With the total vehicle energy given in (D-10) and the damper dissipation function given in (D-9), the equation of motion of the vehicle and the damper system can be obtained as

$$\frac{d}{dt} \frac{\partial T}{\partial \dot{W}_X} - W_Z \frac{\partial T}{\partial \dot{W}_Y} + W_Y \frac{\partial T}{\partial \dot{W}_Z} = 0$$

$$\frac{d}{dt} \frac{\partial T}{\partial \dot{W}_Y} - W_X \frac{\partial T}{\partial \dot{W}_Z} + W_Z \frac{\partial T}{\partial \dot{W}_X} = 0$$

$$\frac{d}{dt} \frac{\partial T}{\partial \dot{W}_Z} - W_Y \frac{\partial T}{\partial \dot{W}_X} + W_X \frac{\partial T}{\partial \dot{W}_Y} = 0$$

$$\frac{d}{dt} \frac{\partial T}{\partial \dot{\alpha}} - \frac{\partial T}{\partial \alpha} + \frac{\partial F}{\partial \dot{\alpha}} = 0 \quad (D-11)$$

The rotational equation of motion of the vehicle can be written in the form of Euler's rigid body equation as

$$\begin{cases} A\dot{W}_X + (C - A) W_Z W_Y = T_X \\ A\dot{W}_Y - (C - A) W_X W_Z = T_Y \\ A\dot{W}_Z = T_Z \end{cases} \quad (D-12)$$

where the torques T_X , T_Y , and T_Z are,

$$\begin{aligned} T_X = & -M [\dot{W}_X (\gamma^2 + b^2 + a^2 + 2b \gamma \sin \alpha - 2a \gamma \cos \alpha) \\ & + \dot{\alpha} (2W_X + \dot{\alpha}) (b \gamma \cos \alpha + a \gamma \sin \alpha) \\ & + \ddot{\alpha} (\gamma^2 - a \gamma \cos \alpha + b \gamma \sin \alpha) \\ & + W_Y W_Z (a^2 - b^2 - 2a \gamma \cos \alpha - 2b \gamma \sin \alpha - \gamma^2 \sin^2 \alpha + \gamma^2 \cos^2 \alpha) \\ & + (W_Y^2 - W_Z^2) (ab + a \gamma \sin \alpha - b \gamma \cos \alpha - \gamma^2 \sin \alpha \cos \alpha)] \quad (D-13) \end{aligned}$$

$$\begin{aligned} T_Y = & -M [\dot{W}_Y (b^2 + 2b \gamma \sin \alpha + \gamma^2 \sin^2 \alpha) \\ & + (\dot{W}_Z - W_X W_Y) (ab + a \gamma \sin \alpha - b \gamma \cos \alpha - \gamma^2 \sin \alpha \cos \alpha) \end{aligned}$$

$$\begin{aligned}
& + W_X W_Z (\gamma^2 + b^2 + 2b \gamma \sin \alpha - \gamma^2 \cos^2 \alpha) \\
& + 2W_Y \dot{\alpha} (b \gamma \cos \alpha + \gamma^2 \sin \alpha \cos \alpha) \\
& + 2W_Z \dot{\alpha} (b \gamma \sin \alpha + \gamma^2 \sin^2 \alpha)] \quad (D-14)
\end{aligned}$$

$$\begin{aligned}
T_Z = -M [& \dot{W}_Z (a^2 - 2a \gamma \cos \alpha + \gamma^2 \cos^2 \alpha) \\
& + (\dot{W}_Y + W_X W_Y) (ab + a \gamma \sin \alpha - b \gamma \cos \alpha - \gamma^2 \sin \alpha \cos \alpha) \\
& + W_X W_Y (-a^2 + 2a \gamma \cos \alpha - \gamma^2 \cos^2 \alpha) \\
& + 2W_Z \dot{\alpha} (a \gamma \sin \alpha - \gamma^2 \sin \alpha \cos \alpha) \\
& - 2W_Y \dot{\alpha} (b \gamma \sin \alpha + \gamma^2 \sin^2 \alpha)] \quad (D-15)
\end{aligned}$$

With ball's equation of motion in tube given as,

$$\begin{aligned}
& \frac{7}{5} \gamma \ddot{\alpha} + \dot{W}_X (\gamma - a \cos \alpha + b \sin \alpha) \\
& - W_X^2 (b \cos \alpha + a \sin \alpha) - W_Y^2 (b \sin \alpha + \gamma \sin \alpha \cos \alpha) \\
& - W_Z^2 (a \sin \alpha - \gamma \sin \alpha \cos \alpha) \\
& - W_Y W_Z (a \cos \alpha + b \sin \alpha - \gamma \cos^2 \alpha + \gamma \sin^2 \alpha) \\
& + W_X \dot{\alpha} (a \sin \alpha + b \cos \alpha - a \sin \alpha - b \cos \alpha) \\
& + \left(\frac{C_D \gamma}{N} \right) \dot{\alpha} = 0 \quad (D-16)
\end{aligned}$$

The drag force on the ball consists of two components: the pressure drag and the viscous drag. For the case where the gap between tube and ball is small, as in the GPS nutation damper, and the speed of the ball in the tube is small compared with the speed of sound, it has been determined in Ref. D-3 that the drag force is primarily due to pressure drag. The drag force D,

can be written as

$$D' = \frac{135}{4 \times 64} \left(\frac{\pi^3 \mu \gamma_b}{g^{5/2}} \right) S \triangleq C_D S$$

where

μ = viscosity of gas in tube

$g = (\gamma_i - \gamma_b) \gamma_b$ = gap parameter

γ_i = inside radius of tube

S = speed of ball relative to gas

C_D = dissipation coefficient

$$= \frac{135}{4 \times 64} \frac{\pi^3 \mu \gamma_b}{g^{5/2}}$$

For GPS nutation damper,

$$\mu = 178.1 \times 10^{-6} \times 2.089 \times 10^{-3} \text{ lb}_f \text{ sec/ft}^2$$

$$g = (0.633 - 0.625) / 0.625$$

$$\gamma_i = 0.633 \text{ in.}$$

Hence, value of dissipation coefficient,

$$C_D = .0171 \text{ lb}_f / (\text{ft/sec})$$

To handle the discontinuity at either end of the damper tube, let

$$\dot{\alpha} = -\epsilon \dot{\alpha} \quad \text{at } \alpha = \pm \alpha_{\max}$$

where

$$\alpha_{\max} \approx (8/159) \text{ rad} = 2.9 \text{ deg.}$$

$$\epsilon = 0 \text{ for inelastic collision}$$

$$= 1 \text{ for elastic collision.}$$

The GPS requirement on half cone angle of nutation is to be less than 2 deg'. The discontinuity situation is not expected to be encountered often if the 2 deg. requirement is met. The value of $\epsilon = 1$ would give a conservative result in that less precession energy is dissipated at bottoming. Hence, use of $\epsilon = 1$ is recommended for this reason.

NUTATION DAMPING TIME CONSTANT VERIFICATION

Nominal Solution Undamped Rigid Body Motion

Consider a rigid body with symmetric moment of inertia about the traverse axes, i.e., $I_{XX} = I_{YY}$ in a torque free situation. The Euler's equation is reduced to:

$$\begin{cases} \dot{W}_X = -A W_Y W_Z \\ \dot{W}_Y = A W_Z W_X \\ \dot{W}_Z = 0 \end{cases} \quad (D-17)$$

where

$$A = \left(\frac{I_{ZZ} - I_{XX}}{I_{XX}} \right) = \left(\frac{I_{ZZ}}{I_{XX}} - 1 \right) \triangleq (n - 1)$$

The solution of the above equation can be written as:

$$\begin{cases} W_X = -B \sin \Omega t \\ W_Y = B \cos \Omega t \\ W_Z = W_Z(0) \end{cases} \quad (D-18)$$

$$\text{with } \Omega = A W_Z(0) \quad (D-19)$$

The angular momentum vector is written as:

$$\underline{H} = I_{XX} \underline{W}_X \underline{X}_B + I_{YY} \underline{W}_Y \underline{Y}_B + I_{ZZ} \underline{W}_Z \underline{Z}_B \quad (D-20)$$

Since there is no external torque, the angular momentum is constant. The nominal motion of the rigid body can be visualized as a constant precession about the angular momentum vector with a precession rate Ω and a nutation angle θ which is defined as:

$$\tan \theta = \frac{H_t}{H_s} = \frac{\sqrt{I_{XX}^2 W_X^2 + I_{YY}^2 W_Y^2}}{I_{ZZ} W_Z} = \frac{I_{YY} B}{I_{ZZ} W_Z} \quad (D-21)$$

Therefore:

$$B = \left(\frac{I_{ZZ}}{I_{YY}} \times \tan \theta \right) W_Z \quad (D-22)$$

For small value of θ , (6) becomes

$$B \approx \left(\frac{I_{ZZ}}{I_{YY}} \times \theta \right) W_Z \quad (D-23)$$

A relationship between the rigid body's angular momentum and rotational energy useful for later development of the energy sink approximation is:

$$\begin{cases} T = \frac{1}{2} I_{XX} (W_X^2 + W_Y^2) + \frac{1}{2} I_{ZZ} W_Z^2 = \frac{H_t^2}{2I_{XX}} + \frac{H_s^2}{2I_{ZZ}} \\ H^2 = H_t^2 + H_s^2 \end{cases} \quad (D-24)$$

$$\text{Hence } H_t^2 = \left(\frac{I_{XX} I_{ZZ}}{I_{ZZ} - I_{XX}} \right) \left(2T - \frac{H^2}{I_{ZZ}} \right) \quad (D-25)$$

From (5)

$$\sin^2 \theta = \frac{H_t^2}{H^2} = \left(\frac{I_{XX} I_{ZZ}}{I_{ZZ} - I_{XX}} \right) \left(\frac{2T}{H^2} - \frac{1}{I_{ZZ}} \right) \quad (D-26)$$

Nutation Damping Time Constant

The GPS nutation damper consists of a tube aligned with respect to the vehicle spin axis. A ball inside the tube is dissipating the nutation energy via viscous drag force retarding the ball's motion. An approximation procedure known as the energy sink concept assumes that the dissipation of nutation energy does not change the system's angular momentum (which is dominantly spin angular momentum). Hence equation (D-26) can be differentiated with terms \dot{H} neglected in this approximation, i.e.,

$$2 \sin \theta \cos \theta \dot{\theta} = \frac{2I_{ZZ}\dot{T}}{(n-1)H^2} \quad (D-27)$$

For small value of θ ,

$$\theta \dot{\theta} = \frac{2I_{ZZ}\dot{T}}{(n-1)H^2} \quad (D-28)$$

A further approximation involves

$$H^2 \approx H_S^2 = I_{ZZ}^2 \omega_Z^2 \quad (D-29)$$

Hence

$$\dot{\theta} \approx \left[\frac{1}{(n-1)I_{ZZ}\omega_Z^2} \right] \dot{T} \quad (D-30)$$

The energy dissipation \dot{T} can be expressed as the product of the drag force the ball experienced and the velocity of the ball, i.e.,

$$\dot{T} = -fv \quad (D-31)$$

with drag force,

$$f = C_D V$$

and the ball velocity,

$$V = \gamma \dot{\alpha}$$

Hence the energy dissipation rate,

$$\dot{T} = -C_D \gamma^2 \dot{\alpha}^2 \quad (D-32)$$

where α is the position of ball in tube defined as in Figure D-2,

γ = is radius of damper tube,

C_D = is dissipation coefficient

From analysis of nutation damper, the motion of the ball in tube was obtained as

$$\begin{aligned} \frac{7}{5} \gamma \ddot{\alpha} + \dot{W}_X (\gamma - a \cos \alpha + b \sin \alpha) - W_Y^2 (b \cos \alpha + \gamma \sin \alpha \cos \alpha) \\ - W_X^2 (b \cos \alpha + a \sin \alpha) - W_Z^2 (a \sin \alpha - \gamma \sin \alpha \cos \alpha) \\ - W_Y W_Z (a \cos \alpha + b \sin \alpha - \gamma \cos^2 \alpha + \gamma \sin^2 \alpha) \\ + \frac{C_D \gamma}{M} \dot{\alpha} = 0 \end{aligned} \quad (D-33)$$

With the geometry of mounting such that $b = 0$ and introducing the small angle approximations $\sin \alpha \approx \alpha$, $\cos \alpha \approx 1$ and neglecting terms W_X^2 and W_Y^2 as they are small for small nutation angle θ , equation (17) becomes

$$\left(\frac{7\gamma}{5}\right) \ddot{\alpha} + \left(\frac{C_D \gamma}{M}\right) \dot{\alpha} + W_Z^2 (\gamma - a) \alpha = W_Y W_Z (a - \gamma) - \dot{W}_X (\gamma - a) \quad (D-34)$$

Using the expression of W_Y as given in equations (2) and (7)

$$W_Y = \Omega n W_Z \cos \Omega t \quad (D-35)$$

Similarly,

$$\dot{W}_X = -\theta n W_Z \Omega \cos \Omega t$$

Equation (18) can be reduced to the following form:

$$\begin{aligned} \ddot{\alpha} + \left(\frac{5C_D}{7M} \right) \dot{\alpha} + \left[\frac{5(\gamma - a)W_Z^2}{7\gamma} \right] \alpha \\ = -\theta \left[\frac{5(\gamma - a)(2n - n^2)W_Z^2}{7\gamma} \right] \cos \Omega t \end{aligned} \quad (D-36)$$

The solution of the standard second order linear differential equation of the form

$$\ddot{\alpha} + 2\underline{b} \dot{\alpha} + \underline{a}^2 \alpha = \underline{c} \theta \cos \Omega t \quad (D-37)$$

has been obtained in standard textbooks as:

$$\alpha = \frac{c\theta}{\sqrt{(\underline{a}^2 - \Omega^2)^2 + 4\underline{b}^2 \Omega^2}} \cos(\Omega t + \phi) \stackrel{\Delta}{=} \theta \alpha_o \cos(\Omega t + \phi) \quad (D-38)$$

Compare (20) and (21),

$$\begin{aligned} 2\underline{b} &= 5 C_D / (7M) \\ \underline{a}^2 &= 5(\gamma - a)W_Z^2 / (7\gamma) \\ \underline{c} &= -5(\gamma - a)(2n - n^2)W_Z^2 / (7\gamma) \end{aligned} \quad (D-39)$$

From (22),

$$\dot{\alpha} = -\theta \alpha_o \Omega \sin(\Omega t + \phi) \quad (D-40)$$

Substitute (24) into (16)

$$\dot{T} = -\theta^2 C_D \gamma^2 \alpha_o^2 \Omega^2 \sin^2(\Omega t + \phi) \quad (D-41)$$

The average value over a full period, i.e.,

$$\Omega t_p = 2\pi, \text{ is}$$

$$\bar{\dot{\theta}} = -\frac{1}{2} C_D \gamma^2 \alpha_o^2 \Omega^2 \theta^2 \quad (D-42)$$

$$\text{since } \frac{1}{t_p} \int_0^{t_p} \sin^2 (\Omega t + \phi) dt = \frac{1}{2}$$

Substitution of (26) into (14) gives

$$\dot{\theta} = \left[\frac{1}{(n-1)I_{ZZ}W_Z^2} \right] \left[-\frac{1}{2} C_D \gamma^2 \alpha_o^2 \Omega^2 \theta^2 \right]$$

or

$$\dot{\theta} = - \left[\frac{C_D \gamma^2 \alpha_o^2 \Omega^2}{2(n-1)I_{ZZ}W_Z^2} \right] \theta \quad (D-43)$$

The time constant of nutation damping can now be written as:

$$T_c = \frac{2(n-1)I_{ZZ}W_Z^2}{C_D \gamma^2 \alpha_o^2 \Omega^2} \quad (D-44)$$

where

$$\begin{cases} \alpha_o = \sqrt{\frac{c}{(\underline{a}^2 - \Omega^2)^2 + 4\underline{b}^2 \Omega^2}} \\ 2\underline{b} = 5 C_D / (7M) \\ \underline{a}^2 = 5(\gamma - a)W_Z^2 / (7\gamma) \\ \underline{c} = -(2n - n^2)\underline{a}^2 \\ \Omega = (n - 1)W_Z \end{cases}$$

The predicted nutation damping time constant for the two cases of $W_Z = 100$ RPM and $W_Z = 10$ RPM are computed as follows:

Case 1:

$$r = 13.25 \text{ ft.}$$

$$a = 10.25 \text{ ft.}$$

$$m = 0.018 \text{ slug}$$

$$C_D = 0.0171 \text{ lb}_f/(\text{ft}/\text{sec})$$

$$I_{XX} = I_{YY} = 77 \text{ slug-ft}^2$$

$$I_{ZZ} = 94 \text{ slug-ft}^2$$

$$W_Z = 100 \text{ RPM} = 10.47 \text{ rad/sec.}$$

$$n = 1.22$$

$$\Omega = 2.31$$

$$2b = 0.6789$$

$$\underline{a}^2 = 17.728$$

$$\underline{c}^2 = -16.84$$

$$\alpha_o = -1.348$$

$$T_c = 155.755 \text{ sec.}$$

Case 2:

$$W_Z = 10 \text{ RPM} = 1.047 \text{ rad/sec.}$$

$$n = 1.22$$

$$\Omega = 0.231$$

$$2b = 0.6786$$

$$\underline{a}^2 = 0.17728$$

$$\underline{c} = -0.1684$$

$$\alpha_o = -0.84275$$

$$T_c = 398.497 \text{ sec.}$$

The nutation half cone angle history corresponding to Case 1 and Case 2 considered above are plotted in Figures D-3 and D-4 respectively. These results are obtained using the nutation damping simulation program where the detailed dynamics of the damper ball and rigid body dynamics are considered.

100 RPM

$$\begin{cases} I_{xx} = 76.3 \\ I_{yy} = 78.3 \\ I_{zz} = 94.1 \end{cases}$$

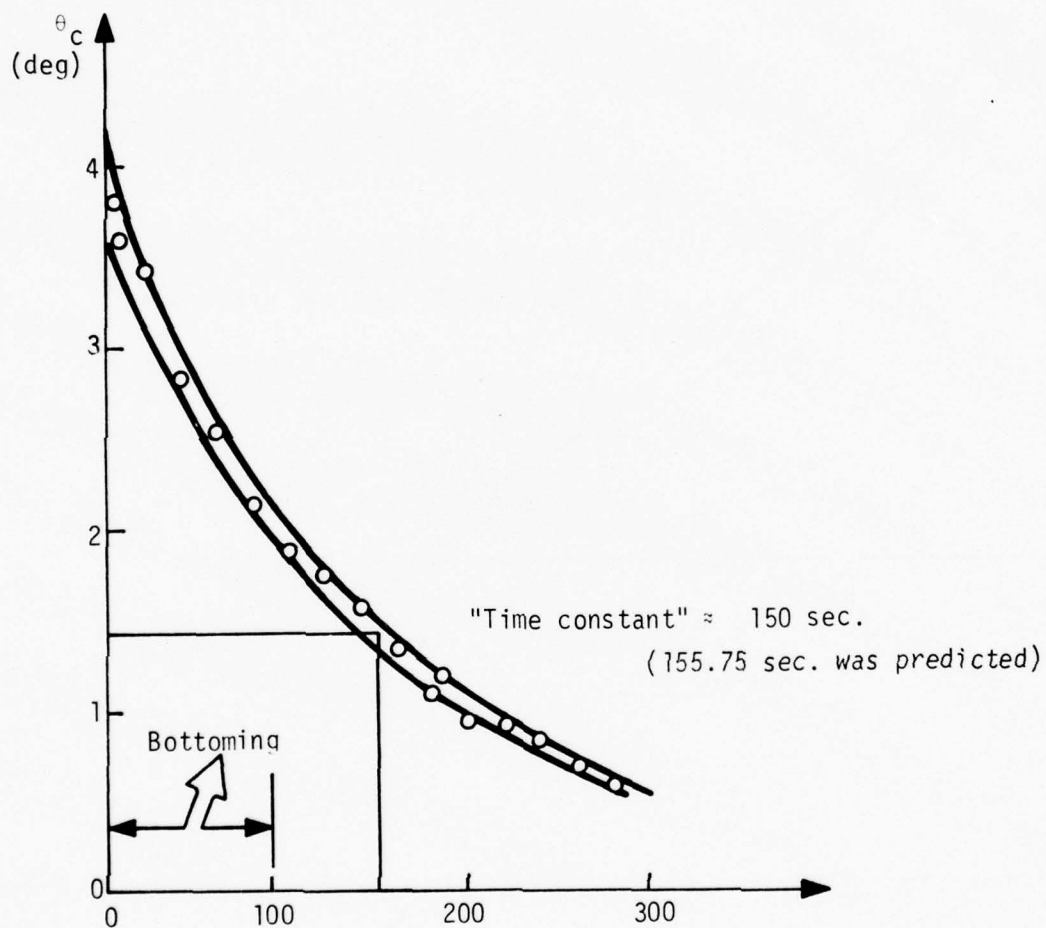


Figure D-3. Simulation Data

10 RPM

$$\begin{cases} I_{xx} = 76.3 \\ I_{yy} = 78.3 \\ I_{zz} = 94.1 \end{cases}$$

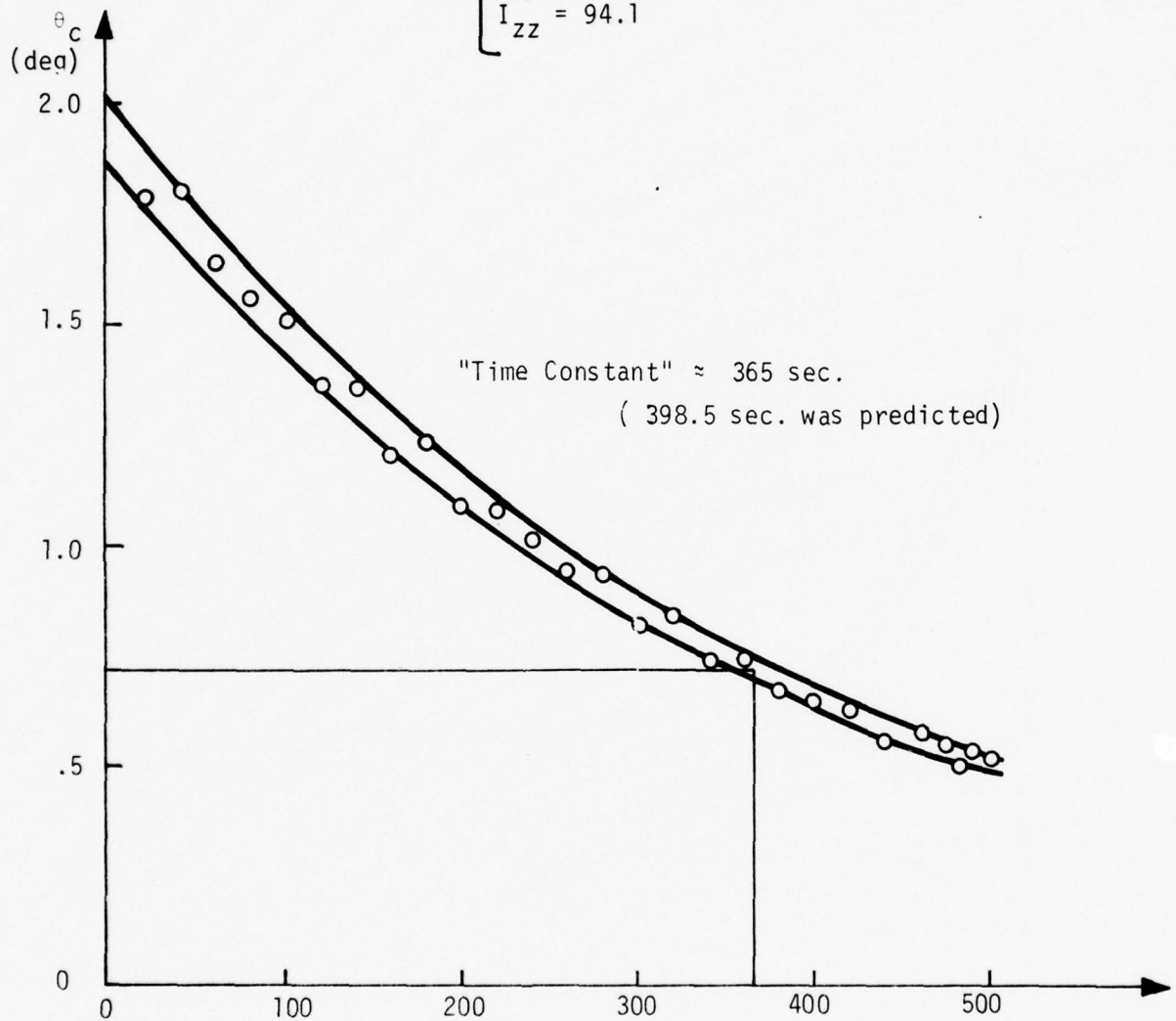


Figure D-4. Simulation Data

REFERENCES

- D-1. Yu, E.Y., "Spin Decay, Spin-Precession Damping, and Spin-Axis Drift of the Telstar Satellite," The Bell System Technical Journal, September 1963.
- D-2. Auelmann, R.R. and Lane, P.T., "Design and Analysis of Ball-In-Tube Nutation Dampers," Proceeding of Symposium on Dual Spin Spacecraft, 1967.
- D-3. Bauer, A.B. and DuPuis, R.A., "Fluid Drag on a Sphere Rolling in a Tube," Journal of Applied Mechanics, ASME, September 1967.

APPENDIX E

MODEL FOR GPS DIGITAL SPIN SUN SENSOR (SSS)

APPENDIX E

MODEL FOR GPS DIGITAL SPIN SUN SENSOR (SSS)

This appendix documents the GPS spin sun sensor (SSS) model. It has been programmed on a digital computer, and the simulation performs satisfactorily. Figure E-1 shows a flowchart of the math model which is based on the data of the references and the assumptions listed in this appendix. The main simulation program will provide the model with the sun vector in the spin reference frame and the spin rate at each sample instant. The model will provide a flag indicating whether or not a pipper command pulse will occur during the next sample interval, the time to the pipper pulse from the current sample instant, and the solar aspect angle at the pipper pulse occurrence.

DISCUSSION OF THE MODEL

A flowchart of the preliminary math model for the SSS is shown in Figure E-1. It accepts from the main program the spin rate and the sun vector in the spin reference frame at the sampling instant. To simulate the asynchronous pipper pulse within a synchronous simulation, both a flag and the predicted pipper pulse time from the current sampling instant is output when the pipper pulse is predicted to occur within the next sample period, T_{samp} . The measured solar aspect angle, nominally the angle between the Z axis and the sun vector and specifically the angle between the sun vector and the sensor Z axis, will be computed at the time of the pipper pulse, quantized, and output to the main program along with the flag and pipper pulse time. To perform these computations, the model must be initialized with the angular alignment of the sensor and the orientation of the spin vector with respect to the vehicle.

The SSS model described in Figure E-1 is based on the 1/8/75 spin sun sensor procurement specification and the assumptions listed in Table E-1. Table E-1 lists the initialization data required by the model. Table E-2 lists the input data to the model from the main program, and Table E-3 lists the outputs computed by the model. The intermediate variables internal to the model are described in Table E-4.

The notation $[\theta]j$ denotes a rotational transformation by the angle θ about the j axis. Transformations used in the model and those suggested to be used in the main program to obtain SW, the sun vector in the spin frame at the sampling instant t , are defined in Figures E-2 through E-7.

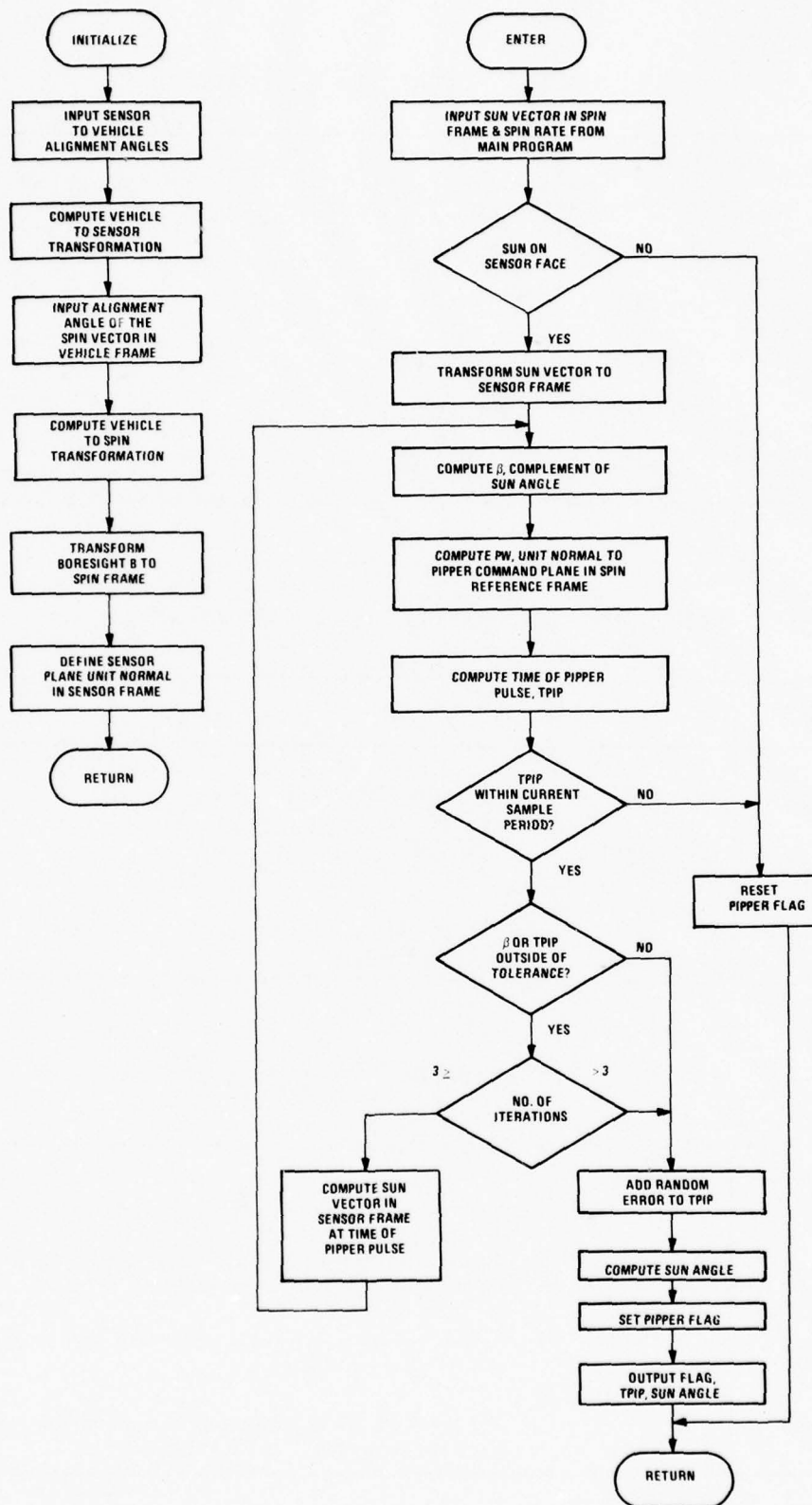


Figure E-1. GPS SSS Model Top Level Flowchart

TABLE E-1. INITIALIZATION DATA

Variable	Units	Description
α_S	Degrees	Figure E-6
β_S	Degrees	Figure E-6
γ_S	Degrees	Figure E-6
α_W	Degrees	Figure E-7
β_W	Degrees	Figure E-7

TABLE E-2. INPUT DATA FROM MAIN PROGRAM

Variable	Units	Description
T_{SAMP}	Seconds	SSS Sample Period
ω_S	Radians/ Second	Spin Rate
$\bar{S}_W(t)$		Sun Vector in Spin Reference Frame at Sample Instant

TABLE E-3. SSS OUTPUT TO MAIN PROGRAM

Variable	Units	Description
T_{pipper}	Seconds	Time from beginning of current sample interval to time of pipper pulse.
SUN_{ANG}	Degrees	Angle between Z sensor axis and sun vector (solar aspect angle).
I_{pipper}		Flag set to 1 if proper pulse occurs during current interval. Set = 0 otherwise.

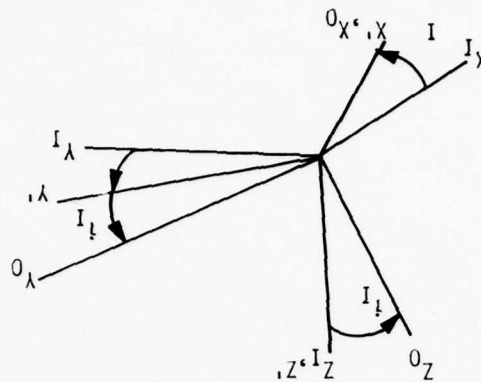
TABLE E-4. INTERNAL VARIABLES

Variable	Units	Description
$[T_{V/S}]$	Radians	Sensor to vehicle transformation. Transpose of $[T_{S/V}]$. (See Figure E-6.)
$[T_{W/V}]$		Vehicle to spin transformation. (See Figure E-7.)
$[T_{W/S}]$		Sensor to spin transformation $[T_{W/S}] = [T_{W/V}] [T_{S/V}]^T$
\bar{B}_W		Boresight vector in spin frame. (See Figure E-5.)
\bar{N}_S		Normal to sensor plane in sensor frame. (See Figure E-5.)
θ		Sensor measured value of complement of the sun angle.
\bar{P}_W		Sensor plane normal vector in spin frame.
\bar{S}_S		Sun vector in sensor frame.
ITER		Iteration counter.
$\hat{\bar{K}}_S$		Unit vector along sensor Z axis.
T_P	Seconds	Value of T_{pipper} from previous iteration.
θ'	Radians	Value of θ from previous iteration.

The method of solution for the pipper command and pulse time and the analysis performed to develop the model are documented in the subsection entitled "Method of Solution." The analysis showing the effect of the quasi-stationary spin axis orientation is also documented. The model does not include sensor dynamics or anomalies in the optics.

ASSUMPTIONS

- The orientation of the spin axis to the vehicle axes is defined in Figure E-7 and is constant. Nominally, the spin axis and the Z vehicle axis are aligned.
- The sensor reference frame and orientation to the vehicle axes are as defined in Figures E-5 and E-6. Nominally, the Z sensor axis is parallel to the spin axis.



INERTIAL FRAME

- X_I - in celestial equatorial plane pointed toward vernal equinox
- Y_I - in celestial equatorial plane at 90 degrees right ascending
- Z_I - perpendicular to equatorial plane (nominally toward Polaris)

ORBIT FRAME

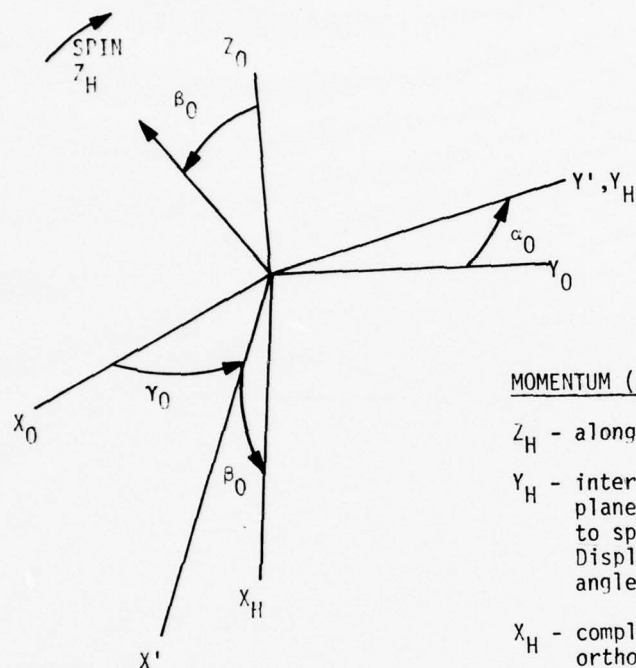
- X_O - ascending node
- Y_O - lies in orbit plane and 90 degrees from X_O
- Z_O - perpendicular to orbit plane (right-hand triad)

TRANSFORMATION FROM INERTIAL FRAME TO THE ORBIT ORIENTED INERTIAL FRAME IS

$$\begin{bmatrix} T_{O/I} \end{bmatrix} = \begin{bmatrix} i_I \end{bmatrix} \times \begin{bmatrix} \alpha_I \end{bmatrix} Z$$

where α_I = right ascension of ascending node
 i_I = orbit inclination

Figure E-2. Definition of Transformation from the Stellar Inertial Frame to the Orbit Frame



MOMENTUM (H) FRAME

Z_H - along spin vector

Y_H - intersection of orbit plane and plane normal to spin vector. Displaced from Y_0 by angle γ_0 .

X_H - completes right-hand orthogonal triad

$$\begin{bmatrix} T_{H/O} \end{bmatrix} = \begin{bmatrix} \beta_0 \end{bmatrix}_Y \begin{bmatrix} \gamma_0 \end{bmatrix}_Z \quad \phi = 0$$

This is a time varying transformation driven by the control system where

γ_0 = the angle from X_0 about Z_0 to the projection of the spin vector on the orbit plane X_0Y_0

β_0 = the angle between the spin vector and the orbit plane normal

Figure E-3. Transformation from the Orbit (O) Frame to the Momentum (H) Frame

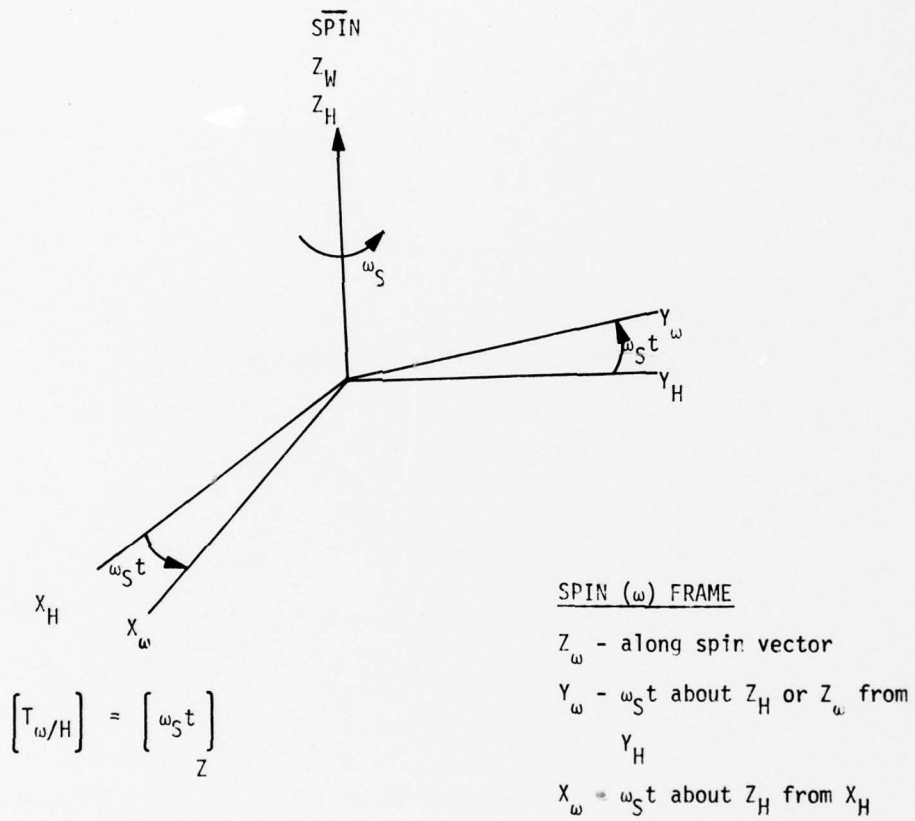
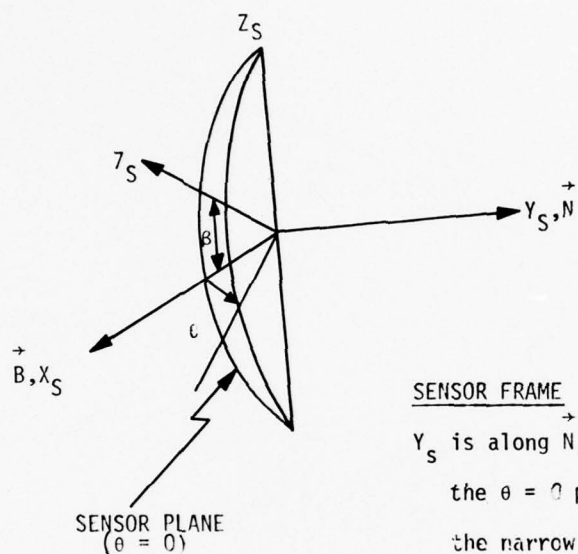


Figure E-4. Transformation from the Momentum (H) Frame to the Spin (ω) Frame



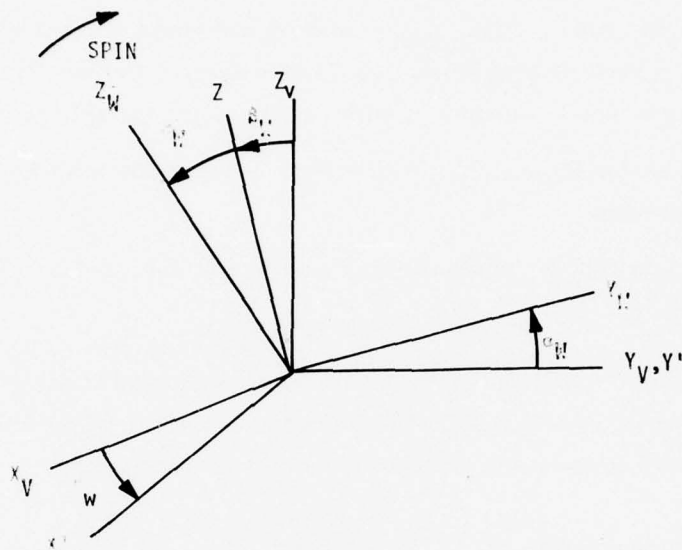
SENSOR FRAME

Y_S is along N , the normal to the $\theta = 0$ plane (plane of the narrow field of view).

X_S is along B , the boresight which is the intersection of the plane $\theta = 0$ and the plane $\beta = 0$.

Z_S completes the right-hand orthogonal triad.

Figure E-5. Definition of GPS SSS Sensor Reference Frame



$$\begin{bmatrix} T_{W/V} \end{bmatrix} = \begin{bmatrix} T \text{ SPIN/VEHICLE} \end{bmatrix} = \begin{bmatrix} \alpha_W \end{bmatrix}_X \begin{bmatrix} \beta_W \end{bmatrix}_Y$$

This is a constant transformation where

α_W = angle between the Z_V axis and the projection of the spin vector on the $X_V - Z_V$ plane

β_W = angle between the spin vector and the $X_V - Z_V$ plane

Figure E-7. Definition of GPS Spin Reference Frame and Transformation from Vehicle to Spin Reference Frame

- The sample period T_{SAMP} will be 0.05 sec or shorter to preclude the sun vector from entering the active region of the sensor from the opposite side of the vehicle during one sample period.
- The rate of angular displacement of the spin vector in inertial space will be less than $0.01 \text{ deg}/T_{\text{SAMP}}$ so that angular displacement of the spin axis during T_{SAMP} will be negligible. This will allow prediction of the pipper pulse from the spin rate and geometry without accounting for spin vector displacement.
- At each sample instant, the simulation main program will provide the SSS model with
 1. Spin rate W_S about the spin axis in rad/sec, and
 2. $\bar{S}_W^{(t)}$, the sun vector in the spin frame.
- The pipper command pulse occurs $0.25 \text{ deg}/\cos \beta$ ahead of the crossing of the sensor ($\theta = 0$) plane. The repeatability of the pulse with respect to $\theta = 0$ is 3 arc minutes for repeated crossings at constant β .

METHOD OF SOLUTION

The method of solution is to predict, from the sun vector, sensor plane unit normal vector and the spin rate, the time of the pipper command pulse, and the measured solar aspect angle at that instant. It is assumed that the spin axis is quasi-stationary as explained in the next subsection.

Define the pipper command plane with unit normal \bar{P}_S to contain the sensor Z axis and the sun vector at the time of the pipper command pulse. The unit normal \bar{P}_S can be defined in terms of \bar{N}_S , the normal to the sensor ($\theta = 0$) plane shown in Figure E-5. \bar{P}_S is the result of the rotation of \bar{N}_S $0.25 \text{ deg}/\cos \beta$ about the Z sensor axis, where β is the complement of the measured solar aspect angle also shown in Figure E-5.

$$\bar{P}_S = (-0.25/57.3) * (1/\cos \beta) \bar{N}_S \quad (\text{E-1})$$

This relationship between the pipper command plane, sensor plane, and aspect angle is defined in Reference E-1. At the time of the pipper command pulse, the sun vector lies in the pipper command plane; therefore, the sun vector \bar{S} and the normal \bar{P} are perpendicular at this instant. Thus,

$$\bar{S} \cdot \bar{P} = 0 \quad (E-2)$$

The solution of Equation (E-2) will allow the prediction of the pippier pulse time. If sensor, vehicle, and spin reference frames all have Z axes aligned, the solution is of closed form. However, these frames, in general, will not be aligned, so an iterative solution is shown in Figure E-2. The solution of Equation (E-2) will be done in the spin reference frame so that only rotations about one axis need to be considered. The sun vector in the spin frame,

$$\bar{S}_W = [T_{W/H}] [T_{H/O}] [T_{O/I}] \bar{S}_I \quad (E-3)$$

where the transformations from the inertial frame to the spin frame are defined in Figures E-3, E-4, and E-5, will be input from the main program at the sampling instant. The pippier command plane unit normal in the spin frame

$$\bar{P}_W = [T_{W/V}] (T_{S/V})^T [(-0.25/57.3) 1/\cos \beta]_Z \bar{N}_S \quad (E-4)$$

will be computed in the model. The transformations $[T_{W/V}]$ and $[T_{S/V}]$ are defined in Figures E-7 and E-8. The initial value of β is computed from the sun vector \bar{S}_W at the sample instant:

$$\beta = \sin^{-1} (\hat{k}_S \cdot [T_{S/V}] [T_{W/V}]^T \bar{S}_W) \quad (E-5)$$

At the instant of the pippier pulse, T_{pippier} , the sun vector in the spin frame will be

$$\bar{S}_W(T_{\text{pippier}}) = [W_S T_{\text{pippier}}]_Z \bar{S}_W \quad (E-6)$$

because the spin frame rotates about the Z axis. W_S is the spin rate (about the Z spin axis) and T_{pippier} is measured from the sample instant. Incorporating (E-4) and (E-6) into (E-2),

$$\left([W_S T_{\text{pippier}}]_Z \right) \bar{S}_W \cdot \bar{P}_W = 0 \quad (E-7)$$

Evaluating Equation (E-7), one obtains

$$(\sin W_S T_{\text{pippier}})(S_y P_x - S_x P_y) + (\cos W_S T_{\text{pippier}})(S_x P_x + S_y P_y) = -S_z P_z \quad (E-8)$$

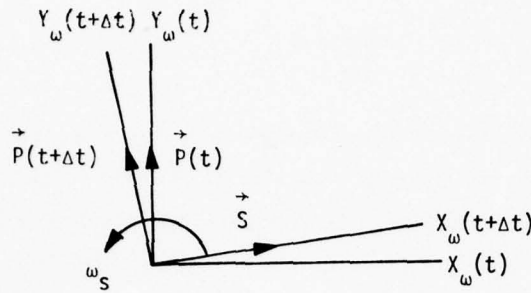


Figure E-8. Sun Vector Rotation

which has the form

$$\sin \theta B + \cos \theta A = -K$$

Equation (E-8) can be reduced by trigonometry identities to

$$\begin{aligned} \sin(W_S T_{\text{pipper}} + \phi) &= \frac{-S_z P_z}{(S_x^2 P_x^2 + S_y^2 P_y^2 + S_y^2 P_x^2 + S_x^2 P_y^2)^{\frac{1}{2}}} \\ &= \frac{-S_z P_z}{\sqrt{(1-S_z^2)(1-P_z^2)}} \end{aligned}$$

where

$$\phi = \sin^{-1} \frac{S_x P_x + S_y P_y}{\sqrt{(1-S_z^2)(1-P_z^2)}}$$

Then,

$$T_{\text{pipper}} = \left[\sin^{-1} \left(\frac{-S_z P_z}{\sqrt{(1-S_z^2)(1-P_z^2)}} \right) - \sin^{-1} \left(\frac{S_x P_x + S_y P_y}{\sqrt{(1-S_z^2)(1-P_z^2)}} \right) \right] \frac{1}{W_S} \quad (\text{E-9})$$

Examining the second term, we see that the opposite sign is needed so that, for positive spin rate and P_x , P_y , S_x , S_y positive, the time T_{pipper} will be positive for the time required for the sensor to rotate so that the sun vector is perpendicular to the plane normal \bar{P} (Figure E-9). Examining the first term, we see also that the sign is wrong because the sensor must be rotated farther to cross the sun vector when S_z and P_z are of the same sign than when they are either zero or of opposite signs (Figure E-9). Thus,

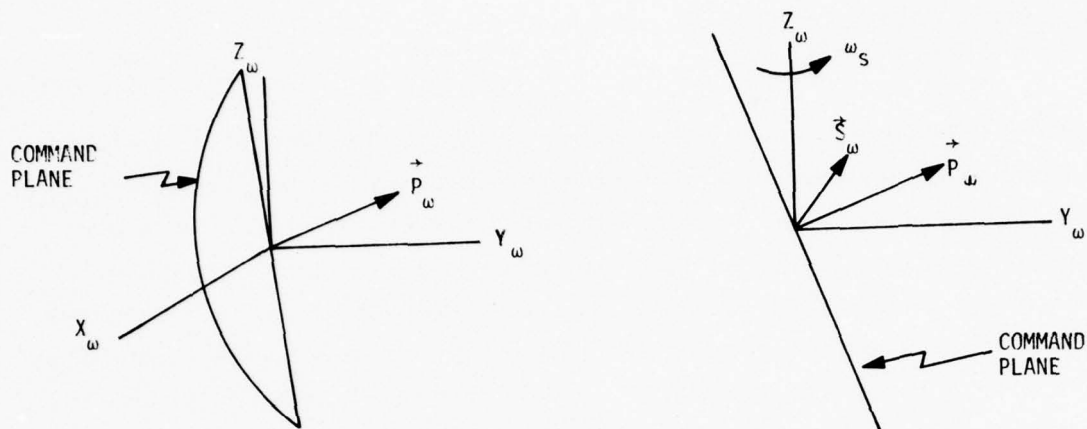


Figure E-9. Sun Vector Sensor Geometry

$$T_{\text{pipper}} = \frac{1}{W_S} \left[\sin^{-1} \left(\frac{S_z P_z}{\sqrt{(1-S_z^2)(1-P_z^2)}} \right) + \sin^{-1} \left(\frac{S_x P_x + S_y P_y}{\sqrt{(1-S_z^2)(1-P_z^2)}} \right) \right] \quad (\text{E-10})$$

Because the sensor frame is not aligned to the spin frame, the measured θ is recomputed for the sun vector in the sensor frame at T_{pipper} . Equation (E-10) is then iterated with \bar{P} based on the new value of θ . This iterative process can be repeated until the T_{pipper} and/or θ converge to acceptable tolerances or for a maximum number of iterations.

If $T_{\text{pipper}} > T_{\text{samp}}$, the pipper command will occur following the next sampling. If $T_{\text{pipper}} < 0$, the pipper command has already occurred in a previous sample period.

There is also a random error which must be added to T_{pipper} . It is the 3 arc minute repeatability of the pipper command at $\theta=0$. This repeatability is assumed to be the same for repeated passes through any angle θ . The random time error will be modeled by a nominally distributed random number representing the uncertainty in the time of the pipper pulse. The 1 sigma value of this time uncertainty is

$$\sigma t_{\text{rand}} = \frac{1/20}{57.3} \frac{1}{W_S} \text{ sec}$$

If the spin rate is variable, a random number generator which has a variable standard deviation will be needed.

SIMULATION ACCURACY WITH ASSUMPTION OF QUASI-STATIONARY SPIN AXIS

The GPS SSS is designed to operate in the spin rate range of 5 to 100 rpm. To model the sun crossing pippier pulse time but maintain a relatively long sample period T_{SAMP} , it is necessary to predict the time within the sample period during which the pippier pulse occurs. It is assumed that the rate of change of the spin vector orientation is sufficiently small (less than $.01 \text{ deg}/T_{\text{SAMP}}$) so that the angular motion of the sensor with respect to the sun vector can be approximated by the angular motion about the spin axis location at the last sample instant. Then the prediction of pippier pulse time is a straightforward computation from the spin rate and the sun vector in the spin frame at the last sample instant. If the spin vector orientation will be changing faster than $.01 \text{ deg}/T_{\text{SAMP}}$, then the model needs to be changed to use an iterative method or to extrapolate the sun vector to the spin frame at the instant of pippier crossing.

The maximum spin axis orientation rate according to the Reference E-3 precession control mode is $.136 \text{ deg per jet firing}$. The duration of firing is $.111 \text{ sec}$ and firing occurs once per revolution. Since the precession equations are derived from

$$\dot{\bar{T}} = \frac{\delta \bar{H}}{\delta t} + \bar{W} \times \bar{H}$$

or

$$\bar{T} \approx \bar{W} \times \hat{h}k$$

$$T_x = W_y h$$

$$T_y = -W_x h$$

the jet torque causes rate rather than acceleration. The precession rate will be $.136 \text{ deg}/.111 \text{ sec} = 1.66 \text{ deg/sec}$.

This rate of change of the spin axis orientation does not occur as a continuous function, but the rate is present for about 60 deg out of each rotation. With a sampling period of $.005 \text{ sec}$, the error in spin axis orientation knowledge at the predicted pippier pulse time would be about $.008 \text{ deg}$ in the worst case. Worst case will occur when the pippier pulse occurs at the end of the sample interval. This will be an error of $.008 \text{ deg}$ in the aspect angle measurement with negligible error in the pippier pulse time.

REFERENCES

- E-1. Procurement Specification, Spin Sun Sensor, No. MC 432-0216, January 8, 1975.
- E-2. Prime Item Development Specification for the Attitude, Velocity, and Control Subsystem of the NAVSTAR Global Positioning System Phase I, No. CID-SV-103, Part 1 of 2, October 4, 1974.
- E-3. Viewgraphs on the AVCS from PDR at Rockwell, November 1974.
- E-4. Preliminary Design Review Data Package, Spin Sun Sensor, No. MC 432-0216, Adcole Corporation, March 31, 1975.

APPENDIX F

REACTION JET MODEL FOR GPS INDEPENDENT ANALYSIS

APPENDIX F

REACTION JET MODEL FOR GPS INDEPENDENT ANALYSIS

This appendix presents the model for the GPS reaction jets. This model is based on the model used in the 3XATS simulation. Both ATS and GPS use Rocket Research Corporation monopropellant hydrazine thrusters. Any data that was not available from Rockwell was extracted from ATS documents.

MODEL DESCRIPTION

The model consists of an initialization section and a normal operation section. The initialization section performs one-time computations and clears outputs and counters. The normal operation section receives jet commands from the controller and outputs total jet force and total jet torque on the spacecraft. The following are system characteristics included in the model:

- Thrust increases with catalyst temperature which increases when the jet is firing and decreases when the jet is not firing. The time constant for heating is less than that for cooling.
- No thrust is developed if the jet command is less than the minimum on time.
- Thrust start and stop times lag the jet command start and stop times due to valve response time and hydrazine burn response.
- Eighteen thrusters are used.
- Thruster torque depends on variable spacecraft cg location.

The following are jet system characteristics not included in the model:

- Dynamics of the thrust rise at turn-on and thrust decay at turn-off must be considered because of the impact on computer run time. The static model will be adequate for all but difficult limit cycle cases. These limit cycle cases should be studied using a single-axis simulation and correlated with static model results. A dynamic model can be provided if necessary.

- Changes in thrust due to supply pressure reduction with fuel consumption is not modeled. The supply pressure changes will be very slow. Stability should be analyzed with both high and low supply pressure by changing the thrust level initialization inputs.
- Dynamic changes in thruster position and angular alignment are not considered. The spacecraft is very stiff. Cases of extreme position and angular alignment should be run.

The jet model flow diagram is shown in Figure F-1. The left arrow (\leftarrow) within boxes indicates replacement, i. e., the expression on the right replaces the variable on the left. Mathematical subscripts are used. Symbols used in the flow diagram are defined in the sections below. Comments appear outside the boxes to describe the operations within the boxes.

INITIALIZATION DATA

Table F-1 lists the initialization parameters, nominal values, tolerance, and source of data. This data is to be input at the start of each run.

INPUT AND OUTPUT DATA

Table F-2 lists the input data that the jet model expects from the calling program each time the jet subroutine is executed in the normal mode.

Table F-3 lists the output data from the jet model subroutine. Other subroutine variables may be outputs if the user desires.

INTERNAL VARIABLES

Internal variables used in the flow diagram are defined in Table F-4.

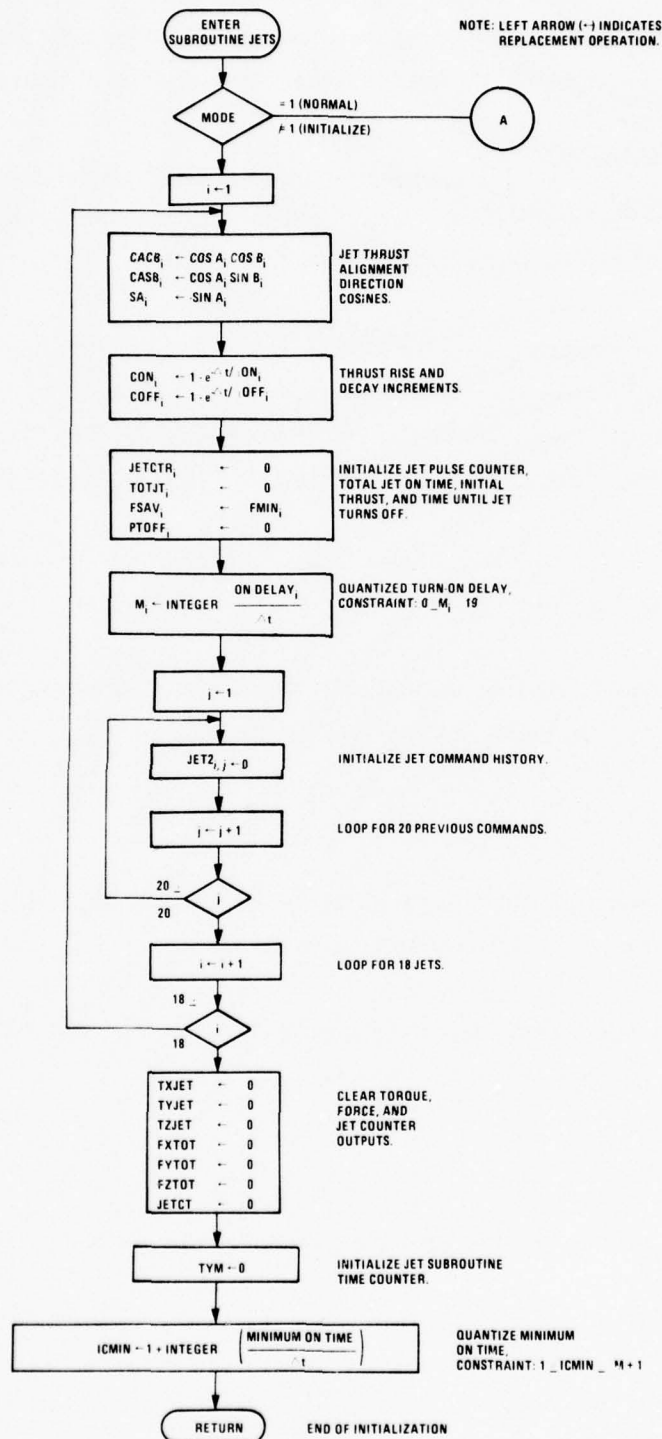


Figure F-1. Flow Diagram of Reaction Jet Model

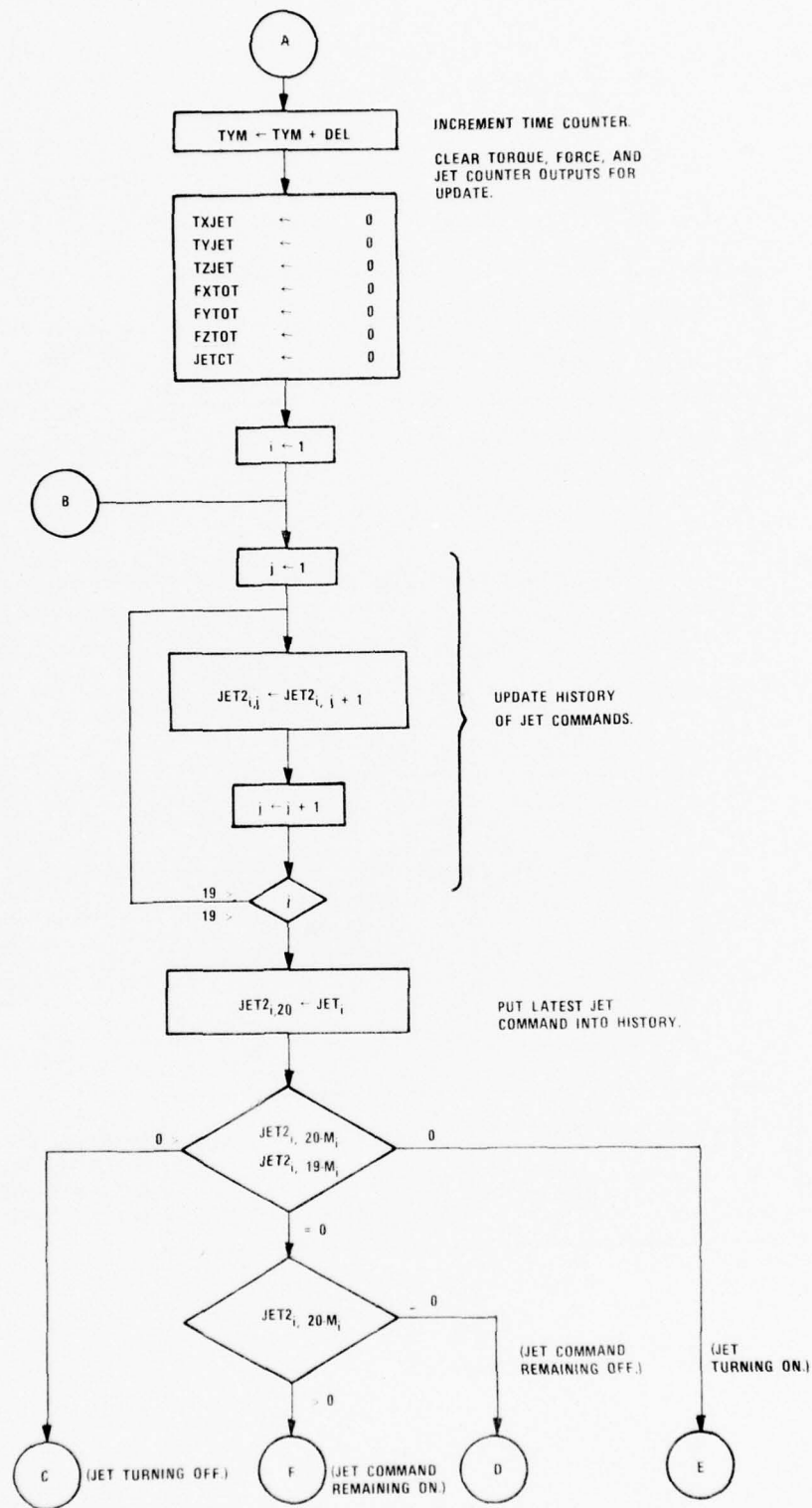


Figure F-1. Flow Diagram of Reaction Jet Model (continued)

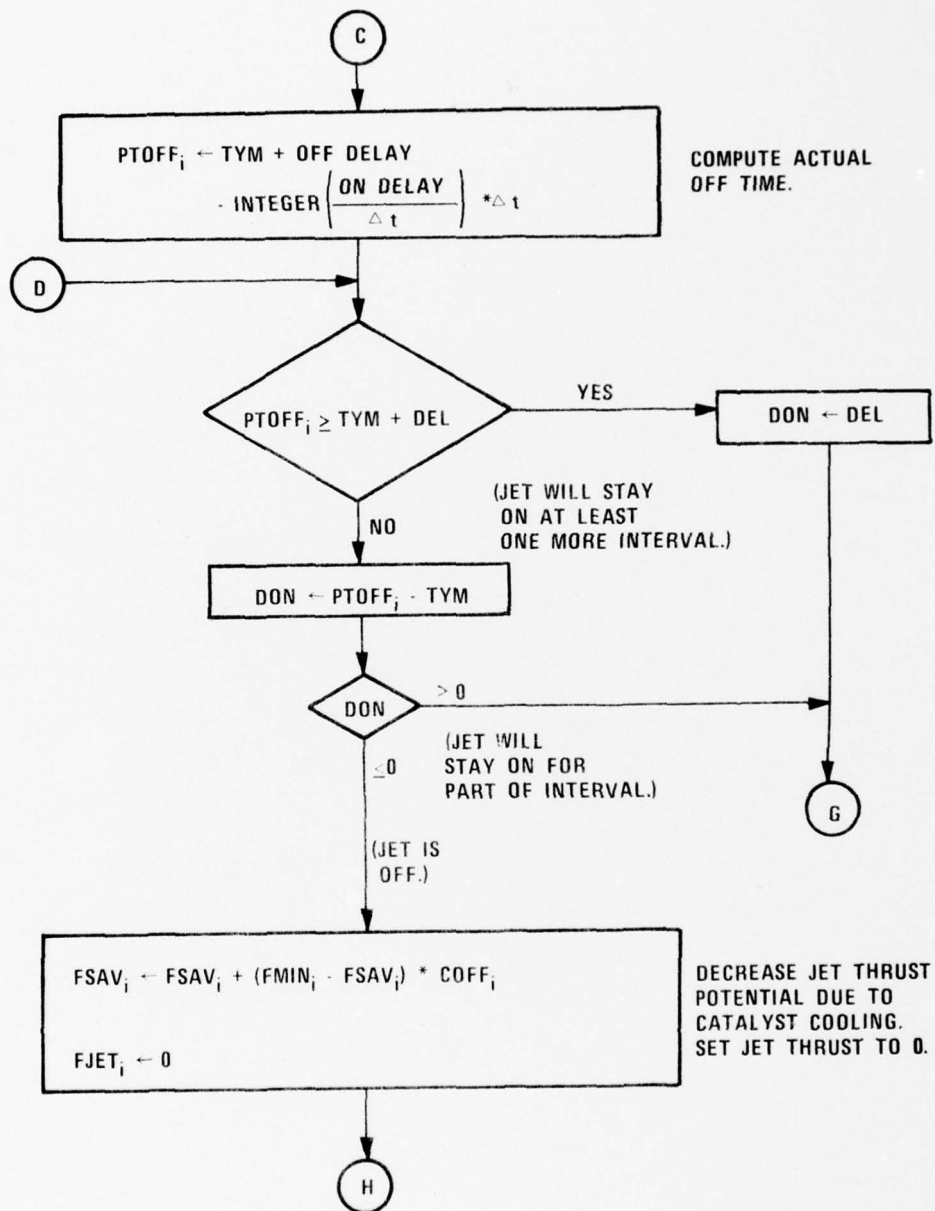


Figure F-1. Flow Diagram of Reaction Jet Model (continued)

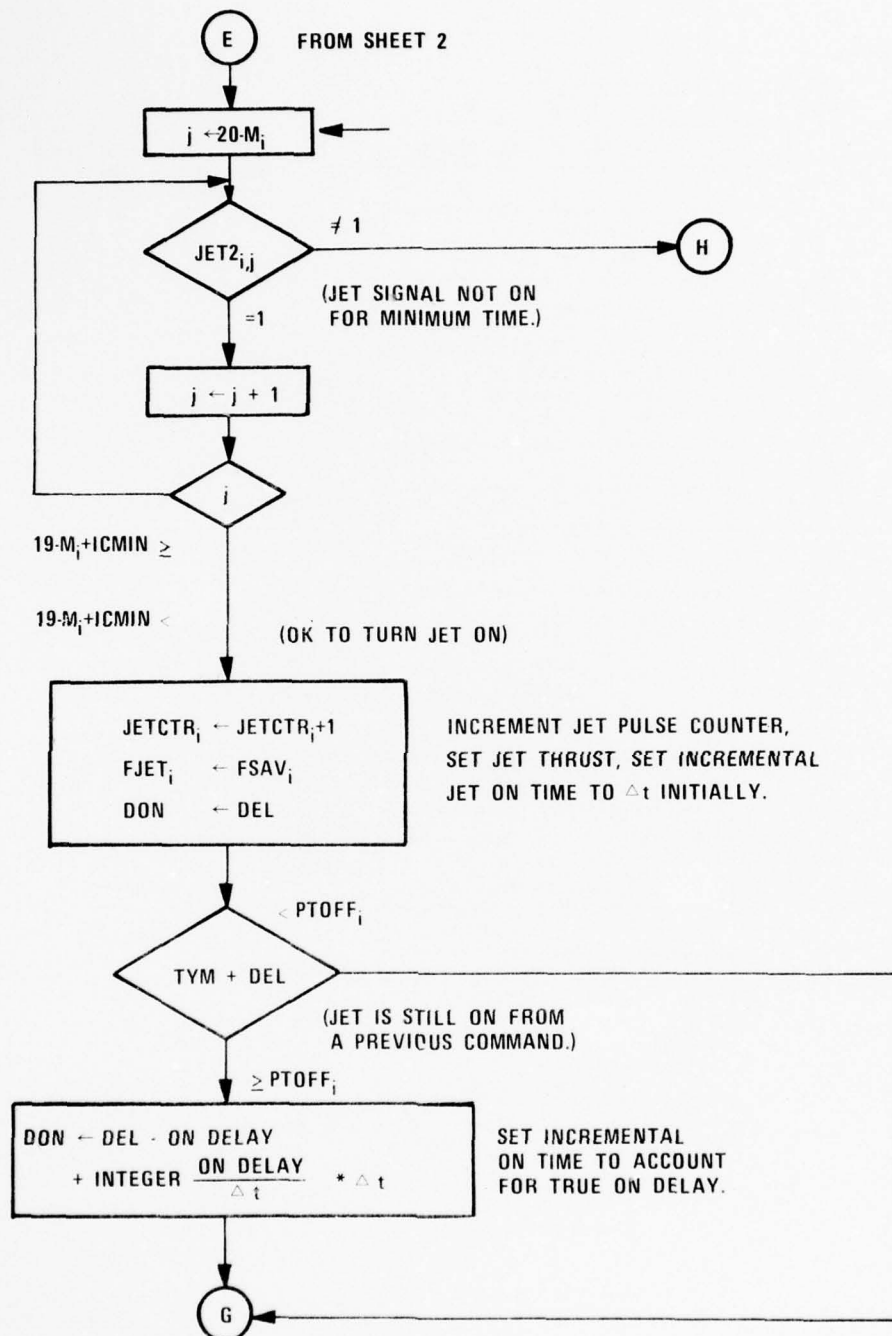


Figure F-1. Flow Diagram of Reaction Jet Model (continued)

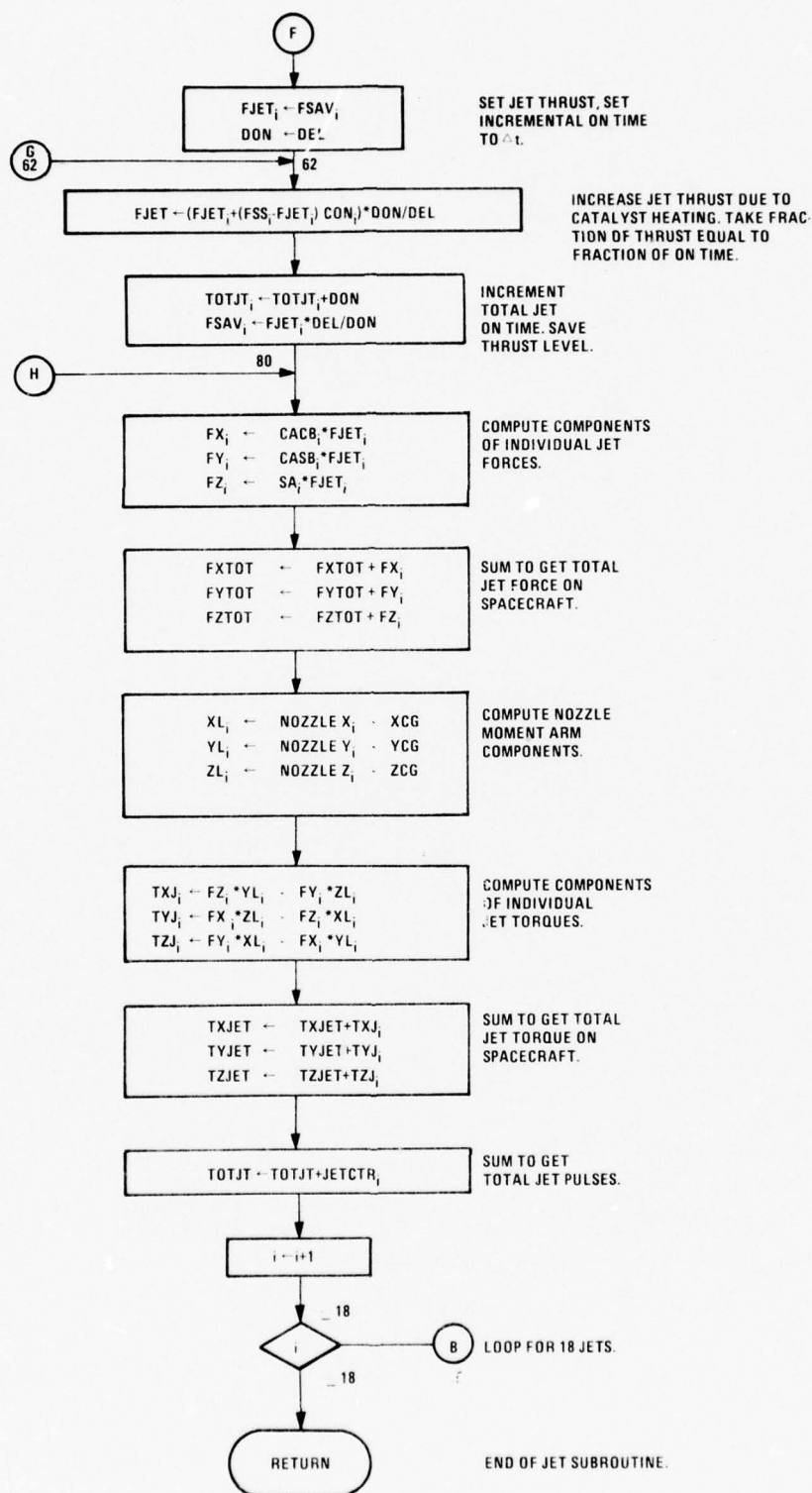


Figure F-1. Flow Diagram of Reaction Jet Model (concluded)

TABLE F-1. INITIALIZATION DATA FOR JET MODEL

Parameter	Subscript	Units	Nominal Value	Source	Tolerance	Source
Nozzle X coordinate	1	feet	2.833	Note 1	Not available	None
	2		2.833			
	3		2.833			
	4		2.833			
	5		-2.833			
	6		-2.833			
	7		-2.833			
	8		-2.833			
	9		2.667			
	10		2.667			
	11		2.667			
	12		2.667			
	13		-2.667			
	14		-2.667			
	15		-2.667			
	16		-2.667			
	17		2.817			
	18		-2.817			
Nozzle Y coordinate	1	feet	-0.417	Note 1	Not available	None
	2		0.417			
	3		0.417			
	4		-0.417			
	5		-0.417			
	6		0.417			
	7		-0.417			
	8		0.417			
	9		-0.708			
	10		-0.708			
	11		0.708			
	12		0.708			
	13		-0.708			
	14		-0.708			
	15		0.708			
	16		0.708			
	17		0			
	18		0			

Notes:

1. Scaled from Rockwell drawing V505-900003, Rev. C, 1+27-75.
2. Rockwell GPS PDR handout.
3. Coordination meeting notes, 3/20/75.
4. Rockwell Specification MC 321-0009, 10/24/74.
5. Rockwell Specification MC 321-0011, 10/24/74.
6. GPS 0.1 LBF REA, Qualification Test Report, CDRL Item A005, March 31, 1976.
7. GPS 5.0 LBF REA, Qualification Test Report, CDRL Item A005, March 31, 1976.
8. Pairs match to $\pm 5\%$, 3σ . Pairs are 9 and 14, 10 and 13, 12 and 15, 11 and 16, 3 and 6, 4 and 5, 1 and 7, 2 and 8, 6 and 7, 2 and 4, 1 and 3, 5 and 8, 9 and 15, 10 and 16, 12 and 14, 11 and 13.

TABLE F-1. INITIALIZATION DATA FOR JET MODEL (continued)

Parameter	Subscript	Units	Nominal Value	Source	Tolerance	Source
Nozzle Z coordinate	1	feet	-0.458	Note 1	Not available	None
	2		-0.458			
	3		0.458			
	4		0.458			
	5		-0.458			
	6		-0.458			
	7		0.458			
	8		0.458			
	9		-0.175			
	10		0.175			
	11		-0.175			
	12		0.175			
	13		-0.175			
	14		0.175			
	15		-0.175			
	16		0.175			
	17		0.567			
	18		-0.567			
Jet alignment A (rotation from \hat{X}_A about \hat{Y})	1	deg	270	Note 2	+2, 3 σ	Note 3
	2		270			
	3		90			
	4		90			
	5		270			
	6		270			
	7		90			
	8		90			
	9		0			
	10		0			
	11		0			
	12		0			
	13		0			
	14		0			
	15		0			
	16		0			
	17		90			
	18		270			
Jet alignment B (rotation from \hat{X}_B about \hat{Z})	1	deg	0	Note 2	+2, 3 σ	Note 3
	2		0			
	3		0			
	4		0			
	5		0			
	6		0			
	7		0			
	8		0			
	9		90			
	10		90			
	11		270			
	12		270			
	13		90			
	14		90			
	15		270			
	16		270			
	17		0			
	18		0			

TABLE F-1. INITIALIZATION DATA FOR JET MODEL (continued)

Parameter	Subscript	Units	Nominal Value	Source	Tolerance	Source
Jet thrust at 204°C catalyst, FMIN	1	lbs	0.09	Notes 6 and 7	$\pm 10\%$, 3σ	Notes 4 and 8
	2		0.09			
	3		0.09			
	4		0.09			
	5		0.09			
	6		0.09			
	7		0.09			
	8		0.09			
	9		0.09			
	10		0.09			
	11		0.09			
	12		0.09			
	13		0.09			
	14		0.09			
	15		0.09			
	16		0.09			
Jet thrust at 35°C catalyst, FMIN	17		4.0			
	18		4.0			
Jet thrust at highest catalyst temperature, FSS	1	lbs	0.1	Notes 6 and 7	Not available	None
	2		0.1			
	3		0.1			
	4		0.1			
	5		0.1			
	6		0.1			
	7		0.1			
	8		0.1			
	9		0.1			
	10		0.1			
	11		0.1			
	12		0.1			
	13		0.1			
	14		0.1			
	15		0.1			
	16		0.1			
	17		5.0			
	18		5.0			
Thrust rise time constant, τ_{ON}	1	sec	0.4	Notes 6 and 7	Not available	None
	2		0.4			
	3		0.4			
	.		.			
	.		.			
	18		0.4			
Thrust decay time constant, τ_{OFF}	1	sec	0.0	Notes 6 and 7	Not available	None
	2		0.0			
	3		0.0			
	.		.			
	.		.			
	18		0.0			

TABLE F-1. INITIALIZATION DATA FOR JET MODEL (concluded)

Parameter	Subscript	Units	Nominal Value	Source	Tolerance	Source
Jet on delay	1	sec	0.025	Notes 6 and 7	Not available	None
	2		0.025			
	3		0.025			
	.		.			
	.		.			
Jet off delay	18	sec	0.025	Notes 6 and 7	Not available	None
	1		0.075			
	2		0.075			
	3		0.075			
	.		.			
Minimum on time	18	sec	0.075	Notes 4 and 5	Not available	None
	--		0.05			

TABLE F-2. INPUT DATA FOR JET MODEL

Definition	Flow Diagram Symbol	Dimension	Type	Units
Mode control flag	Mode	18	Integer	
Jet command from controller (Subscript is jet number)	Jet		Integer	
Spacecraft cg X coordinate	XCG		Real	
Spacecraft cg Y coordinate	YCG		Real	
Spacecraft cg Z coordinate	ZCG		Real	

1 = Normal

1 = On
0 = Off

TABLE F-3. OUTPUT DATA FOR JET MODEL

Definition	Flow Diagram Symbol	Dimension	Type	Units
Total number of jet operations	JETCT		Integer	
Number of operations for each jet	JETCTR	18	Integer	
Accumulated on time for each jet	TOTJT	18	Real	Seconds
X component of total jet force on spacecraft	FXTOT		Real	Pounds
Y component of total jet force on spacecraft	FYTOT		Real	Pounds
Z component of total jet force on spacecraft	FZTOT		Real	Pounds
Total jet torque about X axis	TXJET		Real	Foot pounds
Total jet torque about Y axis	TYJET		Real	Foot pounds
Total jet torque about Z axis	TZJET		Real	Foot pounds

TABLE F-4. INTERNAL VARIABLES FOR JET MODEL

Definition	Flow Diagram Symbol	Dimension	Type	Units
Thrust direction cosine	CACB	18	Real	---
Thrust direction cosine	CASB	18	Real	---
Thrust direction cosine	SA	18	Real	---
Thrust rise increment	CON	18	Real	---
Thrust decay increment	COFF	18	Real	---
Potential jet thrust from previous cycle	FSAV	18	Real	Pounds
Predicted time for jet thrust to go off	PTOFF	18	Real	Seconds
Quantized on delay	M	18	Integer	Cycles
History of jet commands	JET2	18 x 20	Integer	---
Time since start of run	TYM		Double precision	Seconds
Quantized minimum on time	ICMIN		Integer	Cycles
Incremental jet on time	DON		Real	Seconds
Actual jet thrust	FJET	18	Real	Pounds
X component of jet force	FX	18	Real	Pounds
Y component of jet force	FY	18	Real	Pounds
Z component of jet force	FZ	18	Real	Pounds
X component of nozzle moment arm	XL	18	Real	Feet
Y component of nozzle moment arm	YL	18	Real	Feet
Z component of nozzle moment arm	ZL	18	Real	Feet
X component of jet torque	TXJ	18	Real	Foot pounds
Y component of jet torque	TYJ	18	Real	Foot pounds
Z component of jet torque	TZJ	18	Real	Foot pounds
Jet index	i		Integer	
General index	j		Integer	

APPENDIX G

GPS DEPLOYMENT MODEL

APPENDIX G

GPS DEPLOYMENT MODEL

The following equations will be used for simulation of the GPS rotational dynamics during deployment. These equations will be incorporated in the one-body simulation to investigate the effect of deployment on the pitch and roll jet channels.

The following primary assumptions were made in developing these equations:

1. Panels are treated as point masses.
2. Mass of the boom is neglected.
3. A "linear" deployment linkage is assumed.

ROTATIONAL DYNAMICS

Referring to Figure G-1 and Appendix C for notation, the angular momentum during deployment is given by

$$\bar{H} = \bar{I}_O \omega_O + \sum_i m_i (\bar{r}_O + \bar{r}_i + \bar{\rho}_i) \times \dot{\bar{\rho}}_i \quad (G-1)$$

where

$$I_O = J_O - mM(r_O, r_O) + \sum_i m_i M(r_i + \rho_i, r_i + \rho_i) \quad (G-2)$$

The rotational differential equations of motion are given by

$$T = I_O \dot{\omega}_O + \dot{I}_O \omega_O + \sum_i m_i (\dot{\bar{r}}_O \times \dot{\bar{\rho}}_i) + \sum_i m_i (r_O + r_i + \rho_i) \times \ddot{\bar{\rho}}_i + \omega_O \times H \quad (G-3)$$

The deployment linkage, Figure G-2, is such that $\beta \cong 2\alpha$. With this linear relationship, derivatives appearing in Equations (G-1) through (G-3) can be evaluated as follows:

$$\rho_i = \begin{Bmatrix} 0 \\ (-1)^i (a + b) \sin \alpha_i \\ (b - a) \cos \alpha_i \end{Bmatrix}$$

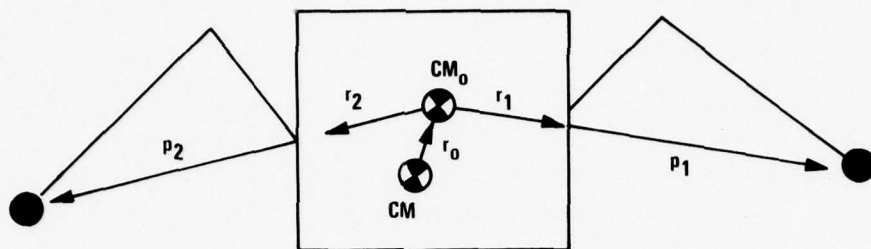


Figure G-1. Notation for Deployment Model

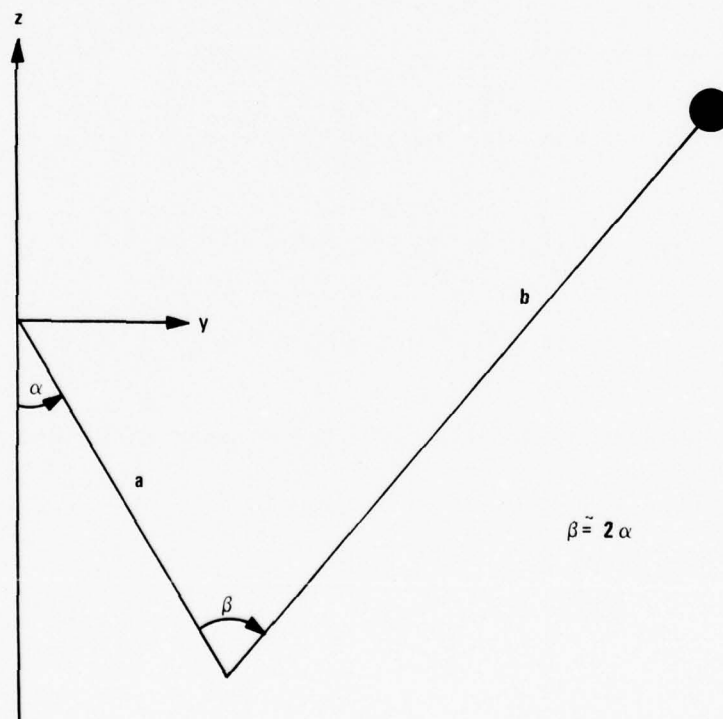


Figure G-2. Deployment Mechanism Linkage Model

$$\dot{\rho}_i = \begin{Bmatrix} 0 \\ (-1)^i (a+b) \cos \alpha_i \dot{\alpha}_i \\ (a-b) \sin \alpha_i \dot{\alpha}_i \end{Bmatrix}$$

$$\ddot{\rho}_i = \begin{Bmatrix} 0 \\ (-1)^i [(a+b) \cos \alpha_i \ddot{\alpha}_i - (a+b) \sin \alpha_i \dot{\alpha}_i^2] \\ (a-b) \sin \alpha_i \ddot{\alpha}_i + (a-b) \cos \alpha_i \dot{\alpha}_i^2 \end{Bmatrix}$$

$$\mathbf{r}_O = -\sum_i \frac{m_i}{m} (\mathbf{r}_i + \rho_i)$$

$$\dot{\mathbf{r}}_O = -\sum_i \frac{m_i}{m} \dot{\rho}_i$$

$$\ddot{\mathbf{r}}_O = -\sum_i \frac{m_i}{m} \ddot{\rho}_i$$

$$\dot{\mathbf{i}}_O = -m[M(\dot{\mathbf{r}}_O, \mathbf{r}_O) + M^T(\dot{\mathbf{r}}_O, \mathbf{r}_O)] + \sum_i m_i [M(\dot{\rho}_i, \mathbf{r}_i + \rho_i) + M^T(\dot{\rho}_i, \mathbf{r}_i + \rho_i)]$$

The hinge torques are given by

$$\overline{T}_{Di} = \bar{\rho}_i \times m_i \frac{d^2 \bar{R}_i}{dt^2} = \bar{\rho}_i \times \frac{d^2}{dt^2} (\bar{\mathbf{r}}_O + \bar{\mathbf{r}}_i + \bar{\rho}_i) + \bar{\rho}_i \times m_i \bar{a}_{cm}$$

$$T_{Di} = \rho_i \times [\ddot{\mathbf{r}}_O + \ddot{\rho}_i + \dot{\omega}_O \times (\mathbf{r}_O + \mathbf{r}_i + \rho_i) + 2\omega_O \times (\dot{\mathbf{r}}_O + \dot{\rho}_i)]$$

$$+ \omega_O \times \omega_O \times (\mathbf{r}_O + \mathbf{r}_i + \rho_i)] + \rho_i \times a_{cm}$$

The hinge torques are produced by spring forces which will be modeled as

$$T_{Di} \cdot \begin{Bmatrix} 1 \\ 0 \\ 0 \end{Bmatrix} = d_{oi} + d_{1i} \alpha_i + d_{2i} \dot{\alpha}_i$$

APPENDIX H

SOLAR PRESSURE TORQUE AND FORCE MODEL

APPENDIX H

SOLAR PRESSURE TORQUE AND FORCE MODEL

This appendix summarizes the preliminary solar pressure force and torque model developed for the digital simulation evaluation of GPS stability and control analysis.

The solar force results from the photo momentum transfer to the vehicle surfaces exposed to solar illumination. The magnitude and direction of the solar force developed on a given vehicle surface are functions of the vehicle-sun attitude, the geometry of the surface, and the physical characteristics of the surface. The solar torque will be developed if the vehicle center of mass is not coincident with the center of total net force.

The model described in this appendix was based on the vehicle geometrical configurations deduced from the Rockwell drawing No. V505-900003 titled "Spacecraft General Arrangement Baseline Configuration - GPS," January 27, 1975.

VEHICLE GEOMETRY FOR SOLAR TORQUE EVALUATION

The GPS spacecraft configuration has been approximated by surfaces of simple geometry to facilitate the evaluation of solar force and torque. This simplified geometry consists of five flat surfaces, six cylindrical surfaces, one segment of a cone, and fourteen complete cylindrical surfaces for the representation of vehicle main body, solar panels, thruster cone, and antenna in on-orbit configuration. The stowed vehicle during the spinning phase is approximated by a complete cylindrical surface. The geometries of the simplified vehicle configurations are shown in Figure H-1.

Total solar pressure force and torque experienced by the vehicle can be evaluated as the vector sum of the forces and torques exerted on the approximating surfaces. Nominal geometries including size, location, and orientation of the surfaces for the GPS vehicle are summarized in a later section of this appendix. These data are based on the Rockwell drawing No. V505-900003 titled "Spacecraft General Arrangement Baseline Configuration - GPS," January 27, 1975. The computations involved in the evaluation of the force and torque contributed by these elementary surfaces are described in the sections that follow.

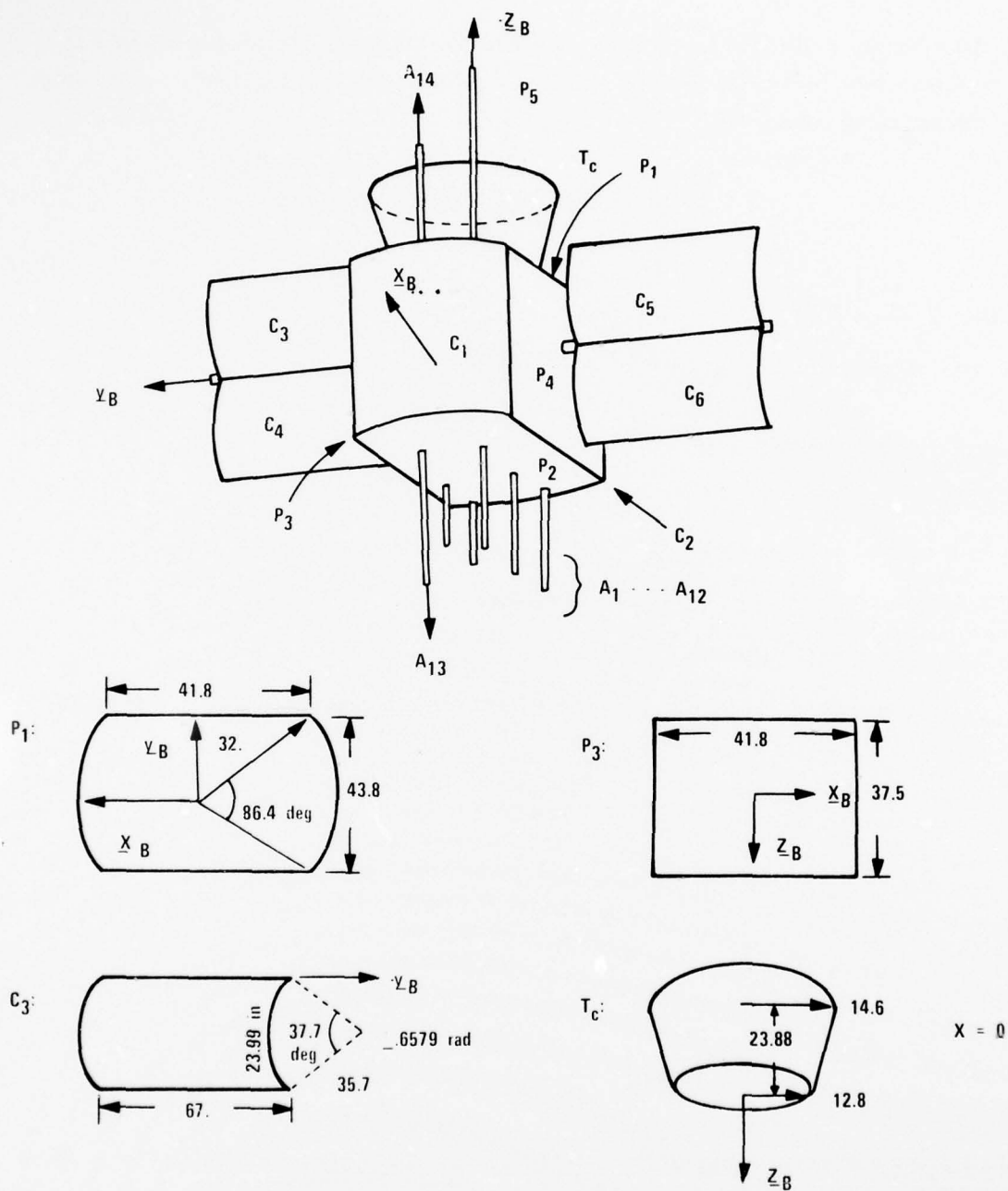


Figure H-1. Simplified GPS Geometry and B-Frame Definition

Solar Pressure on Flat Surface

A flat surface, defined in terms of the surface normal \underline{N} and geometrical center \underline{C} , develops a solar pressure force \underline{F} and torque $\underline{\tau}$ about vehicle center of mass as given in the following equations:

$$\underline{F} = -F_n \underline{N} + F_t [(\underline{N} \cdot \underline{S}) \underline{N} - \underline{S}] / |(\underline{N} \cdot \underline{S}) \underline{N} - \underline{S}| \quad (\text{H-1})$$

$$\underline{\tau} = \underline{C} \times \underline{F} \quad (\text{H-2})$$

where

\underline{S} = LOS vector to sun

$$F_n = [(1 + s\rho) \cos^2 \psi + \frac{2}{3} \rho (1 - s) \cos \psi] \text{ PA}$$

$$F_t = [(1 - s\rho) \cos \psi \sin \psi] \text{ PA}$$

$$P = \text{solar pressure} = 1 \times 10^{-7} \text{ lb/ft}^2$$

ρ = fraction of incident radiation reflected

s = fraction of reflected radiation that is specular

\underline{C} = position vector of surface geometrical center from vehicle center of mass

$$\cos \psi = (\underline{N} \cdot \underline{S})$$

Note that, for the case $\underline{N} = \underline{S}$,

$$|(\underline{N} \cdot \underline{S}) \underline{N} - \underline{S}| = 0$$

This portion of computation in Equation (H-1) should be bypassed. This is when there is no tangential force.

Solar Force on Cylindrical Surfaces

From the geometry of Figure H-2, the location, orientation and size of a cylindrical surface can be completely specified in terms of the following parameters:

\underline{C} = position vector of the geometrical center of the surface

\underline{N} = normal vector at \underline{C} (orientation)

\underline{T} = tangent vector at \underline{C} (orientation)

r = radius of the cylinder (size)

θ_o = angular width of the cylinder (size)

l = length of the cylinder (size)

The evaluation of solar force on a cylindrical surface can be carried out by the subdivision into n flat surface elements as shown in Figure H-3. The i^{th} flat surface element is defined in terms of the location of its geometrical center \underline{C}_i and the normal vector \underline{N}_i which are related to the cylinder parameters as

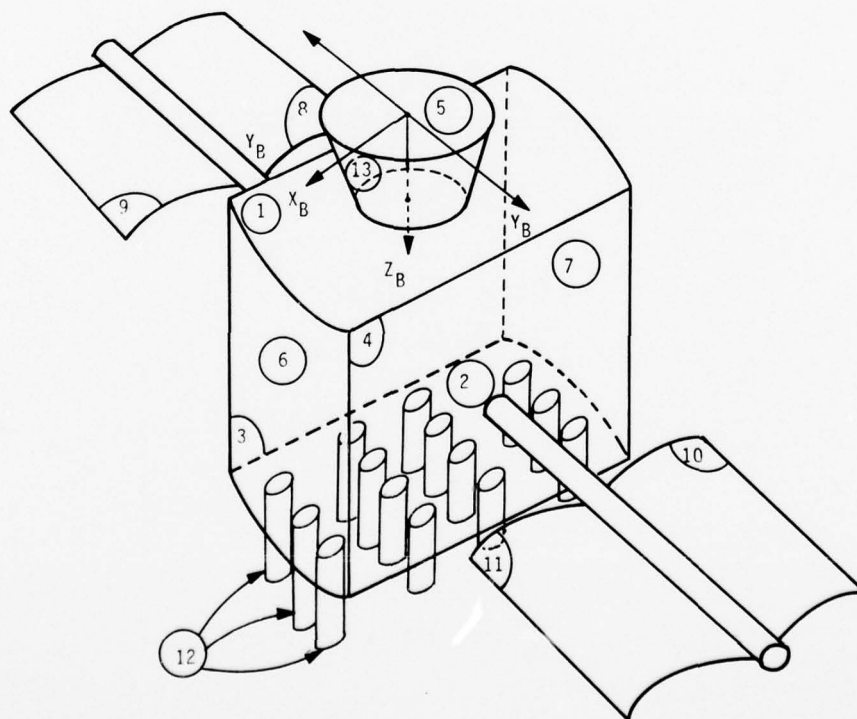


Figure H-2. Surface Numbering Notation

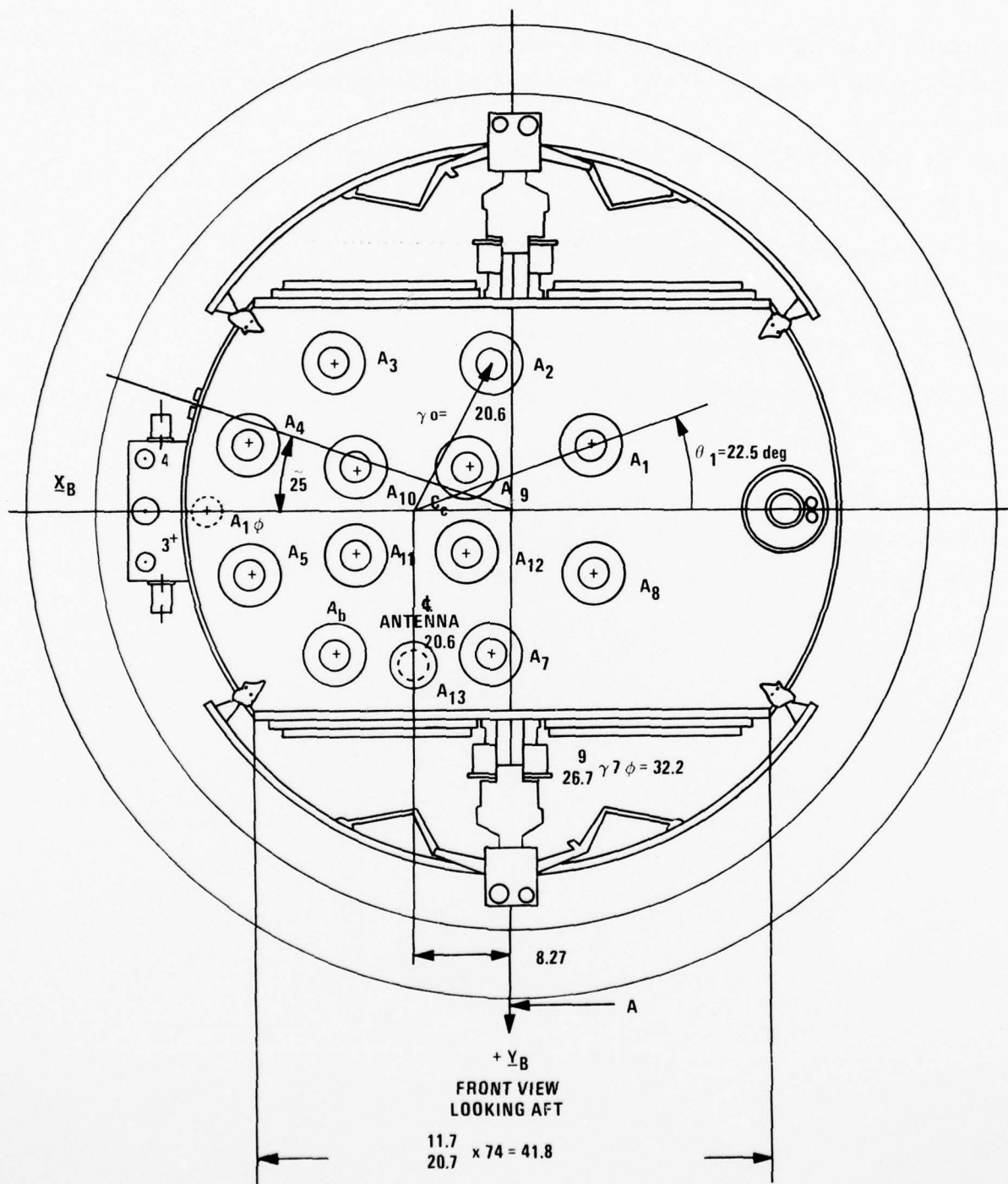


Figure H-3. Definition of Antenna Rods

$$\underline{C}_i = \underline{C} - r\underline{N} + r\underline{N}_i \quad (\text{H-3})$$

$$\underline{N}_i = \cos \theta_i \underline{N} + \sin \theta_i \underline{T} \quad (\text{H-4})$$

where

$$\theta_i = -\theta_0/2 - \Delta/2 + i\Delta, \quad i = 1, 2, \dots, n \quad (\text{H-5})$$

$$\Delta = \theta_0/n$$

The area of i^{th} surface element is

$$A_i = r \cdot \Delta \cdot \ell \quad (\text{H-6})$$

The solar forces and torques developed on these flat surface elements can be computed using Equations (H-1) and (H-2). Let the forces and torques be denoted as \underline{F}_i and $\underline{\tau}_i$.

The total force and torque developed by the cylindrical surface are \underline{F}_c and $\underline{\tau}_c$ evaluated as

$$\underline{F}_c = \sum_{i=1}^n \underline{F}_i \quad (\text{H-7})$$

$$\underline{\tau}_c = \sum_{i=1}^n \underline{\tau}_i \quad (\text{H-8})$$

For the case of a full cylindrical surface, such as the antenna, the cylinder is defined in terms of following parameters:

\underline{C} = position vector of the center of the cylinder from vehicle center of mass

\underline{L} = unit vector along the cylinder axis

r = radius of cylinder

ℓ = length of cylinder

The solar force \underline{F} and torque $\underline{\tau}$ about vehicle center of mass become

$$\underline{F} = -F_n \underline{N} - F_t \underline{L} \quad (\text{H-9})$$

$$\underline{\tau} = \underline{D} \times \underline{F} \quad (\text{H-10})$$

where

$$\underline{N} = [\underline{S} - (\underline{S} \cdot \underline{L}) \underline{L}] / |\underline{S} - (\underline{S} \cdot \underline{L}) \underline{L}|$$

$$F_n = [(1 + s\rho/3) \sin^2 \theta + \rho(1 - s)(\pi/6) \sin \theta] \text{ PA}$$

$$F_t = [(1 - s\rho) \sin \theta \cos \theta] PA$$

$$A = \text{projected cylinder area} = 2lr$$

$$\cos \theta = (\underline{S} \cdot \underline{L})$$

$$D = \underline{C} + r\underline{N}$$

Again, the computations associated with $|\underline{S} - (\underline{S} \cdot \underline{L})\underline{L}|$ should be bypassed for $\underline{S} = \underline{L}$. This is when there is no transverse force.

Solar Force on Conic Surface

From the geometry of Figure H-4, the location, orientation, and size of a conic surface can be completely specified in terms of the following parameters:

\underline{N}_c = unit vector along cone axis

r_a = radius of circle on top

r_b = radius of circle on bottom

\underline{o}_a = center of circle on top

h = height of conical surface

The evaluation of the solar force on a conical surface can be carried out through approximations using flat surface elements. Each surface element is a trapezoid which can be represented by a surface normal \underline{N}_i and the location of its geometrical center \underline{C}_i as depicted in Figure H-4. These parameters are related to the defining parameters of the conical surface as

$$\underline{N}_i = \cos \theta_c \cos \alpha_i \underline{X}_c + \cos \theta_c \sin \alpha_i \underline{Y}_c + \sin \theta_c \underline{N}_c \quad (H-11)$$

$$\underline{C}_i = \underline{A}_i + \left[(2r_b + r_1) / (3r_b + 3r_1) \right] [\underline{B}_i - \underline{A}_i] \quad (H-12)$$

where \underline{X}_c and \underline{Y}_c are unit vectors that make $(\underline{X}_c - \underline{Y}_c - \underline{N}_c)$ a right-handed orthogonal triad. For convenience, let

$$\underline{Y}_c = (\underline{N}_c \times \underline{X}_c) / |\underline{N}_c \times \underline{X}_c|, \quad \bar{\underline{X}}_s = -\bar{\underline{Y}}_B = -\bar{\underline{X}}_C$$

$$\alpha_i = i\delta - \delta/2, \quad i = 1, 2, \dots, n$$

$$\delta = \pi/n$$

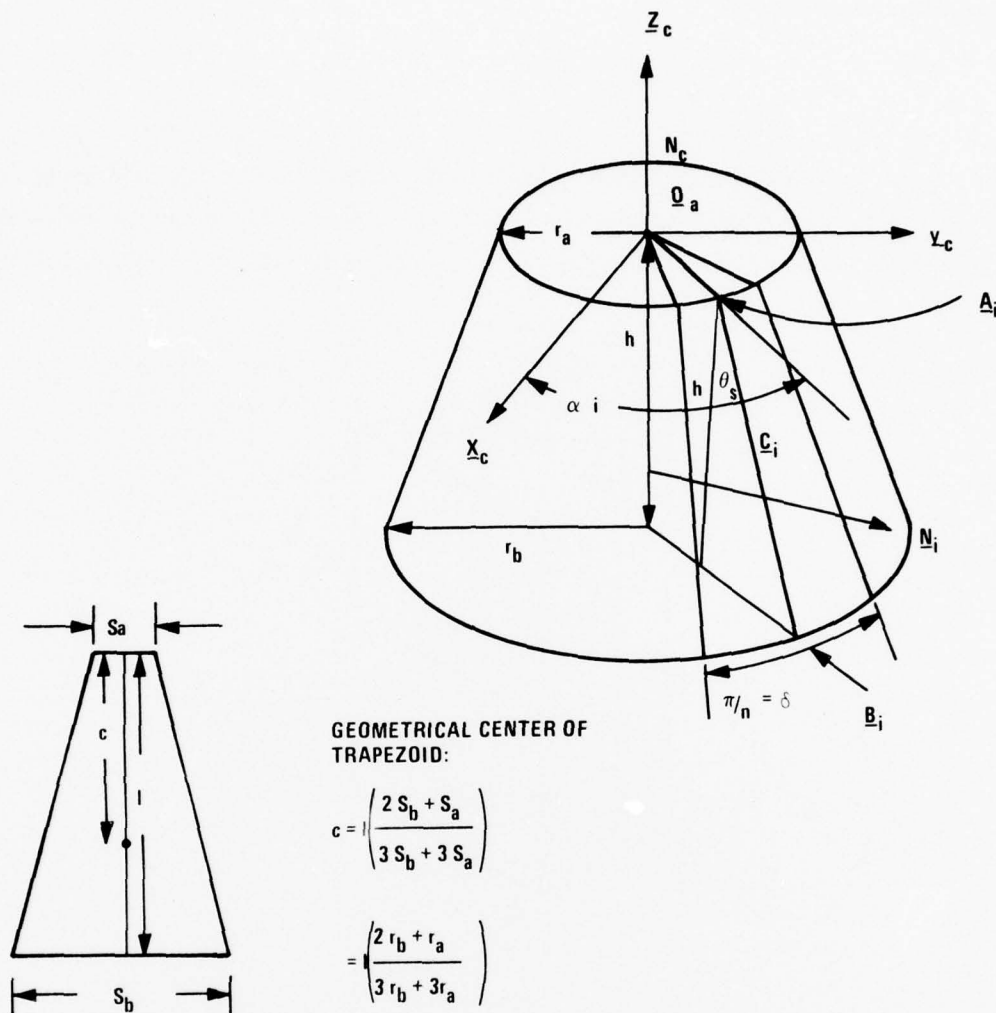


Figure H-4. Geometry of Thruster Cone

$$\underline{A}_i = \underline{O}_a + r_a \cos \alpha_i \underline{X}_c + r_a \sin \alpha_i \underline{Y}_c$$

$$\underline{B}_i = (\underline{O}_a - \ell_1 \underline{N}_c) + r_b \cos \alpha_i \underline{X}_c + r_b \sin \alpha_i \underline{Y}_c$$

$$\theta_c = \tan^{-1} \left((r_b - r_a) / h \right)$$

$$r_1 = r_a + \delta (r_b - r_a) \sqrt{(r_b - r_a)^2 + h^2}$$

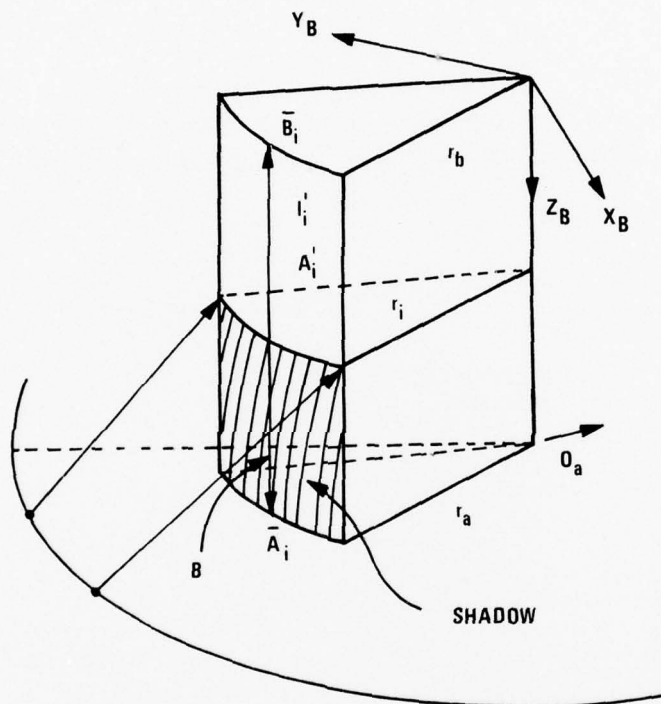
$$\ell_1 = \text{distance between } \underline{A}_i \text{ and } \underline{B}_i$$

$$\ell_1' = \text{distance between } \underline{A}_i' \text{ and } \underline{B}_i'$$

The area of the trapezoid is

$$A_i = \frac{1}{2} (r_1 + r_b) \delta \ell'_1 \quad (\text{H-13})$$

The solar force and torque contributed by each of the trapezoidal surface elements can then be computed using Equations (H-1) and (H-2) with the total force and torque contributed by the thruster cone evaluated in the same manner as Equations (H-7) and (H-8).



Vehicle Nominal Attitude and Shading Considerations

The GPS spacecraft on-orbit attitude is sun and earth oriented. The pitch and roll control allows the vehicle yaw axis to be aligned with local vertical. The vehicle yaw motion is such that the solar array surface normal can be driven to be aligned with sun line for maximum solar exposure. Attitude accuracy requirements are 0.5 deg for roll and pitch and 3 deg for yaw.

In order for the vehicle main body to cast shadow on the solar array, the minimum yaw attitude error must be ψ_s .

$$\psi_s = \tan^{-1}\left(\frac{f}{b/2}\right) \approx \tan^{-1}\left(\frac{12}{23}\right) \approx 27.5 \text{ deg}$$

where

f = clearance between main body and solar array

b = length of main body

Similarly, the main body will not be shaded by the solar array panels. Also, the solar array attitude is driven to within 5 deg of maximum exposure. Hence it can be assumed that the solar array is completely free of shadow. Since the sun vector can be anywhere within the pitch plane, the shading of the thruster cone and the flat surface P_1 interfacing the thruster cone need to be considered. The shading of the antenna is ignored due to the relatively small areas involved.

Shading of Thruster Cone by Surface P_1 --The shading of the thruster cone can be considered in terms of the i^{th} flat surface element described earlier. Referring to the geometry of Figure H-5, the projection of point B_i on the surface P_1 is D_i . Any point located on the surface P_1 satisfies the vector equation

$$(\underline{D}_i - \underline{C}_{P1}) \cdot \underline{N}_{P1} = 0 \quad (\text{H-14})$$

Also, the vector $(\underline{D}_i - \underline{B}_i)$ must be pointed along the sun line, i.e.,

$$(\underline{D}_i - \underline{B}_i) = r\underline{S} \quad (\text{H-15})$$

where r = distance between B_i and D_i . The projection of vector $(B_i - A_i)$ on P_1 along \underline{S} is the vector $(\underline{D}_i - \underline{A}_i)$ which intersects the edge of P_1 at E_i . Hence E_i satisfies the vector equations

$$(\underline{E}_i - \underline{C}_{P1}) \cdot (\underline{E}_i - \underline{C}_{P1}) = r_c^2 \quad (\text{H-16})$$

$$(\underline{E}_i - \underline{A}_i) = t(\underline{D}_i - \underline{A}_i) \quad (\text{H-17})$$

where t = ratio of distance between E_i and A_i to that between D_i and A_i .

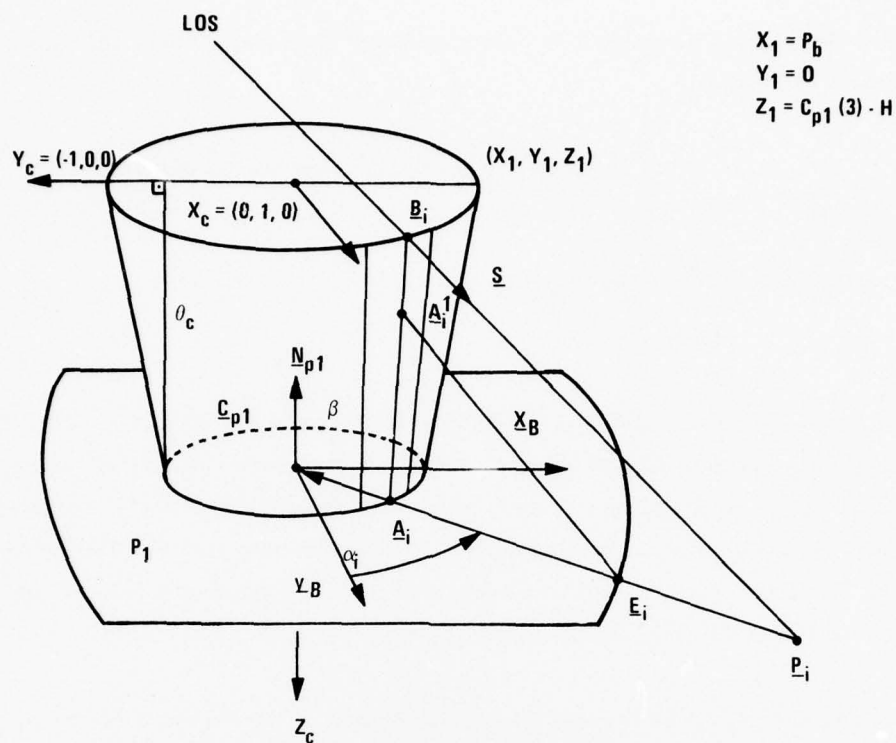


Figure H-5. Shading of Thruster Cone by Plane P_1 Illustrated in Terms of Elementary Surface $A_i \sim B_i$

$$\frac{A_i}{\bar{A}_i} = \frac{A_i}{\bar{A}_i} + (\ell_{AE} / \ell_{AD})(\frac{B_i}{\bar{B}_i} - \frac{A_i}{\bar{A}_i}) \quad (H-18)$$

$$l_{AE} = \text{distance between } \underline{A_i} \text{ and } \underline{E_i}$$

To evaluate the solar force contributed by the unshaded portion of the i^{th} surface element, Equations (H-11), (H-12), and (H-13) can be used with \underline{A}_1 replaced by \underline{A}_1' . It may happen that the entire i^{th} surface element is in the shadow of P_1 . The condition for this situation is that the distance between \underline{C}_{P1} and \underline{D}_i must be less than the radius of surface P_i 's circular edge r_c , i.e.,

$$(\underline{C}_{P1} - \underline{D}_i) \cdot (\underline{C}_{P1} - \underline{D}_i) < r_c^2 \quad (H-19)$$

If the inequality, Equation (H-19), is valid, the computations associated with the i^{th} surface element can be bypassed since it contributes nothing to the total force and torque. Also, it may happen that the entire i^{th} surface element is not shaded by P_1 . This is the case when the sun vector has positive projection along the normal to P_1 , i.e.,

$$\cos \theta_c > (\underline{S} \cdot \underline{N}_{P1}) > 0 \quad (H-20)$$

If the inequality, Equation (H-20), is valid, the point \underline{A}_i is set to be identical to \underline{A}_1 .

Shading of Surface P_1 by Thruster Cone--Since the circle defining the open end of the thruster cone is parallel to the surface P_1 , the projection of this circle on P_1 is always a circle of identical size as shown by the parallelograms of Figure H-6. The geometries of the shadow on surface P_1 for four different sun line configurations are considered for the following discussions. The shadow of thruster cone on P_1 will be characterized as a flat surface of area A_s with normal \underline{N}_s and geometrical center \underline{C}_s . Equations (H-1) and (H-2) are then used to compute the contribution of solar force \underline{F}_s and torque $\underline{\tau}_s$ as if A_s were not shaded. Hence, the effective solar force and torque contributed by the shaded surface P_1 is

$$\underline{F}_{P1} = \underline{F}_{P1}^{(0)} - \underline{F}_s$$

$$\underline{\tau}_{P1} = \underline{\tau}_{P1}^{(0)} - \underline{\tau}_s$$

where

$\underline{F}_{P1}^{(0)}$ and $\underline{\tau}_{P1}^{(0)}$ are force and torque computed for a completely unshaded surface P_1 .

Let the center of the circle where thruster cone joins P_1 be \underline{C}_a , and let the center of the circular shadow of the end of thruster cone on P_1 be \underline{C}_b . Position of \underline{C}_b can be solved from the vector equation

$$(\underline{C}_b - \underline{C}_a) \cdot \underline{N}_{P1} = 0$$

$$\underline{C}_b - (\underline{C}_a + h \underline{N}_{P1}) = -\underline{\ell}_s$$

where $\underline{\ell} = \text{length of } [\underline{C}_b - (\underline{C}_a + h \underline{N}_{P1})]$.

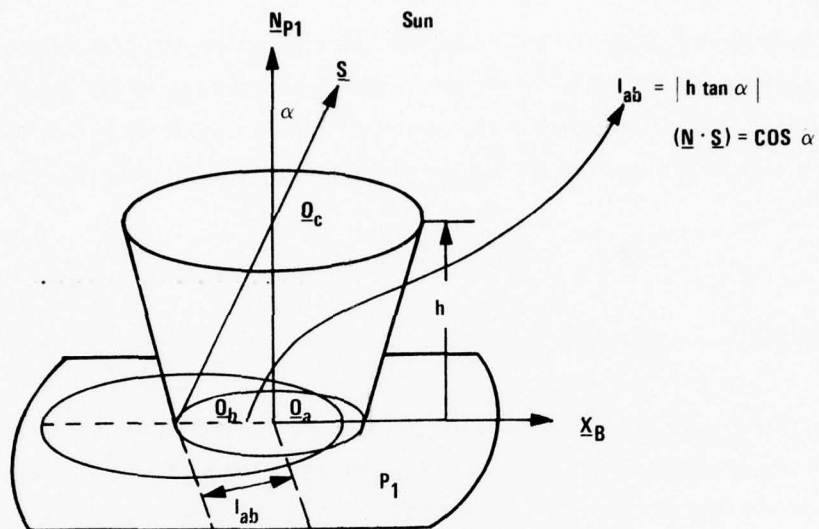


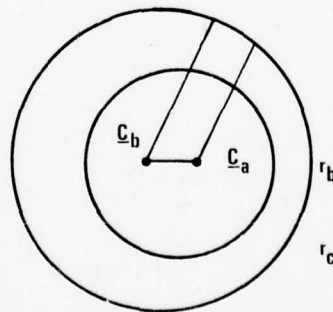
Figure H-6. Shading of Plane P_1 by Thruster Cone

The normal of the shadow on P_1 is of course $\underline{N}_S = \underline{N}_{P1}$. To evaluate \underline{F}_S and $\underline{\tau}_S$, the quantities \underline{C}_S and A_S are defined for four cases:

Case 1: $l_{ab} \leq r_b - r_a$

$$\underline{C}_S = \underline{C}_b$$

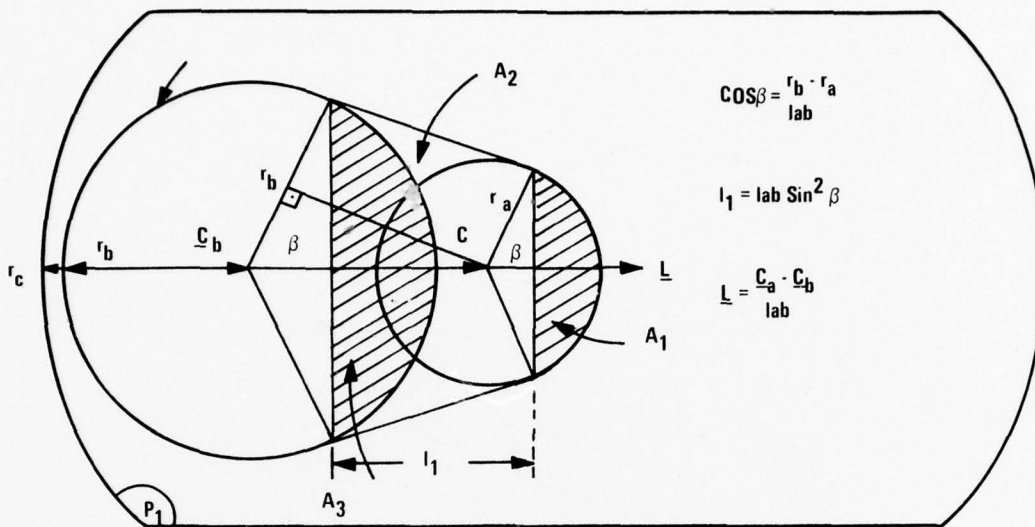
$$A_S = \pi r_b^2$$



$$l_{ab} + r_b \leq r_c$$

$$r_b - r_a < l_{ab} \leq r_c - r_b$$

Case 2:



$$\cos \beta = \frac{r_b \cdot r_a}{l_{ab}}$$

$$l_1 = l_{ab} \sin^2 \beta$$

$$L = \frac{C_a - C_b}{l_{ab}}$$

$$A_1 = \frac{1}{2} r_a^2 [2\beta - \sin 2\beta]$$

$$C_1 = C_a + \frac{(C_a - C_b)}{l_{ab}} \frac{2/3 r_a \sin^3 \beta}{\beta - \cos \beta \sin \beta}$$

$$A_2 = \frac{1}{2} (2r_a \sin \beta + 2r_b \sin \beta) l_{ab} \sin^2 \beta$$

$$\begin{aligned} C_2 &= [C_a + L(r_a \cos \beta)] - L h (2r_b + r_a) / (3r_b + 3r_a) \\ &= C_a + L [(r_a \cos \beta) - l_{ab} \sin^2 \beta (2r_b + r_a) / (3r_b + 3r_a)] \end{aligned}$$

$$A_3 = \frac{1}{2} r_b^2 [2\beta - \sin^2 \beta]$$

$$C_3 = C_b + L (\frac{2}{3} r_b \sin^3 \beta) / (\beta - \cos \beta \sin \beta)$$

Total area of shadow:

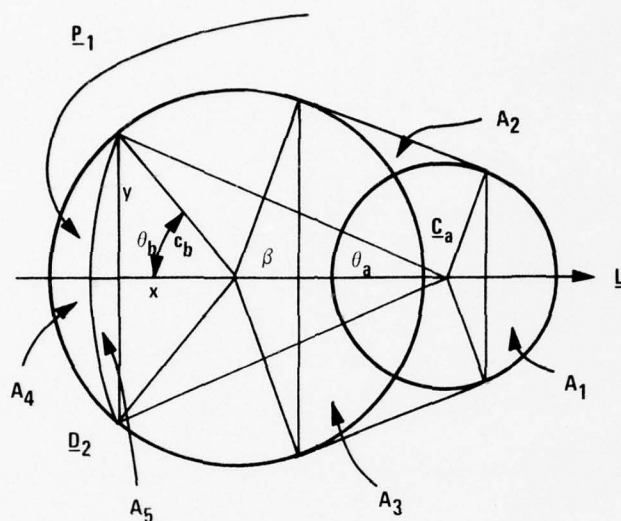
$$A_s = A_1 + A_2 + \frac{1}{2} \pi r_b^2 - A_3$$

Centroid position of A_s :

$$C_s = \frac{1}{A_s} [A_1 C_1 + A_2 C_2 + \frac{1}{2} \pi r_b^2 C_b - A_3 C_3]$$

Case 3: $r_b + r_c \geq l_{ab} > r_c - r_b$

$$r_b + r_c \geq l_{ab} > r_c - r_b$$



$$A_4 = \frac{1}{2} r_b^2 [2\theta_b - \sin 2\theta_b]$$

$$C_4 = C_b - \frac{L}{\theta_b} \left(\frac{(2/3) r_b \sin^3 \theta_b}{\theta_b - \cos \theta_b \sin \theta_b} \right)$$

$$A_5 = \frac{1}{2} r_c^2 [2\theta_c - \sin 2\theta_c]$$

$$C_5 = C_a - \frac{L}{\theta_c} \left(\frac{(2/3) r_c \sin^3 \theta_c}{\theta_c - \cos \theta_c \sin \theta_c} \right)$$

Total area of shadow:

$$A_s = A_1 + A_2 + \frac{1}{2} \pi r_b^2 - A_3 - A_4 + A_5$$

Centroid of A_s :

$$C_s = \frac{1}{A_s} [A_1 C_1 + A_2 C_2 + \frac{1}{2} \pi r_b^2 C_b - A_3 C_3 - A_4 C_4 + A_5 C_5]$$

where

$$\cos 2\theta_b = [(D_1 - C_b) \cdot (D_2 - C_b)] / [(D_1 - C_b) \cdot (D_1 - C_b)]$$

AD-A056 812

HONEYWELL INC MINNEAPOLIS MINN SYSTEMS AND RESEARCH --ETC F/G 17/7
INDEPENDENT STABILITY AND CONTROL ANALYSIS OF NAVIGATION DEVELO--ETC(U)
JAN 78 R E POPE, M D WARD, M F BARRETT F04701-75-C-0135

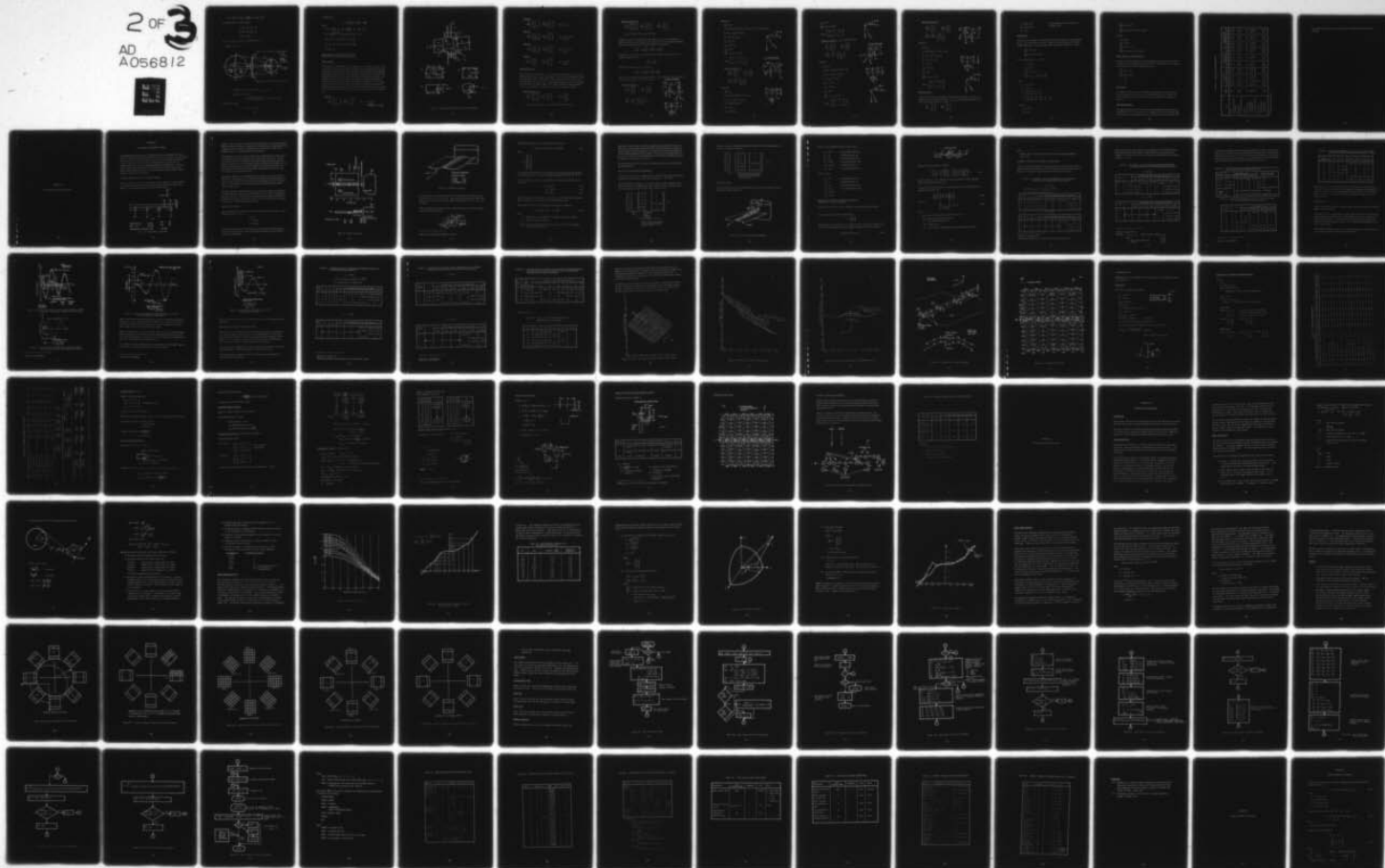
UNCLASSIFIED

78SRC10-VOL-2

SAMSO-TR-78-74-VOL-2

NL

2 OF 3
AD
A056812



$$\cos 2\theta_c = [(\underline{D}_1 - \underline{C}_a) \cdot (\underline{D}_2 - \underline{C}_a)] / [(\underline{D}_1 - \underline{C}_a) \cdot (\underline{D}_1 - \underline{C}_a)]$$

\underline{D}_1 and \underline{D}_2 satisfy the vector equation

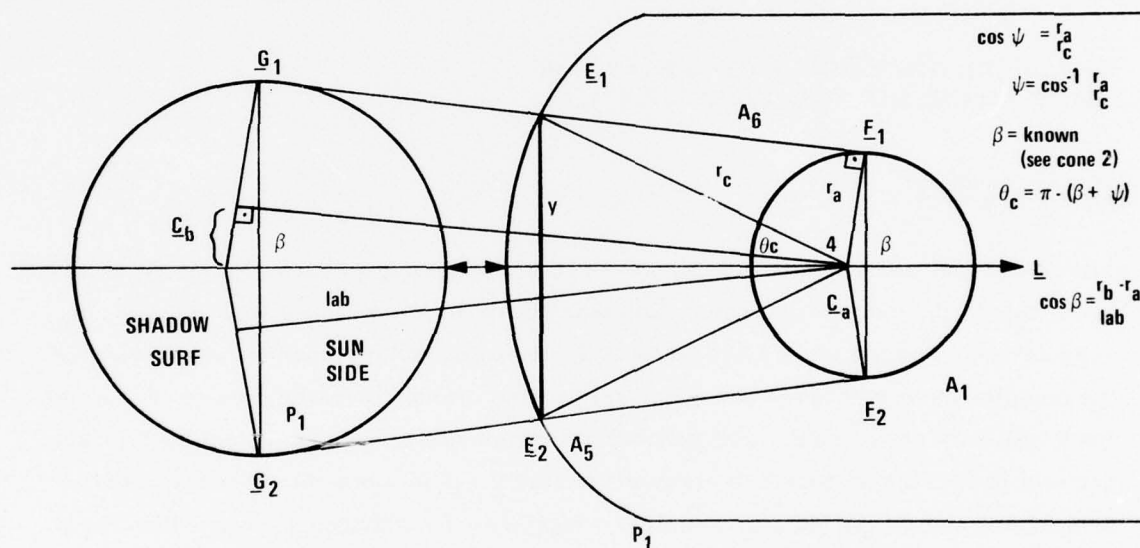
$$(\underline{D} - \underline{C}_a) \cdot (\underline{D} - \underline{C}_a) = r_c^2$$

$$(\underline{D} - \underline{C}_b) \cdot (\underline{D} - \underline{C}_b) = r_b^2$$

$$(\underline{D} - \underline{C}_a) \cdot \underline{N}_{P1} = 0$$

$A_1, A_2, A_3, \underline{C}_1, \underline{C}_2$ and \underline{C}_3 are as defined in Case 3.

Case 4: $\ell_{ab} > r_b + r_c$



$$A_6 = \frac{1}{2} (2r_a \sin \beta + 2r_c \sin \theta_c) (r_c \cos \theta_c + r_a \cos \beta)$$

$$\underline{C}_6 = [\underline{C}_a + \underline{L} (r_a \cos \beta)] - \underline{L} \frac{2r_c \sin \theta_c + r_a \sin \beta}{3r_c \sin \theta_c + 3r_a \sin \beta} (r_c \cos \theta_c + r_a \cos \beta)$$

Total area of shadow:

$$A_s = A_1 + A_5 + A_6$$

Centroid of A_s :

$$\underline{C}_s = \frac{1}{A_s} [A_1 \underline{C}_1 + A_5 \underline{C}_5 + A_6 \underline{C}_6]$$

where

$$\cos 2\theta_c = [(\underline{E}_1 - \underline{C}_a) \cdot (\underline{E}_2 - \underline{C}_a)] / [(\underline{E}_1 - \underline{C}_a) \cdot (\underline{E}_1 - \underline{C}_a)]$$

$$\underline{E}_i = \underline{F}_i + \sqrt{r_c^2 - r_a^2} (\underline{G}_i - \underline{F}_i) / |\underline{G}_i - \underline{F}_i| \quad i = 1, 2$$

$$\underline{F}_i = \underline{C}_a + r_a \cos \theta \underline{L} + (-1)^{i+1} r_a \sin \theta \underline{M}$$

$$\underline{G}_i = \underline{C}_b + r_b \cos \theta \underline{L} + (-1)^{i+1} r_b \sin \theta \underline{M}$$

$$\underline{M} = \underline{N}_{P1} \times \underline{L}$$

SIMPLIFIED GPS VEHICLE GEOMETRY FOR SOLAR FORCE AND TORQUE EVALUATION

Planar Surfaces

The five planar surfaces include P_1 where thruster cone is located, P_2 where antennae are located, P_3 and P_4 adjacent to the solar panels in the directions of $+\underline{Y}_B$ and $-\underline{Y}_B$, respectively, and the plane introduced at the open end of the thruster cone to simplify the complex geometry involved. The vehicle body frame (B-frame), as defined in the Rockwell drawing for spacecraft general arrangement configuration, has its \underline{Y}_B axis parallel to the line of the solar array drive, the \underline{Z}_B axis along the AKM thruster centerline, and the \underline{X}_B axis to complete a right-handed orthogonal triad. The origin of the B-frame is located at the center of the open end of the thruster cone (not the AKM nozzle) as shown in Figure H-7. Let each plane be defined in terms of its surface normal \underline{N}_i , location of surface centroid \underline{C}_i , and area of surface A_i in B-frame coordinates.

Plane P_1 :

$$\begin{pmatrix} \underline{N}_{P1}^B \\ \underline{C}_{P1}^B \end{pmatrix} = \begin{bmatrix} 0 \\ 0 \\ 23.88 \end{bmatrix} \quad \begin{pmatrix} \underline{N}_{P1}^B \\ \underline{C}_{P1}^B \end{pmatrix} = \begin{bmatrix} 0 \\ 0 \\ -1 \end{bmatrix}$$

$$A_{P1} = 43.8 \times 41.8 + (32)^2 \left(\frac{86.4}{57.3} - \sin 86.4 \right)$$

Plane P₂:

$$\begin{pmatrix} \bar{C}_{P2}^B \\ \bar{N}_{P2}^B \end{pmatrix} = \begin{bmatrix} 0 \\ 0 \\ 61.38 \end{bmatrix} \quad \begin{pmatrix} \bar{N}_{P2}^B \end{pmatrix} = \begin{bmatrix} 0 \\ 0 \\ 1 \end{bmatrix} \quad A_{P2} = A_{P1}$$

Plane P₃:

$$\begin{pmatrix} \bar{C}_{P3}^B \\ \bar{N}_{P3}^B \end{pmatrix} = \begin{bmatrix} 0 \\ 21.8 \\ 42.63 \end{bmatrix} \quad \begin{pmatrix} \bar{N}_{P3}^B \end{pmatrix} = \begin{bmatrix} 0 \\ 1 \\ 0 \end{bmatrix} \quad \begin{aligned} A_{P3} &= 37.5 \times 41.8 \\ &= 1567.5 \end{aligned}$$

Plane P₄:

$$\begin{pmatrix} \bar{C}_{P4}^B \\ \bar{N}_{P4}^B \end{pmatrix} = \begin{bmatrix} 0 \\ -21.8 \\ 42.63 \end{bmatrix} \quad \begin{pmatrix} \bar{N}_{P4}^B \end{pmatrix} = \begin{bmatrix} 0 \\ -1 \\ 0 \end{bmatrix} \quad \begin{aligned} A_{P4} &= 37.5 \times 41.8 \\ &= 1567.5 \end{aligned}$$

Plane P₅:

$$\begin{pmatrix} \bar{C}_{P5}^B \\ \bar{N}_{P5}^B \end{pmatrix} = \begin{bmatrix} 0 \\ 0 \\ 0 \end{bmatrix} \quad \begin{pmatrix} \bar{N}_{P5}^B \end{pmatrix} = \begin{bmatrix} 0 \\ 0 \\ -1 \end{bmatrix} \quad \begin{aligned} A_{P5} &= \pi (14.6)^2 \\ &= 669.7 \end{aligned}$$

Cylindrical Surfaces

The six segments of cylindrical surfaces include two main body surfaces, C_1 and C_2 , in the directions of \underline{X}_B and $-\underline{X}_B$, respectively, and two solar panel segments for each of the two solar arrays. Each segment of cylindrical surface is defined in terms of the location of the geometrical center \underline{C} , the normal and tangent vectors at \underline{C} , \underline{N} , and \underline{T} , respectively, the radius, length, and the angular width of the cylinder segment, r , l , and θ , respectively. The cylindrical surfaces are defined as follows:

Cylindrical Surface C₁:

$$\begin{pmatrix} \bar{C}_{C1}^B \\ \bar{N}_{C1}^B \end{pmatrix} = \begin{bmatrix} 30.2 \\ 0 \\ 42.63 \end{bmatrix} \quad \begin{pmatrix} \bar{N}_{C1}^B \end{pmatrix} = \begin{bmatrix} 1 \\ 0 \\ 0 \end{bmatrix} \quad \begin{pmatrix} \bar{T}_{C1}^B \end{pmatrix} = \begin{bmatrix} 0 \\ 1 \\ 0 \end{bmatrix}$$

$$r_{C1} = 32.0, \quad l_{C1} = 37.5, \quad \theta_{C1} = 2 \sin^{-1} (21.9/32.0) \approx 86.4 \text{ deg}$$

Cylindrical Surface C_2 :

$$\begin{pmatrix} \bar{C}_{C2}^B \\ \bar{N}_{C2}^B \\ \bar{T}_{C2}^B \end{pmatrix} = \begin{bmatrix} -30.2 \\ 0 \\ 42.63 \end{bmatrix} \quad \begin{pmatrix} \bar{N}_{C2}^B \\ \bar{T}_{C2}^B \end{pmatrix} = \begin{bmatrix} -1 \\ 0 \\ 0 \end{bmatrix} \quad \begin{pmatrix} \bar{T}_{C2}^B \\ \bar{N}_{C2}^B \end{pmatrix} = \begin{bmatrix} 0 \\ -1 \\ 0 \end{bmatrix}$$

$$r_{C2} = 32.0, \quad l_{C2} = 37.5, \quad \theta_{C2} = 86.4 \text{ deg}$$

Cylindrical surfaces C_3 through C_6 are solar panel surfaces. In the following, the normal and tangent vectors, \bar{N} and \bar{T} , will be defined in terms of the panel fixed frames. Their B-frame definition will be obtained through a transformation as

$$\begin{pmatrix} \bar{N}_C^B \\ \bar{T}_C^B \end{pmatrix} = T_{BP} \begin{pmatrix} \bar{N}_C^P \\ \bar{T}_C^P \end{pmatrix} \text{ and } \begin{pmatrix} \bar{T}_C^B \\ \bar{N}_C^B \end{pmatrix} = T_{BP} \begin{pmatrix} \bar{T}_C^P \\ \bar{N}_C^P \end{pmatrix}$$

The positions of centroid of the cylindrical surfaces will be defined in P-frame with respect to origin of P-frame as

$$[(\bar{C}_C^P) - (\bar{O}_C^P)]$$

Their P-frame definitions are then obtained as

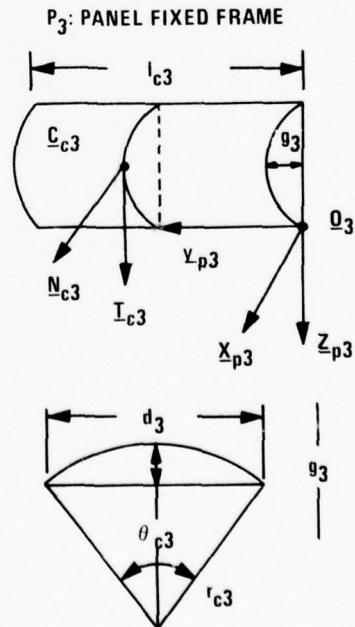
$$\begin{pmatrix} \bar{C}_C^B \\ \bar{N}_C^B \\ \bar{T}_C^B \end{pmatrix} = T_{BP} [(\bar{C}_C^P) - (\bar{O}_C^P)] + (\bar{O}_C^B)$$

Each cylindrical segment is individually defined so that misalignments between segments of arrays and between arrays can be simulated.

Cylindrical Surface C_3 :

$$\begin{pmatrix} \bar{C}_{C3}^{P3} \\ \bar{N}_{C3}^{P3} \\ \bar{T}_{C3}^{P3} \end{pmatrix} = \begin{bmatrix} 1 \\ 0 \\ 0 \end{bmatrix} \quad \begin{pmatrix} \bar{N}_{C3}^{P3} \\ \bar{T}_{C3}^{P3} \end{pmatrix} = \begin{bmatrix} 0 \\ 0 \\ 1 \end{bmatrix}$$

$$\begin{pmatrix} \bar{C}_{C3}^{P3} \\ \bar{N}_{C3}^{P3} \\ \bar{T}_{C3}^{P3} \end{pmatrix} - \begin{pmatrix} \bar{O}_3^{P3} \\ \bar{N}_3^{P3} \\ \bar{T}_3^{P3} \end{pmatrix} = \begin{bmatrix} g_3 \\ l_{C3}/2 \\ -d_3/2 \end{bmatrix} \equiv \bar{DI}$$



Nominally,

$$\underline{Y}_{P3} = \underline{Y}_B$$

α_3 defines \underline{X}_{P3} with respect to \underline{X}_B or \underline{Z}_P with respect to \underline{Z}_B

$$g_3 = r_{C3} - r_{C3} \cos(\theta_{C3/2})$$

$$d_3 = 2r_{C3} \sin(\theta_{C3/2})$$

$$r_{C3} = 32.7 \text{ in}$$

$$\theta_{C3} = 58.6 \text{ deg}$$

$$l_{C3} = 67 \text{ in}$$

$$(\underline{\bar{O}}_3)^B = (0, 21, 9, 42.38)^T$$

$$T_{BP3} = \begin{bmatrix} \cos \alpha_3 & 0 & \sin \alpha_3 \\ 0 & 1 & 0 \\ -\sin \alpha_3 & 0 & \cos \alpha_3 \end{bmatrix}$$

Cylindrical Surface C_4 :

$$(\underline{\bar{N}}_{C4})^{P4} = \begin{bmatrix} 1 \\ 0 \\ 0 \end{bmatrix} \quad (\underline{\bar{T}}_{C4})^{P4} = \begin{bmatrix} 0 \\ 0 \\ 1 \end{bmatrix}$$

$$(\underline{\bar{C}}_{C4})^{P4} - (\underline{\bar{O}}_4)^{P4} = \begin{bmatrix} g_4 \\ l_{C4/2} \\ d_{4/2} \end{bmatrix}$$

Nominally,

$$\underline{Y}_{P4} = \underline{Y}_B$$

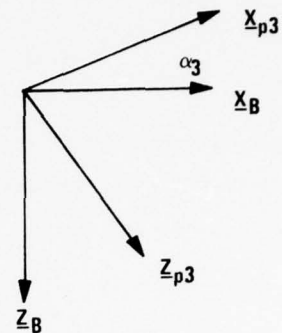
α_4 defines \underline{X}_{P4} with respect to \underline{X}_B

$$g_4 = r_{C4} - r_{C4} \cos(\theta_{C4/2})$$

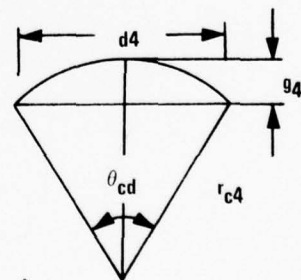
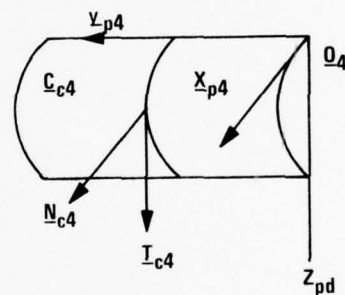
$$d_4 = 2r_{C4} \sin(\theta_{C4/2})$$

$$r_{C4} = 32.7 \text{ in}$$

$$\theta_{C4} = 58.6 \text{ deg}$$



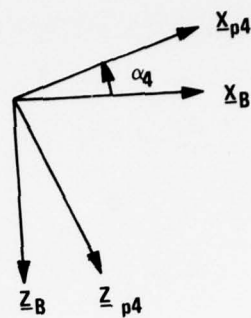
P_4 = PANEL FIXED FRAME



$$l_{C4} = 67 \text{ in}$$

$$\begin{matrix} B \\ (\bar{O}_4) \end{matrix} = (0, 21.8, 38)^T$$

$$T_{BP4} = \begin{bmatrix} \cos \alpha_4 & 0 & \sin \alpha_4 \\ 0 & 1 & 0 \\ -\sin \alpha_4 & 0 & \cos \alpha_4 \end{bmatrix}$$



Cylindrical Surface C₅: P₅: Panel fixed frame

$$\begin{matrix} P5 \\ (\bar{N}_{C5}) \end{matrix} = \begin{bmatrix} 1 \\ 0 \\ 0 \end{bmatrix} \quad \begin{matrix} P5 \\ (\bar{T}_{C5}) \end{matrix} = \begin{bmatrix} 0 \\ 0 \\ 1 \end{bmatrix}$$

$$\begin{matrix} P5 \\ (\bar{C}_{C5}) \end{matrix} - \begin{matrix} P5 \\ (\bar{O}_5) \end{matrix} = \begin{bmatrix} g_5 \\ -l_{C5}/2 \\ -d_5/2 \end{bmatrix}$$

Nominally,

$$\underline{Y}_{P5} = \underline{Y}_B$$

α_5 defines \underline{X}_{P5} with respect to \underline{X}_B

$$g_5 = r_{C5} - r_{C5} \cos(\theta_{C5}/2)$$

$$d_5 = 2r_{C5} \sin(\theta_{C5}/2)$$

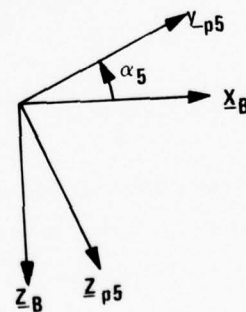
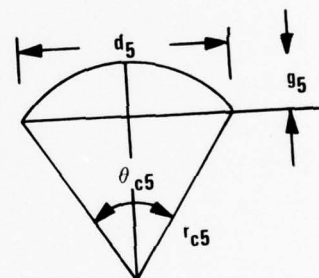
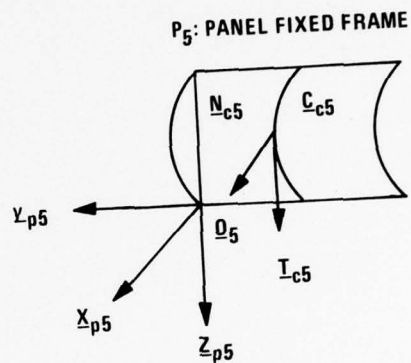
$$r_{C5} = 32.7 \text{ in}$$

$$\theta_{C5} = 58.6 \text{ deg}$$

$$l_{C5} = 67 \text{ in}$$

$$\begin{matrix} B \\ (\bar{O}_5) \end{matrix} = (0, -21.8, 38)^T$$

$$T_{BP5} = \begin{bmatrix} \cos \alpha_5 & 0 & \sin \alpha_5 \\ 0 & 1 & 0 \\ -\sin \alpha_5 & 0 & \cos \alpha_5 \end{bmatrix}$$



Cylindrical Surface C₆:

$$\begin{aligned} \begin{pmatrix} \bar{N}_{C6}^{P6} \\ \bar{C}_{C6}^{P6} \end{pmatrix} &= \begin{bmatrix} 1 \\ 0 \\ 0 \end{bmatrix} & \begin{pmatrix} \bar{T}_{C6}^{P6} \end{pmatrix} &= \begin{bmatrix} 0 \\ 0 \\ 1 \end{bmatrix} \\ \begin{pmatrix} \bar{C}_{C6}^{P6} \end{pmatrix} - \begin{pmatrix} \bar{O}_{C6}^{P6} \end{pmatrix} &= \begin{bmatrix} g_6 \\ -l_{C6}/2 \\ d_{C6}/2 \end{bmatrix} \end{aligned}$$

Nominally,

$$\underline{Y}_{P6} = \underline{Y}_B$$

α_6 defines \underline{X}_{P6} with respect to \underline{X}_B

$$g_6 = r_{C6} - r_{C6} \cos(\theta_{C6}/2)$$

$$d_6 = 2r_{C6} \sin(\theta_{C6}/2)$$

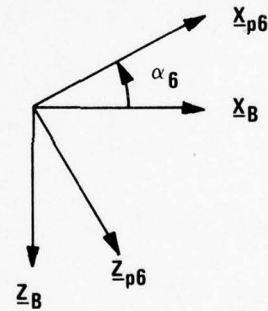
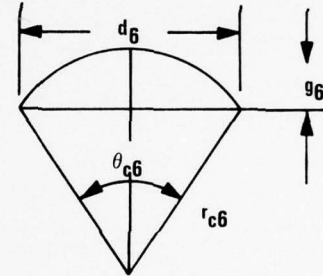
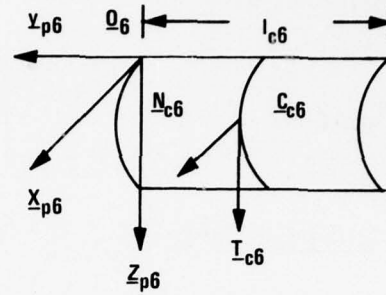
$$r_{C6} = 32.7 \text{ in}$$

$$\theta_{C6} = 58.6 \text{ deg}$$

$$l_{C6} = 67 \text{ in}$$

$$\begin{pmatrix} \bar{O}_6^B \end{pmatrix} = (0, -21.8, 38)^T$$

$$T_{BP6} = \begin{bmatrix} \cos \alpha_6 & 0 & \sin \alpha_6 \\ 0 & 1 & 0 \\ -\sin \alpha_6 & 0 & \cos \alpha_6 \end{bmatrix}$$



Thruster Cone T_C

The orientation, location, and physical dimensions of the thruster cone surface are defined in terms of the parameters (\underline{N}_C , γ_a , γ_b , \underline{O}_a , h) as defined in Section V. In terms of B-frame coordinates, we have

$$\begin{pmatrix} \bar{N}_C^B \end{pmatrix} = \begin{bmatrix} 0 \\ 0 \\ -1 \end{bmatrix} \quad \begin{pmatrix} \bar{O}_a^B \end{pmatrix} = \begin{bmatrix} 0 \\ 0 \\ +h \end{bmatrix}$$

$$\gamma_a = 2.6/2 = 15.0$$

$$\gamma_b = 3.2/2 = 18.5$$

$$h = 23.88$$

B-Frame origin is at center of open end of thruster cone.

Antenna Rods

Antenna rods are simplified as cylindrical surfaces defined in terms of the parameters $(\underline{C}, \underline{L}, \gamma, \ell)$ as described in Section II. Antenna rods A_1 through A_{12} are arranged symmetrically about an axis \underline{L}_C through a point \underline{C}_C as shown in Figure H-3. Hence,

$$(\underline{L}_C)^B = (0, 0, 1)^T$$

$$(\underline{C}_C)^B = (8.27, 0, 61.38)^T$$

For A_1 through A_{12} , i.e., $i = 1, 12$,

$$\gamma_i = 1.25 \text{ in.}$$

$$\ell_i = 18.6 \text{ in.}$$

$$(\underline{L}_i)^B = (0, 0, 1)^T$$

$$(\underline{C}_i)^B = (X_i, Y_i, 61.38)^T + (\underline{C}_C)^B$$

with

$$X_i = -r_o \cos \theta_i$$

$$Y_i = -r_o \sin \theta_i$$

$$r_o = 17.25 \text{ for } i = 1, \dots, 8$$

$$= 6.0 \text{ for } i = 9, \dots, 12$$

$$\theta_i = (i-1) \times 45^\circ + 22.5^\circ \text{ for } i = 1, \dots, 8$$

$$= (i-9) \times 90^\circ + 45^\circ \text{ for } i = 9, \dots, 12$$

For A_{13} ,

$$r_{13} = 1.25 \text{ in.}$$

$$\ell_{13} = 44.3$$

$$(\bar{L}_{13})^B = (0, 0, 1)^T$$

$$(\bar{C}_{13})^B = (8.27, 17.25, 61.38 + \ell_{13}/2)^T$$

For A_{14} ,

$$\gamma_{14} = 0.8 \text{ in.}$$

$$\ell_{14} = 19.1 \text{ in.}$$

$$(\bar{L}_{14})^B = (0, 0, -1)^T$$

$$(\bar{C}_{14})^B = (29.2, 0, 23.88 - \ell_{14}/2)^T$$

Stowed Vehicle as Cylindrical Surface

During the initial spinning phase, the GPS configuration has its solar arrays stowed. A cylindrical surface approximation can be used for evaluating solar force. The cylinder is defined in terms of the following parameters:

$$(\bar{L})^B = (0, 0, 1)^T$$

$$(\bar{C})^B = (0, 0, \ell/2)^T$$

$$\gamma = 35.7$$

$$\ell = 67$$

cg Locations

To evaluate the torque due to solar pressure, the moment arm is the vector difference of location of center of force and the location of vehicle center of mass. In B-frame coordinates, the locations of center of mass for GPS are summarized in Table H-1.

Other Simplifications

The approximating surfaces are assumed to have uniform physical characteristics. For GPS spacecraft exterior surfaces, the coating material is of the Al-Teflon type which, for solar arrays, consists of a cover of AR coat and a layer of UV filter coat.

TABLE H-1. SEQUENCE MASS PROPERTIES

Item	Weight (lb)	Center of Gravity (in.)			Moment of Inertia (slug feet ²)			Product of Inertia (slug feet ²)		
		X	Y	Z	Ixx	Iyy	Izz	Ixy	Ixz	Iyz
Launch	1436	0.00	0.01	35.81	88.0	90.6	104.4	0.83	-0.02	0.01
Less Transfer Orbit Propellant	-6	0.00	0.00	39.40	0.0	-0.6	-0.6	0.00	0.00	0.00
AKM Ignition *	1430	0.00	0.01	35.79	88.0	89.9	103.8	0.83	-0.02	0.01
Less AKM Propellant	-567	0.00	0.00	31.80	-8.4	-8.4	-9.7	0.00	0.00	0.00
On-Orbit										
Array Stowed	863	-0.01	0.02	38.42	76.3	78.3	94.1	0.83	-0.02	0.00
Array Deployed										
In X-X Plane	863	-0.01	0.07	38.11	145.3	72.6	167.9	0.57	-0.02	-0.05
In Z-Z Plane	863	-0.52	0.02	38.48	149.3	72.7	164.3	0.81	0.07	0.00
Less RCS Propellant	-51	0.00	0.00	39.40	0.0	-5.3	-5.3	0.00	0.00	0.00
End Mission										
Array Deployed										
In X-X Plane	811	0.00	0.07	38.03	145.2	67.3	163.0	0.57	-0.02	-0.05
In Z-Z Plane	811	-0.56	0.02	38.43	149.2	67.3	159.0	0.81	0.06	0.00

* Principal axis angular offset

The values of parameters s and ρ for solar pressure evaluation will be furnished by Rockwell.

APPENDIX I

SOLAR ARRAY FLEXIBILITY MODEL

APPENDIX I

SOLAR ARRAY FLEXIBILITY MODEL

A STARDYNE (Control Data version of NASTRAN) finite element program was used to generate a mathematical model of the +Y solar array model. Only the +Y array was modeled, with the pivot point considered to be fixed. The +Y array is structurally identical to the -Y array. However, since each array has independent pitch drive actuators, the model considers each array to be responding separately and independently. The model will be discussed first, with respect to the original coarse model that was used for determining the model structure (i.e., how many structural modes should be included), followed by the final fine mesh model.

COARSE MESH SOLAR ARRAY FLEXIBILITY MODEL

The coarse NDS solar array structural model is shown in Figure I-1. Nodes 5 through 8 are on the boom centerline, at the approximate location of the solar panel to boom hinges. The solar panel sun sensors are located close to Node 8.

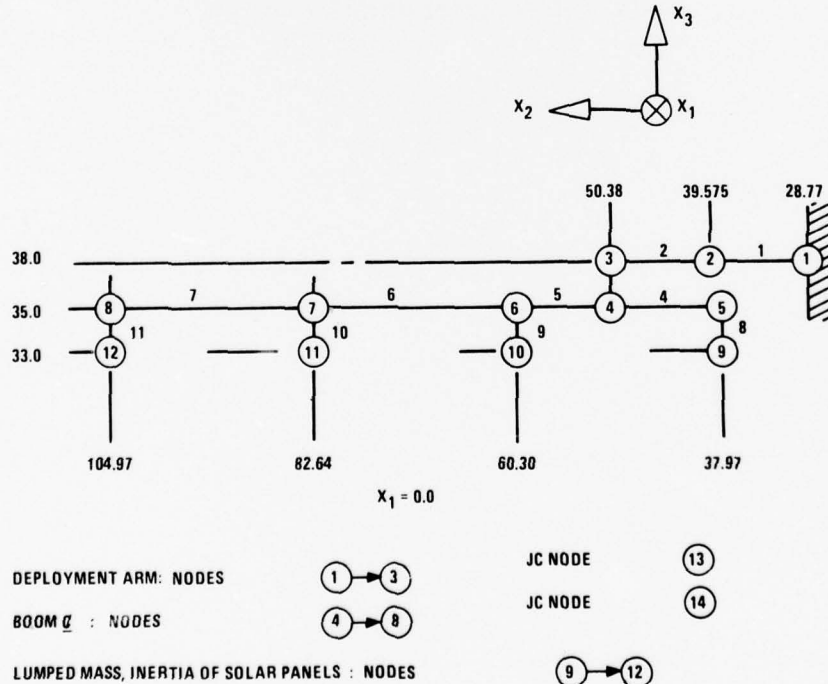


Figure I-1. Math Model--Coarse Mesh

Figures I-2 and I-3 present a layout schematic drawing of the +Y array and the Rockwell vibration test panel orientation, respectively. Based on this test, the equivalent viscous damping ratio for one mode was estimated to be 3.5 percent ($\text{Zeta} = 0.035$). This damping estimate was obtained informally from Rockwell.

The solution for solar array dynamic response can be obtained by direct integration of the equations of motion of the structural math model shown in Figure I-1. However, such a model would have 11 independent nodes with six degrees of freedom per node. Instead, a solution can be obtained using a reduced set of generalized coordinates. The generalized coordinates are the natural frequencies (rad/sec) of the structure. The transformation from the generalized coordinates to the physical math model are the normal modes (mode shapes) of vibration.

The deployed NDS solar array flexibility model is represented by a selected set of n eigenvectors and eigenvalues. The solution for the eigenvector/eigenvalue problem is based on a finite element structural model of the NDS deployed solar array (+Y array) based on available structural drawings obtained from Rockwell through the SAMSO contract monitor office.

The numerical values tabulated in this memo are for a coarse mesh math model based on out-date drawings. The associated natural frequencies are known to be higher than the actual solar array structure, based on informal results of a ground vibration test performed at Rockwell. However this model is sufficiently close in dynamic response characteristics to allow checkout runs to be made.

EQUATIONS OF MOTION

For the NDS solar array model, the base of the STARDYNE elastic structure is at the following station (+Y array):

$$X = 0.0$$

$$Y = 28.77 \text{ in.}$$

$$Z = 38.00 \text{ in.}$$

This point is the location of the inner pivot point of the deployment mechanism and is the centerline of the circular, integrally machined drive tube as shown in Rockwell drawing No. V505-932004.

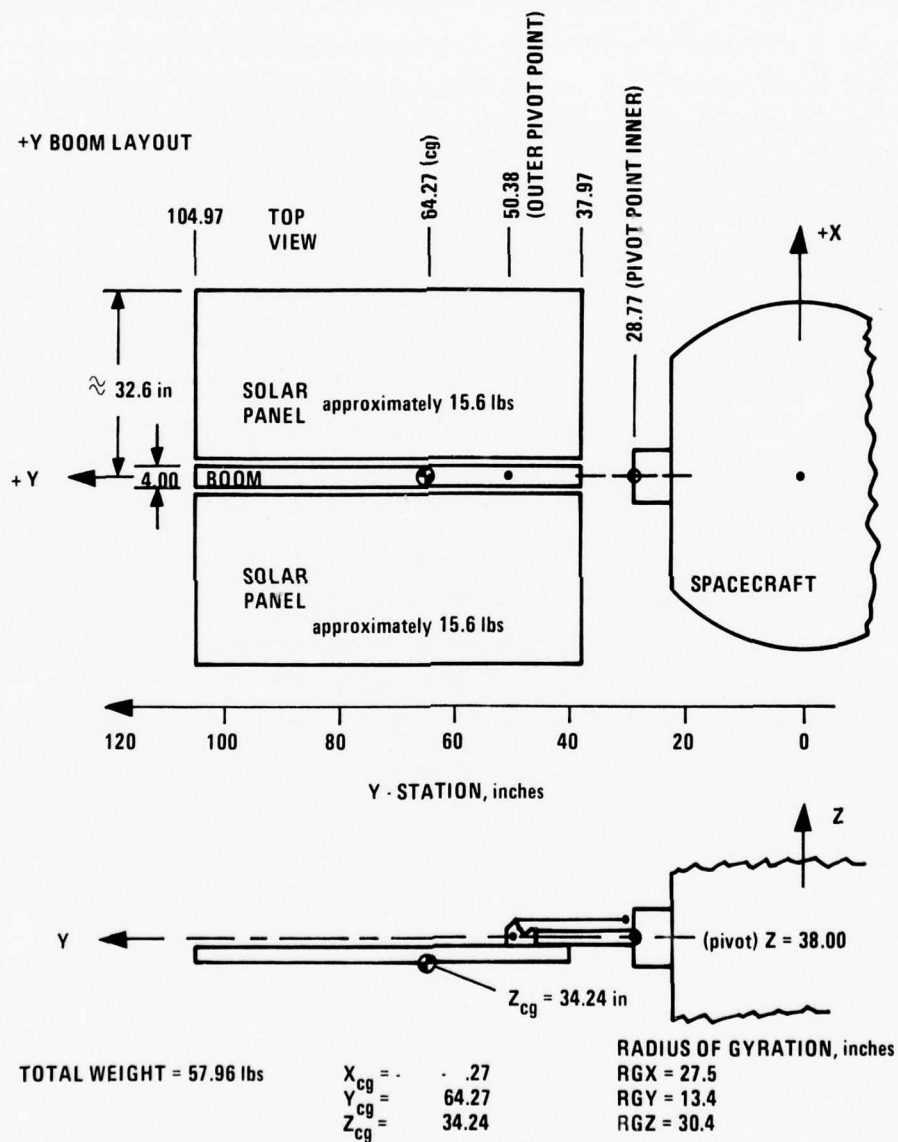


Figure I-2. Solar Array Layout

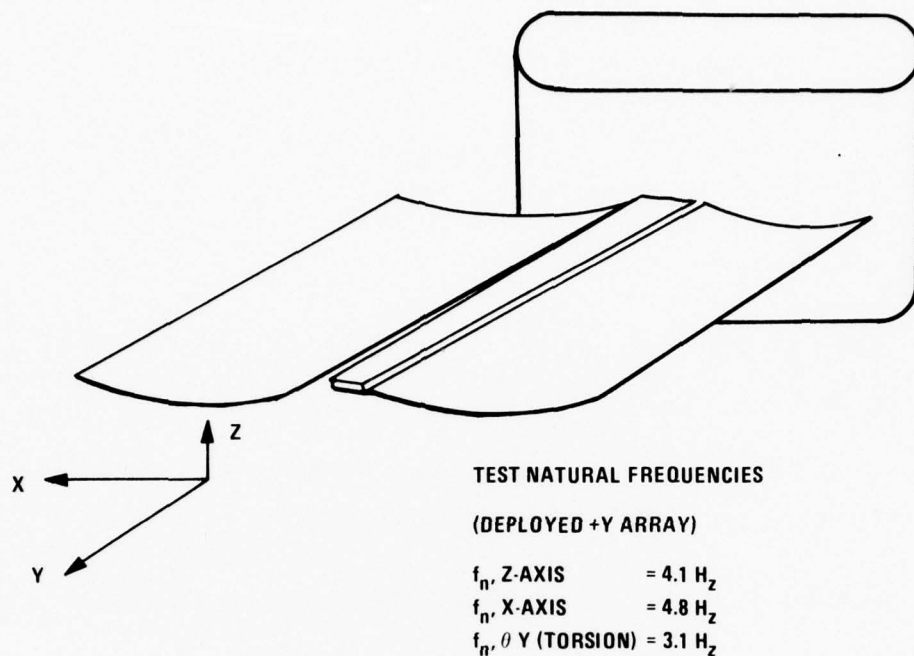
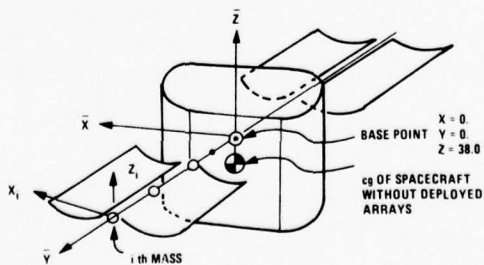


Figure I-3. Rockwell Test Results*

For convenience, the attach point of the elastic structure will be considered to be on the vehicle centerline at Z station 38.0. Thus modal participation factors and the array response torques, moments, and forces will be transformed to $X = 0.0$, $Y = 0.0$, and $Z = 38.00$.

This will simplify the equations required to couple the elastic array model to the rigid body controls simulation model.



*Reference: Rockwell report N18231-26, 2/17/77.

The equations of motion in matrix notation for the +Y array are

$$[m] \{\ddot{u}\} + [c] \{\dot{u}\} + [k] \{u\} = [m][T] \{\ddot{u}\} \quad (I-1)$$

where

$$\{u_i\} = \begin{Bmatrix} X_i \\ Y_i \\ Z_i \\ \theta X_i \\ \theta Y_i \\ \theta Z_i \end{Bmatrix}$$

are motions of panel points on the array relative to the base point. The accelerations of the base point are $\{\ddot{u}\}$. $\{\ddot{u}\}$ has six possible components: $\ddot{X}, \ddot{Y}, \ddot{Z}, \theta\ddot{X}, \theta\ddot{Y}, \theta\ddot{Z}$.

Let the panel points on the array be described by the normal mode coordinate transformation:

$$\{u\} = [\phi] \{\eta\} \quad (I-2)$$

$$\{\dot{u}\} = [\phi] \{\dot{\eta}\} \quad (I-3)$$

$$\{\ddot{u}\} = [\phi] \{\ddot{\eta}\} \quad (I-4)$$

where $[\phi]$ represents the normal modes and the $\{\eta\}$ are a set of generalized coordinates which are uncoupled, second-order, ordinary differential equations.

The response of the n^{th} "mode" or generalized coordinate is expressed as

$$\ddot{\eta}_n + 2\zeta_n \omega_n \dot{\eta}_n + \omega_n^2 \eta_n = -\{y_n\}^T \{\ddot{u}\} \quad (I-5)$$

where

ζ_n = equivalent viscous damping factor assuming 3.5 percent ($\zeta = 0.035$)

ω_n = n^{th} natural frequency (rad/sec)

$\{y_n\}_{6 \times n}$ = model participation factor for base acceleration in each of the six input axes: $\bar{X}, \bar{Y}, \bar{Z}, \theta\bar{X}, \theta\bar{Y}, \theta\bar{Z}$.

Equation (I-5) must be integrated with the satellite main body equations of motion. If each array is represented by the first four elastic modes, then four sets of equations such as Equation (I-5) must be integrated. If solar arrays are pulsed separately, then a total of eight such equations will be required. The +Y array is assumed identical to the -Y array. However, the participation factors will be different (of opposite sign) for rotational base accelerations in θ_X and θ_Z .

The rotational position of the sun sensor at the outer end of the array can be obtained by using Equation (I-2).

ARRAY REACTION FORCES AND MOMENTS

Array dynamic responses are coupled to the spacecraft base point by the elastic forces produced at the attach point by array relative responses: $\{u\} = [\phi]\{\eta\}$

For each generalized coordinate η , a set of three forces and three moments are produced at Node 1 in the STARDYNE math model. These have been transformed to the spacecraft centerline at Z station 38.0. Thus, for the +Y array,

$$\underbrace{\begin{Bmatrix} F_x \\ F_y \\ F_z \\ M_x \\ M_y \\ M_z \end{Bmatrix}}_{\text{base, } n^{\text{th}} \text{ mode}} = \underbrace{\begin{Bmatrix} -VA2 \\ -P \\ VA3 \\ -MA2 \\ -\text{Torque} \\ MA3 \end{Bmatrix}}_{\text{STARDYNE Beam 1 Notation, } n^{\text{th}} \text{ mode}} + \begin{Bmatrix} 0 \\ 0 \\ 0 \\ +28.77*VA3 \\ 0 \\ +28.77*VA2 \end{Bmatrix} \cdot \{\eta_n\}$$

Modal reactions at base point
per unit model deflection of
+Y elastic array

For the -Y array, the modal (or generalized) reaction forces at the base point ($X = 0.0$, $Y = 0.0$, $Z = 38.0$) are as follows:

$$\begin{Bmatrix} F_x \\ F_y \\ F_z \\ M_x \\ M_y \\ M_z \end{Bmatrix}_{\text{base}} = \begin{Bmatrix} -VA2 \\ +P \\ VA3 \\ +MA2 \\ -\text{Torque} \\ -MA3 \end{Bmatrix} + \begin{Bmatrix} 0 \\ 0 \\ 0 \\ -28.77*VA3 \\ 0 \\ +28.77*VA2 \end{Bmatrix} \cdot \{\eta_n\}$$

Modal reactions at base point
per unit modal deflection of
-Y elastic array.

SIGN CONVENTION

The sign convention for the loads acting on spacecraft and the loads acting at +Y array drive point is shown in Figure I-4.

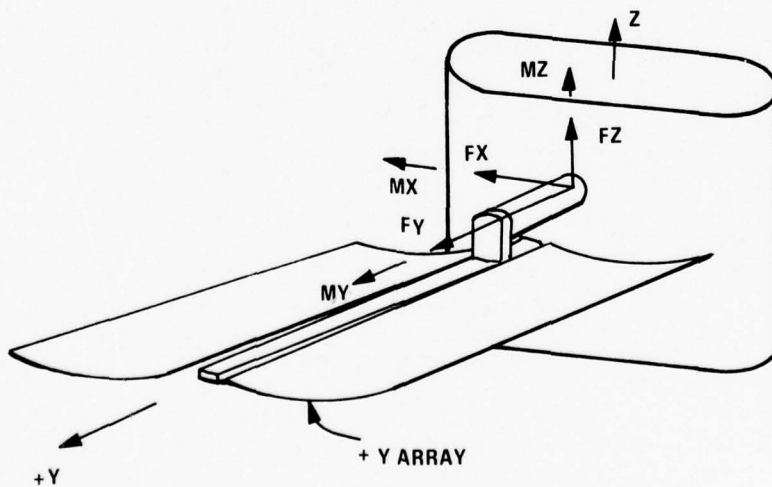


Figure I-4. Structural Analysis Sign Convention

For the +Y array (STARDYNE, Beam 1 loads, end A),

$$\begin{array}{ll}
 F_x = -VA2, & +X1 \text{ tip deflection gives } +F_x \\
 F_y = -P, & +X2 \text{ deflection gives } +F_y \\
 F_z = VA3, & +X3 \text{ tip deflection gives } +F_z \\
 M_x = -MA2, & +X3 \text{ tip deflection gives } +M_x \\
 M_y = -\text{Torque}, & +\theta Y \text{ deflection gives } +M_y \\
 M_z = MA3, & +X3 \text{ tip deflection gives } -M_z
 \end{array}$$

For the -Y array,

$$\begin{array}{ll}
 F_x = VA2 & +X1 \text{ tip deflection gives } +F_x \\
 F_y = P & +X2 \text{ deflection gives } +F_y \\
 F_z = VA3 & +X3 \text{ tip deflection gives } +F_z \\
 M_x = MA2 & +X3 \text{ tip deflection gives } +M_x \\
 M_y = -\text{Torque} & \\
 M_z = -MA3 &
 \end{array}$$

EQUATIONS OF MOTION, FLEXIBLE APPENDAGES COUPLED TO A RIGID SPACECRAFT

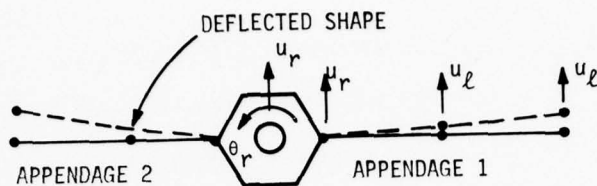
The previous derivation may now be extended to a general math model as follows.

The total displacement set for the spacecraft is

$$\{U_a\} = \begin{Bmatrix} U \\ \bar{U}_r \end{Bmatrix}$$

where the spacecraft rotations $\{\theta_r\}$ are a subset of $\{U_r\}$. For no external loads acting on structure, the undamped equations of motion for displacement set $\{U_a\}$ become

$$[M_{aa}]\{\ddot{u}_a\} + [K_{aa}]\{u_a\} = 0 \quad (I-6)$$



Equation I-6 may be partitioned as follows:

$$\begin{bmatrix} M_{\ell\ell} & M_{\ell r} \\ \hline M_{\ell r}^T & M_{rr} \end{bmatrix} \begin{Bmatrix} \ddot{u}_\ell \\ \ddot{u}_r \end{Bmatrix} + \begin{bmatrix} K_{\ell\ell} & K_{\ell r} \\ \hline K_{\ell r}^T & K_{rr} \end{bmatrix} \begin{Bmatrix} u_\ell \\ u_r \end{Bmatrix} = 0 \quad (\text{I-7})$$

where the subset $\{U_r\}$ of the displacement vector is sufficient to define rigid body motion without additional constraints.

Now introduce the following "hybrid" transformation between modal coordinates $\{\eta\}$ and physical coordinates $\{u\}$:

$$\begin{Bmatrix} u_\ell \\ u_r \end{Bmatrix} = \begin{bmatrix} \phi_{\ell i} & D_{\ell r} \\ \hline 0 & I \end{bmatrix} \begin{Bmatrix} \eta_i \\ u_r \end{Bmatrix} \quad (\text{I-8a})$$

Note that

$$\begin{Bmatrix} U_{\ell \text{ relative to base}} \end{Bmatrix} = [\phi_{\ell i}] \{\eta_i\} \quad (\text{I-8b})$$

where

$[\phi_{\ell i}]$ = matrix of eigenvectors of structure with $\{U_r\} = 0$

$[D_{\ell r}]$ = rigid body transformation matrix
= $[T]$ in STARDYNE write-up

$[I]$ = identity matrix

$\{\eta_i\} = \{\xi_i\}$ = vector of flexible body modal (or generalized) coordinates.

where

$M(x)(t)$, $M_y(t)$, and $M_z(t)$ are jet torques or other external torque applied to spacecraft.

NUMERICAL VALUES OF FLEXIBILITY COEFFICIENTS

Table I-1 presents the equations of motion in terms of generalized coordinates which must be integrated for each solar array. The coefficients for the first four modes are presented. For checkout runs, only the first three modes are necessary.

TABLE I-1. NUMERICAL VALUES FOR GENERALIZED COORDINATE SOLUTION, NDS COARSE MESH SOLAR ARRAYS*

a. +Y Array

$$[I]\{\ddot{\eta}\} + [2\zeta w_n]\{\dot{\eta}\} + [w_n^2]\{\eta\} = -[]^T\{\ddot{u}\}$$

$[I]$ = unity matrix; ζ = 0.035 or less

Mode No.	F_n (Hz)	W_n (rad/sec)	+Y Array Participation Factors (γ_i) for Each Mode					
			\ddot{X}	\ddot{Y}	\ddot{Z}	\ddot{eX}^\dagger	\ddot{eY}^\dagger	\ddot{eZ}^\dagger
1	3.074	19.317	0	0.1676	1.501	10.983	0	0
2	3.491	21.933	1.245	0	0	0	-0.7963	-9.59
3	4.534	28.491	0.0337	0	0	0	0.4983	-0.344
4	10.05	63.171	0.0483	0	0	0	-0.2149	-0.155

b. -Y Array

Mode No.	F_n (Hz)	W_n (rad/sec)	-Y Array Participation Factors (γ_i) for Each Mode					
			\ddot{X}	\ddot{Y}	\ddot{Z}	\ddot{eX}	\ddot{eY}	\ddot{eZ}
1						-10.983	0	0
2						0	-0.7963	+9.59
3						0	0.4983	0.344
4						0	-0.2149	0.155

*Reference: Equation (I-10).

†STARDYNE DYNRE2 values divided by 12.0 to convert inches to feet.

Table I-2 presents the model displacements at node point 8 in the STARDYNE model so that the sun sensor displacements and angles relative to the base point can be computed. If only sun sensor rotations are needed, use only the values in the columns titled θX , θY , and θZ .

TABLE I-2. NUMERICAL VALUES FOR SUN SENSOR DISPLACEMENTS AND ROTATIONS PER UNIT GENERALIZED DISPLACEMENT*

a. +Y Array

Mode No.	F_n	Modal Displacements at Node 8, Coarse Model					
		X (ft/ft)	Y (ft/ft)	Z (ft/ft)	θX (rad/ft)	θY (rad/ft)	θZ (rad/ft)
1	3.074	0	0.0212	1.00	0.0209	0	0
2	3.491	0.9825	0	0	0	-0.0088	-0.0169
3	4.534	1.000	0	0	0	0.2087	-0.0198
4	10.05	-0.1109	0	0	0	0.1284	0.0125

b. -Y Array

Mode No.	F_n	Modal Displacements at Node 8, Coarse Model					
		X (ft/ft)	Y (ft/ft)	Z (ft/ft)	θX (rad/ft)	θY (rad/ft)	θZ (rad/ft)
1					-0.0209	0	0
2		← Same as for +Y Array (above) →			0	-0.0088	+0.0169
3					0	0.2087	+0.0198
4					0	0.1284	0.0125

*Reference: Equation (I-7).

†Example: $\theta Y_{+y \text{ array}} = [0. \quad -0.0088 \quad 0.2087 \quad 0.1284]$ $\begin{Bmatrix} \eta_1 \\ \eta_2 \\ \eta_3 \\ \eta_4 \end{Bmatrix}$
 where
 η_i = generalized displacement,
 i^{th} mode

Tables I-3 and I-4 present the forces and moments applied to a point at the intersection of the solar array pitch drive axis and the spacecraft centerline due to unit generalized deflections of each solar array. These forces and moments should be resolved into the torque summation about the spacecraft cg. For use with elastic arrays, the rigid-body mass of the spacecraft and its cg should not include the solar arrays.

TABLE I-3a. COARSE MESH MODEL INTERNAL FORCES AND MOMENTS, BEAM 1, NODE 1 FOR FIRST FOUR MODES (STARDYNE)*

Beam Load Component	Internal Beam Loads				Conversion to Loads Acting on Base Point
	Mode 1	Mode 2	Mode 3	Mode 4	
VA2, lb	0	-26.619	-19.044	-155.82	FX = -VA2
P, lb	-1.96	0	0	0	FY = -P
VA3, lb	17.5628	0	0	0	FZ = VA3
MA2, in-lb	-1036.8	0	0	0	$MX = \frac{1}{12}(-MA2 + 28.70 VA3)$
Torque, in-lb	0	+204.335	-3380.29	8319.51	$MY = -\text{Torque} \frac{1}{12}$
MA3, in-lb	0	-1695.2	-1787.76	-1530.01	$MZ = \frac{1}{12}(MA3 + 28.77 VA2)$

TABLE I-3b. FORCES AND MOMENTS AT (X = 0, Y = 0, Z = 38.0 inches) DUE TO UNIT GENERALIZED DISPLACEMENTS

Force Component	Units	Internal Beam Loads			
		Mode 1	Mode 2	Mode 3	Mode 4
FX	lb	0	26.619	19.044	155.82
FY	lb	1.96	0	0	0
FZ	lb	17.5628	0	0	0
MX	ft-lb	128.507	0	0	0
MY	ft-lb	0	-17.028	281.69	-693.29
MZ	ft-lb	0	-205.09	-194.64	-501.08

*Reference: Run SSNSOHC

TABLE I-4. FORCES AND MOMENTS AT X = 0, Y = 0, Z = 38.0 INCHES
DUE TO UNIT GENERALIZED DISPLACEMENTS OF -y ARRAY

Force Component	Units	Mode 1	Mode 2	Mode 3	Mode 4
FX	lb	0	26.619	19.044	155.82
FY	lb	-1.96	0	0	0
FZ	lb	17.5628	0	0	0
MX	ft-lb	-128.507	0	0	0
MY	ft-lb	0	-17.028	281.69	-693.29
MZ	ft-lb	0	205.09	194.64	501.08

If the solar array Z axis is shifted more than 5 or 10 deg from the spacecraft Z axis due to pitch rotation of the arrays, then the appropriate coordinate transformations are required. In Table I-1, the array participation factors for $\ddot{\bar{X}}$, $\ddot{\bar{Z}}$, $\theta\ddot{\bar{Z}}$, and $\theta\ddot{\bar{Y}}$ must be rotated. Also the FX, FZ, MX, and MZ forces and moments in Tables I-3b and I-4 must be rotated.

CHECKOUT RUNS

Figures I-5 through I-7 represent transient responses obtained at node 8 due to transient angular acceleration pulses.

For Figure I-5, the array pitch torque is assumed to be 1.0 ft-lb about θY for 50 msec. Using the Rockwell I_{yy} inertia value of 2.2335 slug/ft², this causes an angular acceleration of 0.4477 rad/sec². A reverse input of -0.153846 rad/sec² was applied for 325 msec to kill off the rigid body velocity. This forcing function approximates a solar array drive pulse input.

Two STARDYNE simulations were made, one using the first three modes (up to 4.5 Hz) and a second run using the first four modes (up to 10.0 Hz).

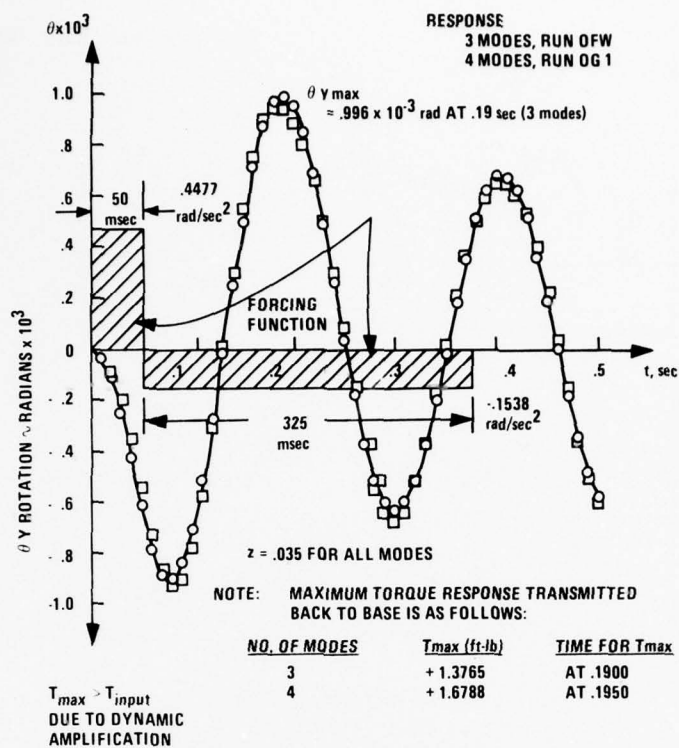


Figure I-5. Relative Angular Displacement in Torsion of NDS Coarse Model to a Single Drive Torque Pulse, STARDYNE DYNRE1 Solution

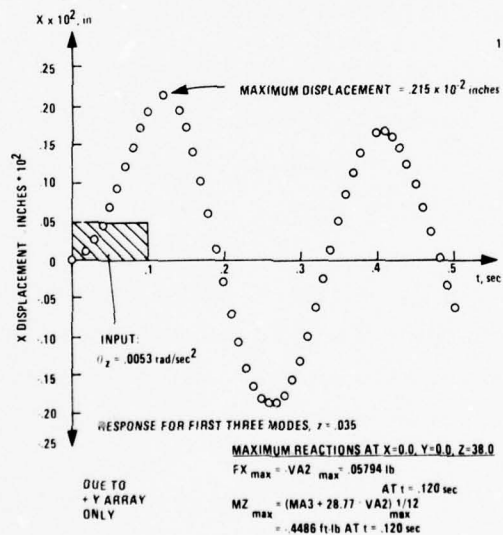


Figure I-6. Relative Boom Tip X Displacement, NDS Coarse Model, Due to Thruster Jet Pulse, STARDYNE DYNRE1 Solution *

*Reference: Run SSNSOQ9

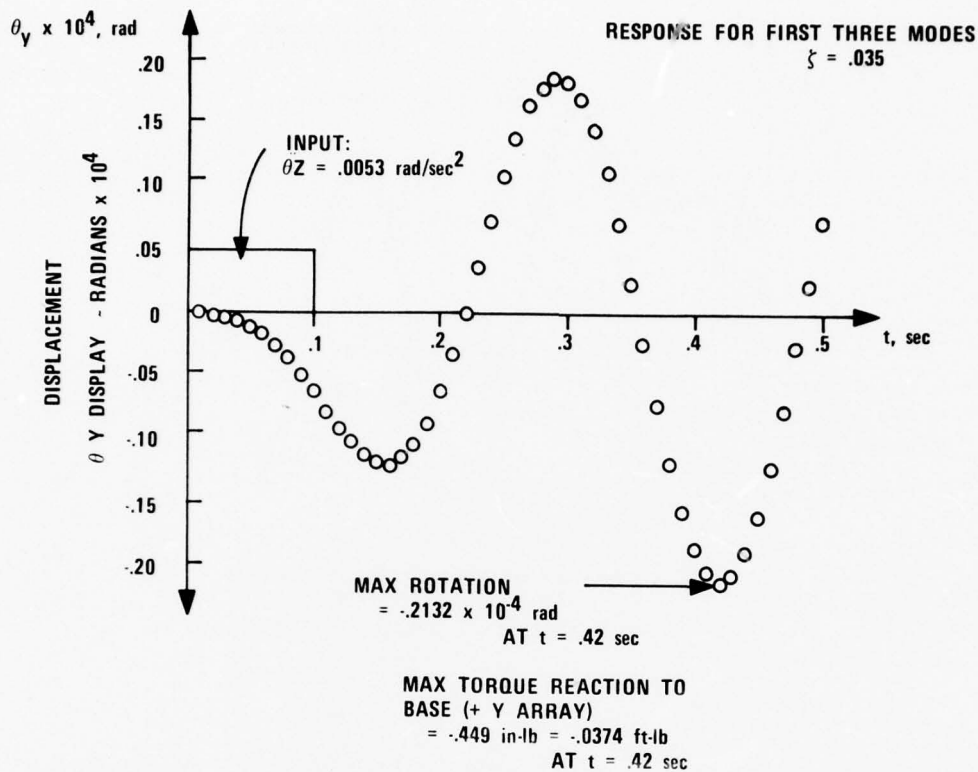


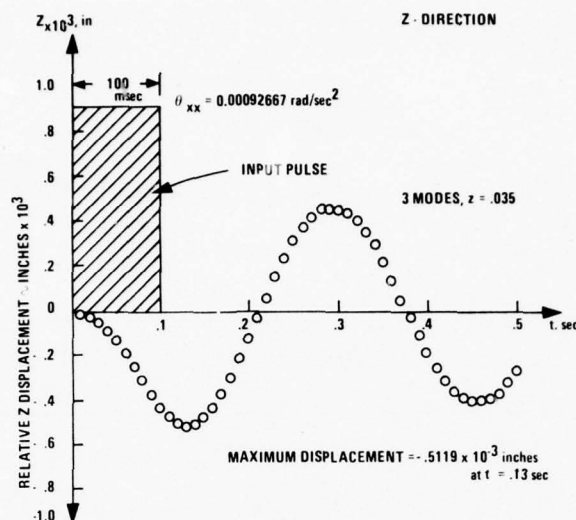
Figure I-7. Boom Tip and Sun Sensor θY Rotation Due to Yaw Thruster Jet Pulse, STARDYNE DYNRE1 Solution*

Figure I-6 presents the simulation for the arrays excited by the thruster jet firing about the yaw axis. Using an inertia estimate of 100 slug ft^2 and a torque of 0.53 ft-lb , an acceleration of 0.0053 rad/sec^2 about the array Z axis was input into the array base. The X response of node 8 at the tip of the boom is plotted.

Figure I-7, also for the same yaw thruster pulse, shows the +y array torsional response which is coupled with the X deflections due to the deployed boom offset from the pivot axis. The DYNRE1 solution was carried out to 2.5 sec and the peak θY response plotted at 0.42 sec is the maximum displacement observed.

For a roll thruster pulse of 0.0834 ft-lb with a rigid body inertia of 90 slug ft^2 , Figure I-8 shows the transient boom tip displacement in the Z direction.

*Reference: Run SSNSOQ9



MAXIMUM +Y ARRAY REACTIONS ON SPACECRAFT
AT X=0., Y=0., Z=38.0

$$FZ = VA3 = -.00899 \text{ lb AT } t = .13 \text{ sec}$$

$$MX = 1/12 (28.77 \times VA3 - MA2)$$

$$= -.0658 \text{ ft-lb at } t = .13 \text{ sec}$$

Figure I-8. Relative Boom Tip Displacement, Z, Due to Single Roll Thruster Pulse

Note that these checkout runs were made with the array Z axis oriented along the spacecraft Z axis.

FINE MESH SOLAR ARRAY FLEXIBILITY MODE

After the solar array flexibility structure had been determined and the latest boom and array stiff data obtained, a fine mesh solar array flexibility model was constructed. Table I-5 presents numerical values for the generalized or modal coordinates of the +Y and the -Y array. (Separate array models are used since they have individual pitch drive control systems and are not physically connected for torsion.)

Table I-6 presents the appropriate mode shape displacements and rotations at the outer ends of each boom ($Y = 104.97$ inches) which is close to the sun sensor.

Table I-7 presents the coupling terms which are used in torque contributions due to array generalized accelerations.

TABLE I-5. NUMERICAL VALUES, GENERALIZED COORDINATE SOLUTION,
NDS FINE MESH SOLAR ARRAYS*

a. +Y Array

$$[I]\{\ddot{\eta}\} + [2\zeta w_n]\{\dot{\eta}\} + [w_n^2]\{\eta\} = -[]^T\{\ddot{u}\}$$

[I] = unity matrix; $\zeta = 0.035$ or less

Mode No.	F_n (Hz)	W_n (rad/sec)	Participation Factors, $[\gamma]^T$, for Each Mode					
			\ddot{X}	\ddot{Y}	\ddot{Z}	$e\ddot{X}^\dagger$	$e\ddot{Y}^\dagger$	$e\ddot{Z}^\dagger$
1	3.9133	24.588	0	0.2149	1.8102	12.159	0.00005	0.00048
2	3.9138	24.591	1.3305	0	0	0.00039	-0.95706	-9.5772
3	5.086	31.958	0.3143	0	0	0	2.6012	-2.8584
4	9.75	61.289	0	-0.2788	0.4589	0.1847	0	0

b. -Y Array

Mode No.	F_n (Hz)	W_n (rad/sec)	Participation Factors, $[\gamma]^T$, for Each Mode					
			\ddot{X}	\ddot{Y}	\ddot{Z}	$e\ddot{X}$	$e\ddot{Y}$	$e\ddot{Z}$
1						-12.159	0.00005	-0.00048
2						-0.00039	-0.95706	9.5772
3						0	2.6012	2.8584
4						-0.1847	0	0

← Same as for +Y Array (above) →

*Reference: Equation (I-5).

[†]STARDYNE DYNRE2 values divided by 12.0 to convert inches to feet.

TABLE I-6. FINE MESH SOLAR ARRAY MODEL, MODE SHAPE AT SUN SENSORS
(Displacement and Rotations per Unit Generalized Displacement)

a. +Y Array*

Mode Number	F_n	Modal Values at Node 8, Fine Mesh Model					
		X (ft/ft)	Y (ft/ft)	Z (ft/ft)	θX (rad/ft)	θY (rad/ft)	θZ (rad/ft)
1	3.9133	-0.00031	0.03157	0.7797	0.01224	0	0
2	3.9138	0.9613	0	0	0	-0.00697	-0.01453
3	5.086	0.2432	0	0	0	0.01852	-0.00388
4	9.75	0	-0.0172	-0.437	-0.00709	0	0

b. -Y Array†

Mode Number	F_n	Modal Values at Node 8, Fine Mesh Model					
		X (ft/ft)	Y (ft/ft)	Z (ft/ft)	θX (rad/ft)	θY (rad/ft)	θZ (rad/ft)
1					-0.01224	0	0
2					0	-0.00697	0.01453
3					0	0.01852	0.00388
4					0.00709	0	0

← Same as +Y Array (above) →

*Reference: Equation (I-2).

†Reference: Run SSNSOQY

TABLE I-7a. NDS FINE MESH SOLAR ARRAY MODEL COUPLING TRANSFORMATIONS
FOR SPACECRAFT TORQUE SUMMATIONS DUE TO GENERALIZED
ACCELERATIONS, FIRST FOUR MODES

Mode No.	M_n General Mass (lb-sec ² /in)	$[M_n][\gamma_{nr}] = [M_n]$ (Participation Factors)					
		\ddot{X}^*	\ddot{Y}^*	\ddot{Z}^*	$\theta\ddot{X}$	$\theta\ddot{Y}$	$\theta\ddot{Z}$
1	0.028288	0	0.00608	0.0512	4.1274	0.000016	0.00016
2	0.044165	0.05876	0	0	0.000208	-0.5072	-5.0756
3	0.022699	0.0071	0	0	0	0.7085	-0.7786
4	0.011422	0	-0.0032	0.0052	0.0253	0	0

* Divide by 12 if used.

TABLE I-7b. $[M_n][\gamma_{nr}]^T$ FOR TORQUE SUMS DUE TO
GENERALIZED ACCELERATIONS

Axis	Mode 1	Mode 2	Mode 3	Mode 4	Array
TXX	4.1274	0.000208	0	0.0253	+Y
TTY	0.000016	-0.5072	0.7085	0	
TZZ	0.00016	-5.0756	-0.7786	0	
TXX	-4.1274	-0.000208	0	-0.0253	-Y
TTY	+0.000016	-0.5072	0.7085	0	
TZZ	-0.00016	5.0756	0.7786	0	

Figures I-9 through I-11 present geometry plots of the fine mesh math model. The deployment arm and fittings were not changed from the previous model (see Figure I-12). The honeycomb aluminum solar panels were modeled as shown in Figure I-13. Triangular plate elements were used because the STARDYNE quadrilateral plate element cannot model a honeycomb panel.

Each panel has a set of four hinges, similar to door hinges, to allow folding for launch. At each end of the panel a linkage is used to hold the panels out in the deployed position for orbit. These links were modeled by scaling off the drawings, and some error in the torsion mode could be caused by inaccuracies in the linkage model.

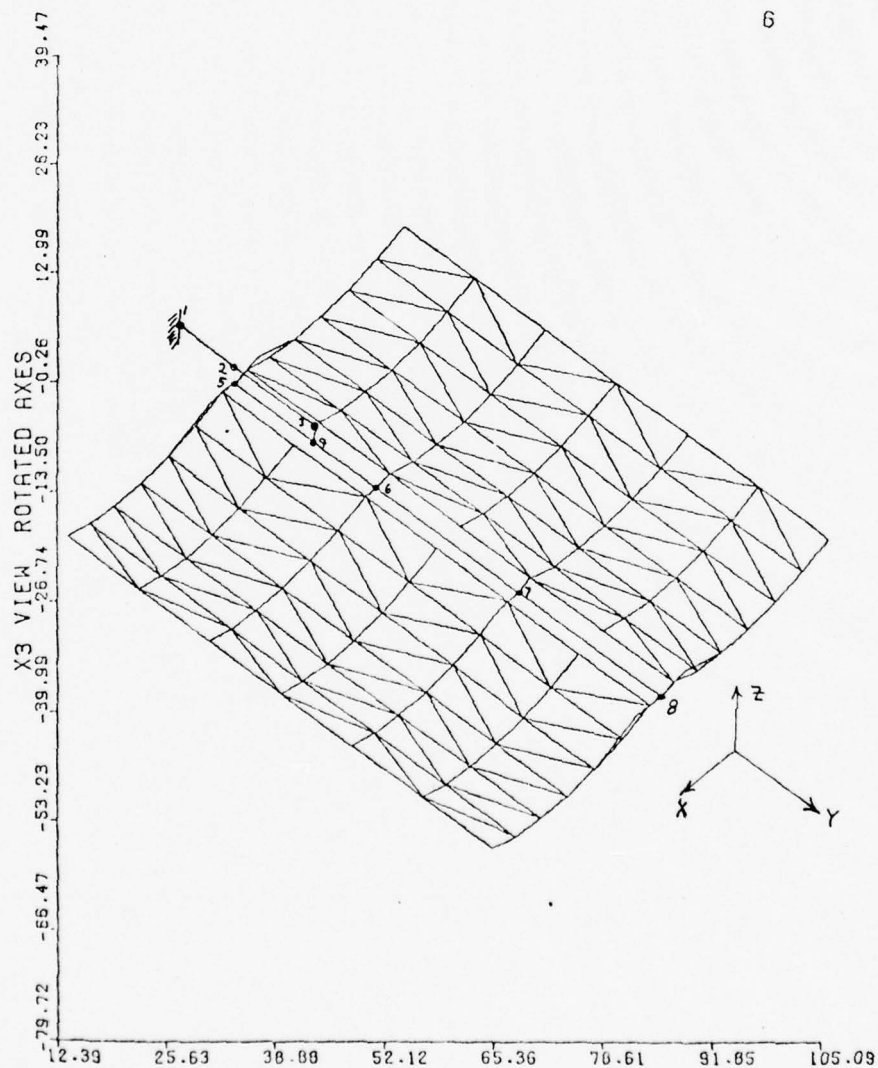


Figure I-9. NDS +Y Array Fine Mesh Dynamic Model, X3 Rotated View

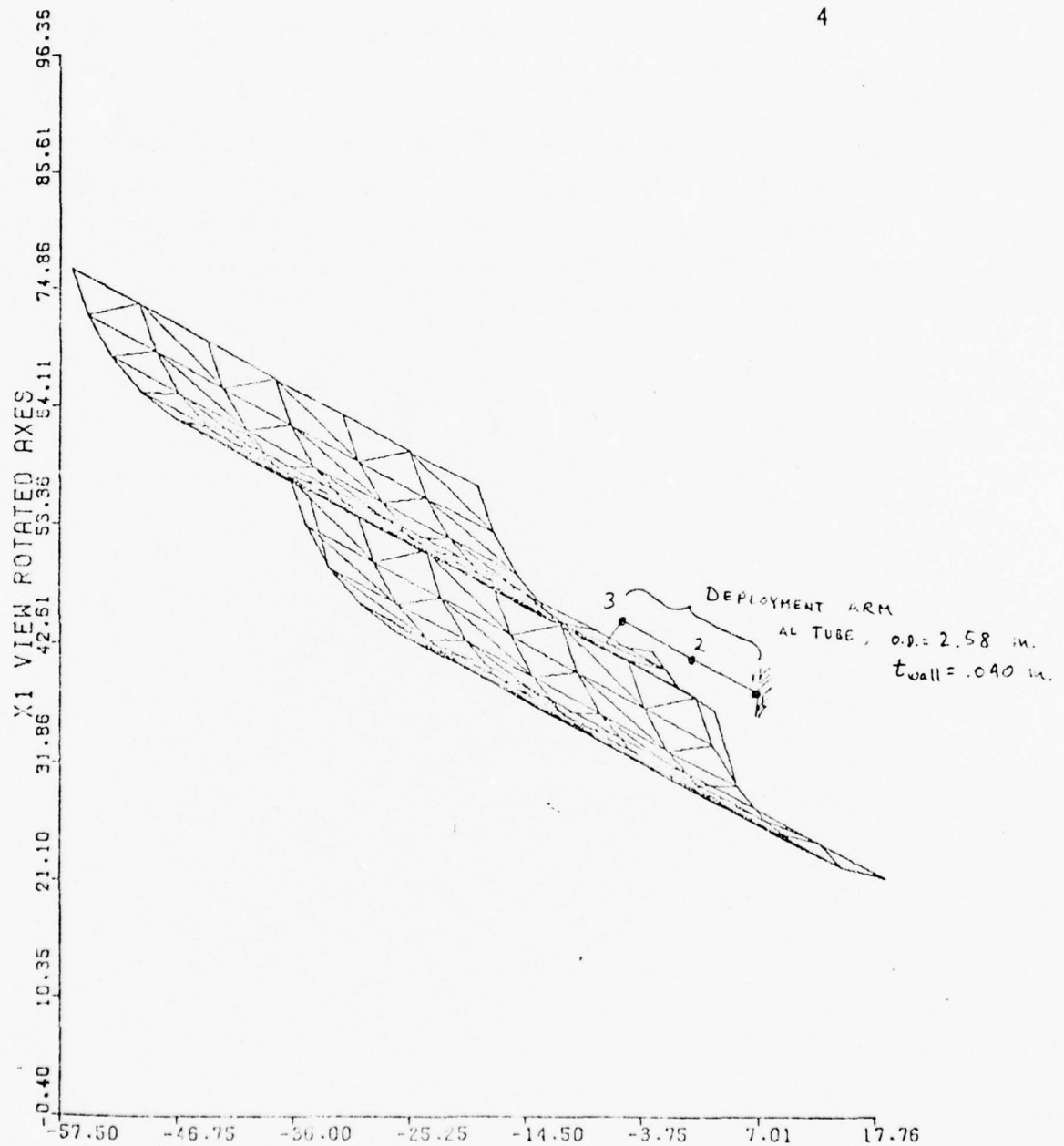


Figure I-10. NDS +Y Array Model, X1 Rotated View

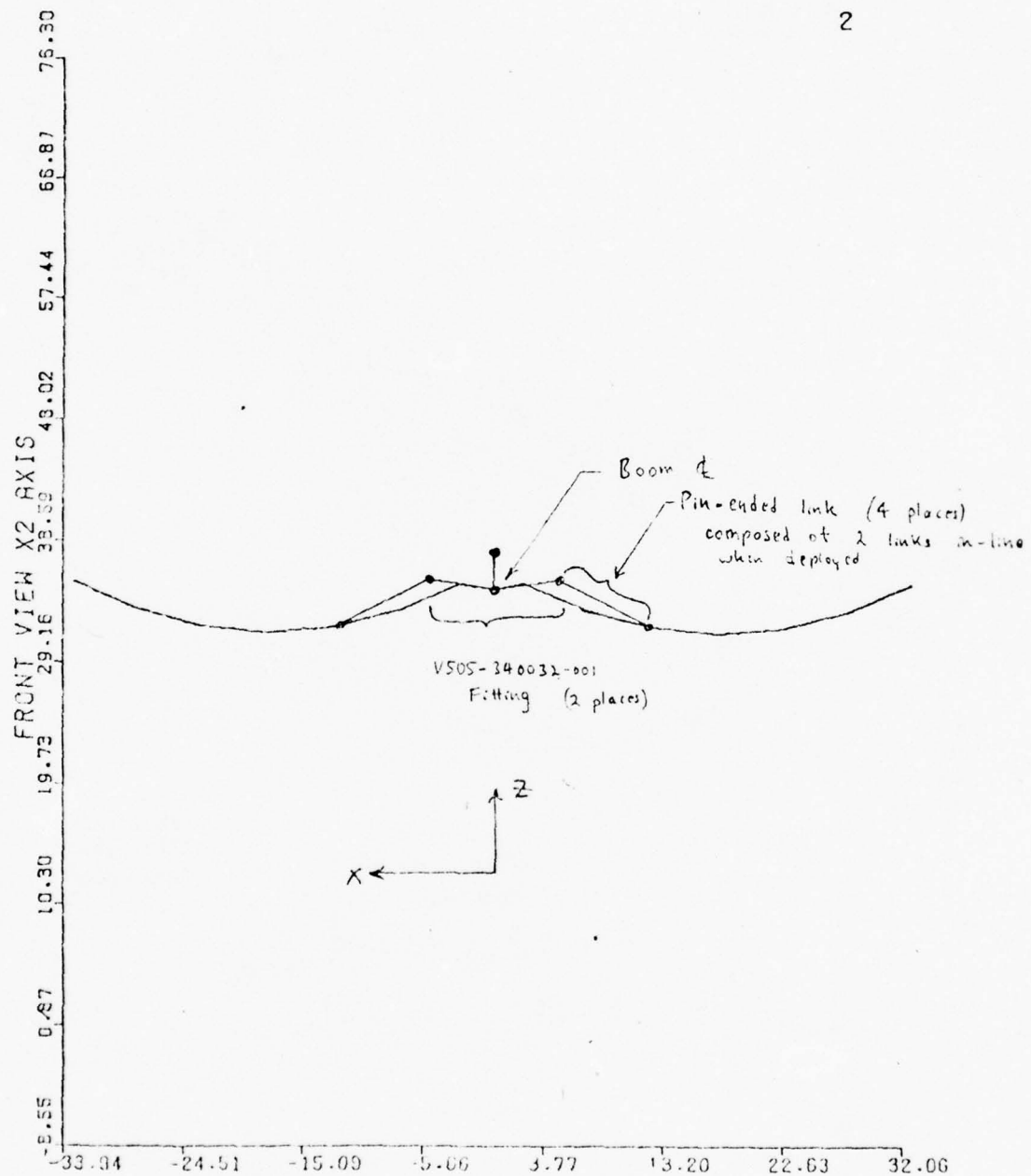


Figure I-11. NDS +Y Array Model End View, Looking Down Y Axis

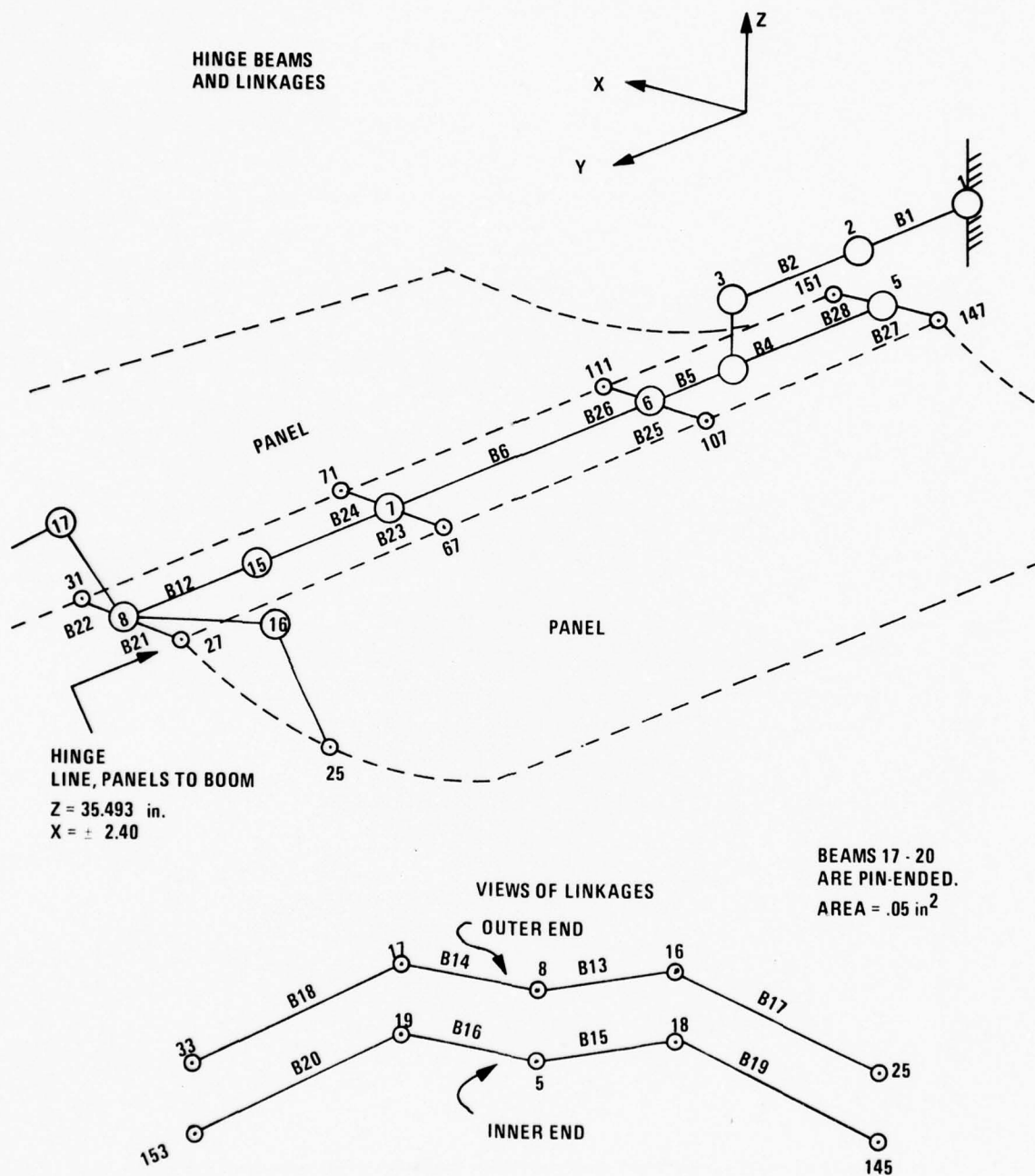


Figure I-12. NDS Solar Array, Fine Mesh Model

SUPPORTING DATA

Supporting data used in development of the fine mesh solar array flexibility model is presented below.

Solar Panel

(Reference: Drawing No. V505-93200)

$$R_o = 32.50 \text{ in.}$$

$$R_i = 32.00 \text{ in.}$$

$$R_{\text{mean}} = 32.25 \text{ in.}$$

$$\text{chord} = 30.59$$

$$\theta = \sin^{-1}(30.59/2)/32.25 = 28.3 \text{ deg}$$

$$t_{\text{core}} = 0.50 \text{ in.}$$

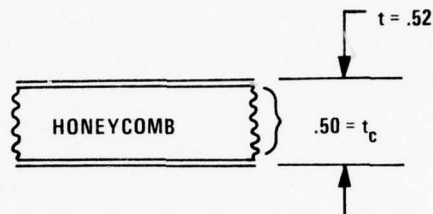
$$t_{\text{face sheets}} = 0.010 \text{ in.}$$

$$\text{Face sheets} = \text{aluminum} \quad E = 10 \times 10^6$$

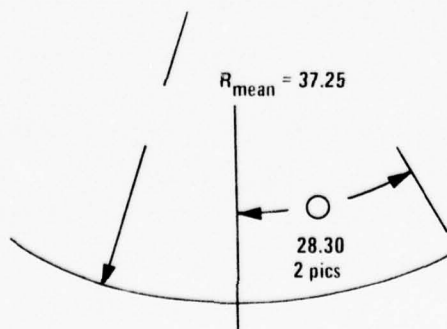
$$\text{core} = 1/4 \text{ cell Al honeycomb, } 2.3 \text{ lb/ft}^3 \text{ density}$$

$$G_c \text{ (core shear modulus)} = 27,000 \text{ psi average in "L" direction}$$

$$\text{average } G_c = \frac{27,000 + 14,000}{2} = 20,500 \text{ psi}$$



Assume isotropic core properties.



Origin for Array Cylindrical Coordination System

ICYL = 2

X2 = H

A = 0 deg at +X3 axis

X3_{cg} = Z station = 33.0

approximately 1.25 in. above inside mean radius

R_{mean} ≈ 32.25

X3 = (32.25 - 1.25) + 33.0

= 64.0 in. (Adjust origin after geometry check)

For -X Array

Point A: X1 = -17.7

X2 = 0

X3 = 64.

Measured Drawing No. V505-932003

From angle = 180 deg + 28.32 = 208.32

To angle = 180 deg - 28.32 = 151.68

Point B: X1 = -0.0

X2 = 0.0

X3 = 64.

Point C: X1 = -10.

X2 = +10.

X3 = 64.

For +X Array

Point A: X1 = +17.7

X2 = 0.

X3 = 64.

Point B: X1 = 50.

X2 = 0.

X3 = 64.

Point C: X1 = 30.

X2 = 10.

X3 = 64.

TABLE I-8. ROCKWELL WEIGHTS DATA

ACC DEPLOYED APPAY X-Y PLANE														
VEH	FC	DESCRIPTION	NC	NO	MC	WEIGHT	XCG	YCG	ZCG	RCX	PGY	RGZ	PXY	PIZ
GPS	FAA	ARRAY			I E	6.92	15.5	71.3	33.0	19.1	9.0	21.1	C.	0.
GPS	FAA	ARRAY			I E	6.92	-15.5	71.3	33.0	19.1	9.0	21.1	C.	0.
GPS	FAA	450002 SUBSTRATE			I C	8.22	-15.5	71.3	33.0	19.4	9.1	21.3	C.	0.
GPS	FAA	450002 SUBSTRATE			I C	8.22	15.5	71.3	33.0	19.4	9.1	21.3	C.	0.
GPS	FCB	SLP PNL SUBST 1	N		I E	0.20	-15.5	71.3	33.0	19.4	9.1	21.3	C.	0.
GPS	FLB	SLP PNL SUBST 1	N		I E	0.20	15.5	71.3	33.0	19.4	9.1	21.3	C.	0.
GPS	FAA	ARRAY SHUNT			I E	2.00	0.0	66.8	35.0	3.0	3.0	3.0	C.	0.
GPS	FAA	SUN SENSOR			I E	0.36	0.0	96.0	33.0	1.0	1.0	1.0	C.	0.
GPS	ARA	340040 ROOM +Y	S		I C	5.61	0.0	71.5	25.0	20.3	1.7	20.3	C.	0.
GPS	ABA	MC470-0145 PLY+Y	S		I C	2.58	0.0	71.5	25.0	20.3	1.7	20.3	C.	0.
GPS	ARA	340030 ROOM A/PY	S		I C	6.30	0.0	71.5	35.0	20.3	1.7	20.3	C.	0.
GPS	ABB	340071 DEPL MECH	S		I C	7.69	-2.0	41.3	27.5	6.7	0.6	6.7	C.	0.
GPS	ABC	340031 LINK	S		I C	0.68	0.0	37.5	37.0	0.1	0.4	0.4	C.	0.
GPS	ABC	340021 LINK	S		I C	0.68	0.0	105.0	27.0	0.1	0.4	0.4	C.	0.
GPS	ABE	340018 STRAP APT	S	4	C	0.20	0.0	71.5	37.5	19.0	9.0	20.0	C.	0.
GPS	HGA	340040 A/P BOX	S		I C	0.04	0.0	71.5	25.0	0.0	0.0	0.0	C.	0.
GPS	HGA	240112 COVER +Y	S		I C	0.25	0.0	71.5	35.0	0.0	0.0	0.0	C.	0.
GPS	HGA	240111 BOX +Y	S		I C	0.57	0.0	71.5	35.0	0.0	0.0	0.0	C.	0.

TABLE I-8. ROCKWELL WEIGHTS DATA (concluded)

GPS	HGA	340105	FIG +Y	5	1 C	0.11	0.0	07.0	28.8	0.0	0.0	0.0	0.0
GPS	HGA	340105	COND ASSY	5	1 C	0.19	0.0	07.0	30.9	0.0	0.0	0.0	0.0
GPS	HGA	A	DP PICTAIL	1	1 C	1.10	0.0	42.0	37.5	7.5	0.0	7.5	0.0
GPS	HAE	451201	SCOM XDCP	1	1	0.18	0.0	0.0	35.0	71.5	0.0	71.5	0.0
GPS	HAF	451208	SOL THERM	1	1	0.45	0.0	0.0	25.0	71.5	0.0	71.5	0.0
GPS	HAG	451200	SOL J-BOX	1	1	0.74	0.0	0.0	35.0	71.5	0.0	71.5	0.0
GPS	HAG	451202	SOL FWP	1	1	0.12	0.0	0.0	35.0	71.5	0.0	71.5	0.0
GPS	HAG	451204	SOL OPLMT	1	1	0.58	0.0	0.0	35.0	71.5	0.0	71.5	0.0
GPS	HGA	TRANSOPES		2		0.66	0.0	75.0	28.0	0.0	0.0	0.0	0.0

***TOTAL WEIGHT = 57.56

XCMENT = -15% XCG = -0.27 PGX = 27.5
 YCMENT = 3725. YCG = 64.27 PGY = 12.4
 ZCMENT = 1584. ZCG = 34.24 PGZ = 30.4

STATUS**PCOUNDS***PERCENT OF TOTAL WEIGHT

ESTIMATED =	16.60	28.6	STAR DYNE	FINE	MESH	MODEL	RESULTS
ACTUAL =	0.0	0.0	WTE	57.96	X CG =	0.0	
CALCULATED =	37.97	65.5			Y CG =	64.645 in.	
HIGH QUALITY =	0.0	0.0			Z CG =	34.279 in.	

MOMENTS OF INERTIA :

LB IN2	43934.1172	IYY =	10347.7539	IZZ =	52453.6016
SLUG FT2	5.4827	IYY =	2.02335	IZZ =	11.5374

PRODUCTS OF INERTIA:

LB IN2	353.2314	IXZ =	-50.2000	IYZ =	-924.1250
SLUG FT2	0.0762	IXZ =	-0.0108	IYZ =	-0.1993

One Solar Panel (-X Array)

Weight = 15.34 lb excluding boom

$$\left. \begin{array}{l} X_{cg} = -15.5 = X1 \\ Y_{cg} = 71.3 = X2 \\ Z_{cg} = 33.0 = X3 \end{array} \right\} \text{STARDYNE Notation}$$

$$\text{Total area, one panel} = 2133.576 \text{ in}^2$$

Modify material density (MATLG 2 card) to make face sheet density match total density.

$$\begin{aligned} \text{Total volume, face sheets} &= \text{AREA} \times 0.020 \text{ in.} \\ &= 2133.576 \times 0.020 \\ &= 42.67152 \text{ in}^3 \end{aligned}$$

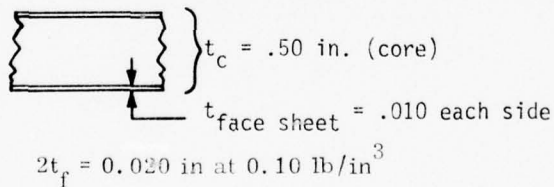
$$\text{Composite gross density} = \frac{15.34 \text{ lb}}{42.67152 \text{ in}^3}$$

$$\rho_2 = 0.35949 \text{ lb/in}^3$$

Solar Panel Distributed Weights

$$\text{Honeycomb core material} = 2.3 \text{ lb/ft}^3$$

$$\rho = \frac{2.3}{1728} = 0.001331 \text{ lb/in}^3$$


$$2t_f = 0.020 \text{ in at } 0.10 \text{ lb/in}^3$$

Composite density based on face sheet thickness is, for 1 square inch of panel,

$$wt_{\text{face}} = 0.10 \text{ lb/in}^3 \times 0.020 \text{ in} = 0.002 \text{ lb}$$

$$wt_{\text{core}} = 0.001331 \times 0.50 = \frac{.0006655}{.0026655} \text{ lb}$$

Increase density of face sheets:

$$\zeta = \frac{0.0026655}{0.002} \times 0.10 = 0.13328 \text{ lb/in}^3$$

to account for core material and face sheets.

Distributed Weight, One Panel

$$\text{AREA} = 72 \text{ tri-plates} \times 29.633 \text{ in}^2 = 2133.576 \text{ in}^2$$

From weights statement, -X panel

$$\text{GPS FAA ARRAY} = 6.92 \text{ lb}$$

$$\text{FAA 450002 SUBSTRATE} \approx 8.22 \text{ lb}$$

$$\text{FDB SLR PNL SUBSTRATE} = \frac{0.20}{15.34} \text{ lb}$$

Weight Shifts on Solar Panel (STARDYNE Run SSNS05A)

(-X panel geometry check)

$$\text{WT} = 15.34 \text{ lb} \quad \left\{ \begin{array}{l} X_{cg} = -17.7 \text{ in.} \\ Y_{cg} = 71.47 \text{ in.} \\ Z_{cg} = 33.1173 \text{ in.} \end{array} \right\} \quad \begin{array}{l} \text{based on uniform} \\ \text{density panels} \end{array}$$

$$\text{Desired cg:} \quad \left\{ \begin{array}{l} X_{cg} = -15.5 \text{ in.} \\ Y_{cg} = 71.3 \text{ in.} \\ Z_{cg} = 33.0 \text{ in.} \end{array} \right\}$$

The model can be simulated, from the distributed weights above, as follows:

Node No.	Weight (lb)	X, in.	W · X
21	0.10653	-33.0	-3.51549
41	0.21306	↓	-7.03098
61	↓		↓
81			
101			
121			
141	0.10653	↓	-3.51549
Totals:	1.27836 = W _{edge}		-42.18588

$$\bar{W} \cdot \bar{X} = 15.34 \times -17.7 = -271.518 \quad - \text{current}$$

$$\text{desired } W \cdot \bar{X} = 15.34 \times -15.5 = -237.77$$

$$\Delta(W \cdot \bar{X}) = 33.748$$

$$W_{\text{edge}} \times (X1_{\text{new}} - X1) = 33.748 \text{ in-lb}$$

$$(X1_{\text{new}} - (-33.0)) = \frac{33.748}{1.27836} = 26.3994 \text{ in.}$$

$$X1_{\text{new}} = 26.39945 - 33.0 = -6.6005 \text{ in.}$$

Weight Shift, -X Panel (X-Direction Shift)

$$W_{\text{edge}} = 1.27836 \text{ lb} \quad X_{\text{edge}} = -33.0 \text{ in.}$$

$$W_{\text{panel}} \cdot \bar{X}_c = 15.34 \times -17.7 = -271.518 \text{ (current)}$$

$$W_{\text{panel}} \cdot \bar{X}_{\text{desired}} = 15.34 \times -15.5 = -237.77 \text{ (desired)}$$

$$\Delta W \cdot X = 33.748 \text{ (to match Rockwell weight report)}$$

$$W_1 = a \cdot W_{\text{edge}} = \text{weight left at outer edge of panel}$$

$$W_2 = (1 - a)W_{\text{edge}} = \text{weight shifted to inner edge of panel}$$

$$W_2(X_{\text{new}} - X_{\text{old}}) = \Delta W \cdot X$$

$$W_2(-2.400744 + 32.99926) = 33.748$$

$$W_2(30.59852) = 33.748 \text{ in-lb}$$

$$W_2 = 1.102929 \text{ lb}$$

Subtract 1.102929 lb from outer edge.

Add 1.102929 lb to inner edge.

Node No.	Node No.	ΔW
21	37	-0.09191075
41	57	-0.1838215
61	77	<div style="text-align: center;"> </div>
81	97	
101	117	
121	137	
141	157	-0.09191075
-X	+X	-1.102929
Panel	Panel	

Node No.	Node No.	ΔW
27	31	+0.09191075
47	51	+0.1838215
67	71	<div style="text-align: center;"> </div>
87	91	
107	111	
127	131	
147	151	+0.09191075
-X	+X	+1.102929
Panel	Panel	

Aluminum Tube, Strut Assembly (Deployment Arm)*

Major portion is machined down to

ID = 2.500 in. diameter

$t_{\text{wall}} \approx 0.040$ in.

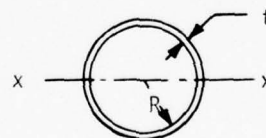
mean diameter = ID + t_{wall}
= 2.540 in.

$$\begin{aligned}
 I_{x-x} &= \pi R^3 t \\
 &= \pi (2.54/2)^3 0.040 \\
 &= 0.2574 \text{ in}^4
 \end{aligned}$$

$$I_{z-z} = I_{x-x} = 0.2574$$

$$A = \pi D t = 0.314 \text{ in}^2$$

$$I_{yy} = Z I_{xx} = 0.52 \text{ in}^4$$



BPROP1 No. 1

* Part No. V505-340052, Reference: D/N V505-932004.

BEAM 3 SECTION PROPS

BPROP 1, No. 2

$$I_y = (Ad^2)(2) = (1.5)(0.25)(2.12)^2(2) = 3.37$$

$$I_z = BH^3/12 = (0.50)(1.50)^3/12 = 0.140$$

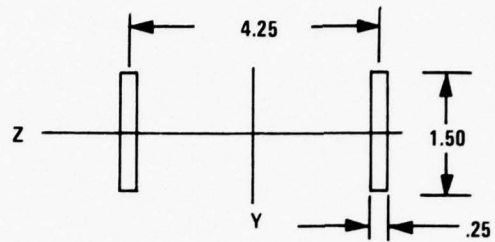
$$I_x = \left\{ ab^3 \left[\frac{16}{3} - 3.36 \frac{b}{a} \left(1 - \frac{b^4}{12a^4} \right) \right] \right\} Z$$

$$a = \frac{1.50}{2} = 0.75$$

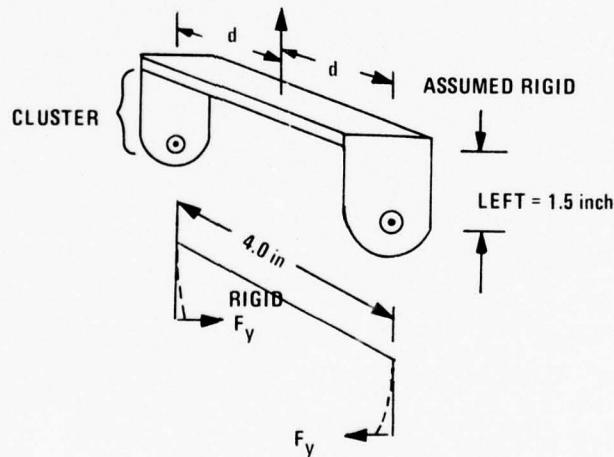
$$b = \frac{0.25}{2} = 0.125$$

$$I_x = 0.014 \leftarrow \text{ignores } 2 \times K \cdot d^2 \text{ stiffness}$$

$$A = (1.50)(0.25)(2) = 0.75 \text{ in}^2$$



BPROP 1 NO. 2



$$\theta = \frac{TL}{JG}$$

$$= T \times K_{\theta\theta}$$

$$K_{\theta\theta} = 9.952 \times 10^6 \text{ in-lb/radian}$$

Use matrix addition

for $\theta X3$, nodes 3 and 4.

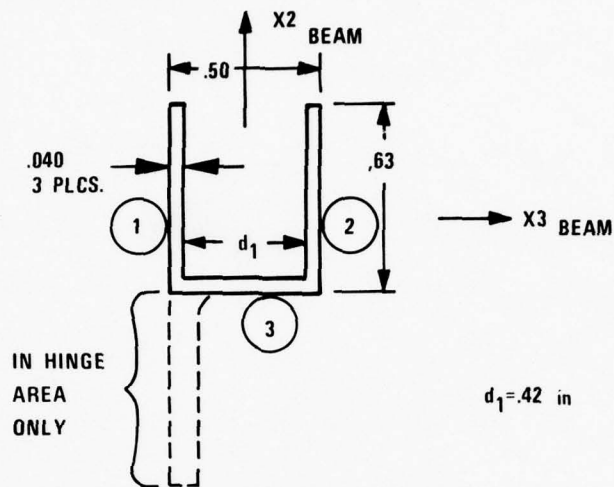
$$K_1 = \frac{3EI_z}{L^3} = \frac{3 \times 10.0 \times 10^6 \times 0.140}{1.5^3} = 1.244 \times 10^6$$

$$K_{\theta\theta} = 2 \cdot K \cdot d^2 = 2 \times 1.244 \times 10^6 \times 2^2$$

Aluminum Channel Beam Along Long Sides of Panel*

Along hinge side (between hinges):

ALONG HINGE SIDE (BETWEEN HINGES)



$$d_1 = .42 \text{ in}$$

Segment	Area	$A \cdot X_2$	$X_2 - \bar{X}_2$	$A(X_2 - \bar{X}_2)^2$	$I_{O_{X_3} - X_3}$	X_2
1 + 2	0.63×0.080 $= 0.0504$	0.015875	0.07375	0.00027413	$\frac{1}{12}(0.08)(0.63)^3$ $= 0.00166698$	0.315
3	0.92×0.040 $= 0.0168$	0.000336	-0.22125	0.00082239	$\frac{1}{12} \times 0.42(0.040)^3$ $=$	0.020
Totals	0.0672	0.016212		0.0010865	0.0016692	

$$\text{Area} = 0.0672 \text{ in}^2$$

$$\bar{X}_2 = \frac{0.016212}{0.0672} = 0.24125$$

$$I_{X_3} = 0.0010965 + 0.0016692$$

$$= 0.002766 \text{ in}^4$$

$$I_{X_2} = \frac{1}{12} 0.63 \times 0.50^3 - \frac{1}{12} 0.59(0.42)^3$$

$$= 0.0065625 - 0.00364266$$

$$I_{X_2} = 0.00292 \text{ in}^4$$

$$J = \sum \delta L t^3 \approx \frac{1}{3}(0.63 + 0.63 + 0.42)(0.040)^3$$

$$= 0.0000358 \text{ in}^4$$

*BPROP1 No. 11, Reference: Rockwell Drawing No. V505-450003.

EFFECT OF DRIVE LINK ADDITION

Because of the discrepancy in model versus test torsional frequency, the effect of adding a flexible torsion lock or drive link was investigated using the coarse mesh model. Figure I-14 shows the modified model with the flexible drive link introduced with nodes 28 and 29.

Table I-9 presents the results of such modification on natural frequencies. The torsional frequency was reduced from 6.84 Hz to from 5.13 to 6.16 Hz, depending on the model of the drive link used. Although test and model frequencies were still in slight disagreement, these results indicate that the torsional frequency would be higher in flight than the test indicates.

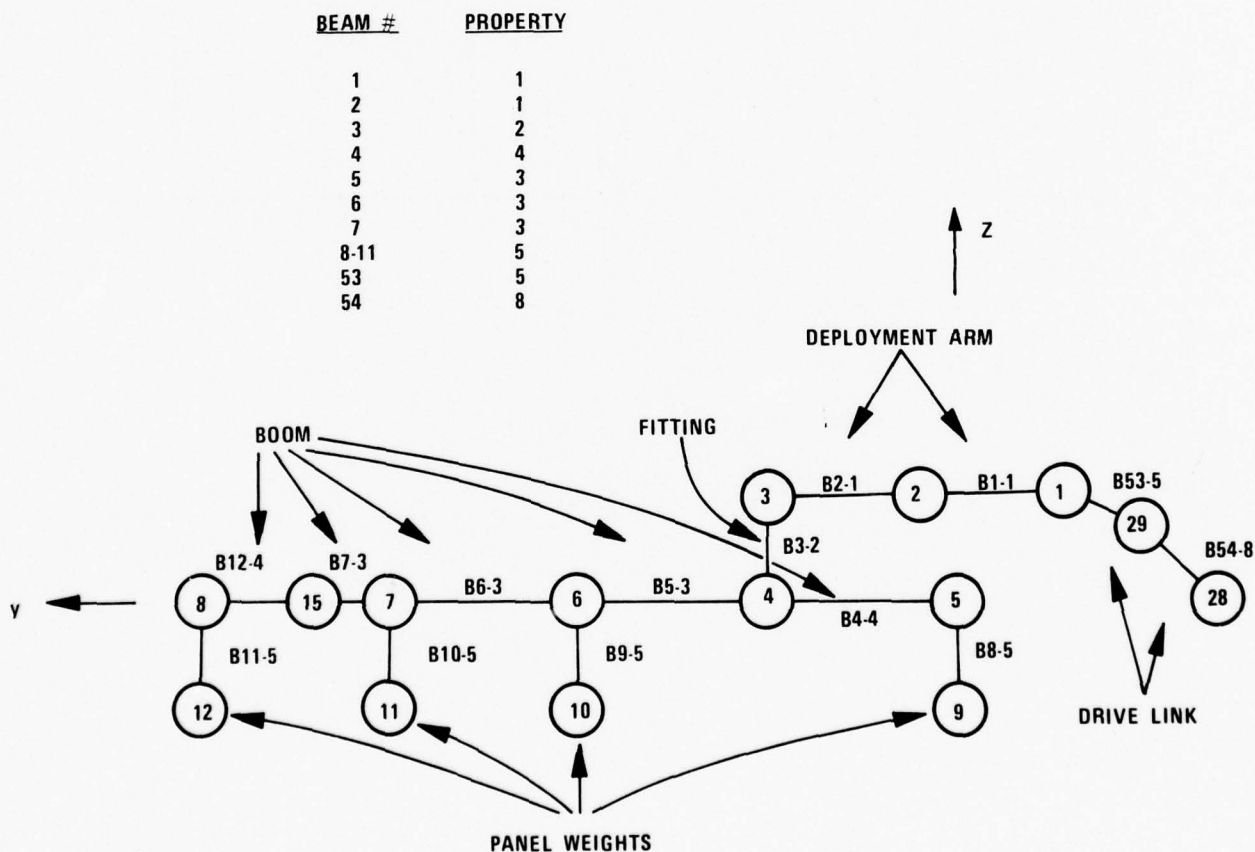


Figure I-14. Present Coarse Model with Flexible Drive Link

TABLE I-9. STARDYNE FREQUENCIES OF MODIFIED MODEL

Mode Shape Description	Test Frequency (Hz)	STARDYNE Model Frequencies (Hz)			
		A	B	C	D
Bending, normal to panel Z-direction	4.1	3.07	3.75	3.75	3.75
Bending, in plane to panels X-direction	4.8	3.49	3.75	3.70	3.74
Torsion about Y-axis	3.1	4.53	6.84	5.13	6.16

Condition:

- A From reference (old boom stiffnesses).
- B With new boom stiffnesses.
- C With drive-link addition.
- D With expanded drive-link addition.

APPENDIX J

COMBINED EARTH SENSOR MODEL

APPENDIX J

COMBINED EARTH SENSOR MODEL

INTRODUCTION

This appendix describes the model developed for the GPS combined earth sensor. The model can be used to evaluate acquisition as well as normal operation.

This model is based on information obtained from Barnes Engineering Company at a meeting in St. Petersburg, Florida on March 13, 1975, and a subsequent phone call, and the Rockwell procurement specification for the sensor.

SENSOR DESCRIPTION

The Combined Earth Sensor is a two-axis, static sensor which incorporates two horizon crossing indicators for spinning mode attitude sensing. The adjective static means the sensor uses no moving parts in the measurement of attitude.

The two-axis sensor consists of an optical system, 24 thermopile detectors, and processing electronics. The 24 detectors are arranged on the focal surface of the optical system. The earth image is tangent to the inner edges of the A detectors at null at the design altitude. Two roll and two pitch measurements are computed sequentially by switching sums and differences of various detector outputs to the input of an integrator. Each measurement is sampled and held for comparison check and possible output. A new roll and new pitch measurement is computed each $1/4$ second. Roll and pitch computations are separated by $1/8$ second. The S detectors are for space reference and are used with the A detectors for accurate

measurements over $+1^\circ$ in the track mode. The A and B detectors are used in the acquisition mode for $+4^\circ$ range. The thermopile detectors have a time constant of 1.4 seconds and are sensitive to the 14 to 16 micron wavelengths (CO_2 band). The sensor continuously tests all signals and rejects spurious or incorrect signals due to sun, moon, or other anomalies.

The two horizon crossing indicators consist of 3 degree by 3 degree square fields of view. One diagonal of each square is parallel to the scan path. One field is 10° from the -X axis toward +Z and the other is 10° from -X toward -Z (Spin rotation is about the Z axis). The detectors are pyroelectric with insignificant time constant.

MODEL DESCRIPTION

The model consists of an initialization and two normal operation sections. The initialization section performs one-time computations and clears outputs and counters. One normal operation section is for the horizon crossing indicators used in the spin phase. The other normal operation section is for two-axis earth sensing.

Characteristics of the horizon crossing indicator model are as follows:

- Inputs to the model are spacecraft position vector from center of earth, and spacecraft attitude direction cosine matrix. Both inputs must be relative to the same reference frame.
- When a sensor line of sight crosses the edge of the earth, the time from the crossing to the sample time is output. If no crossing occurs in the sample interval, the output is set to $-\Delta t$.
- If a sensor line of sight crosses the earth very close to a tangent, there may not be an output. The sample, Δt , should be small

enough so that this loss of output does not happen when attitude determination is critical. Select Δt as follows:

$$\Delta t \leq \frac{1}{W_s} \sqrt{1 - \frac{\ell}{r_e}}^2 \tan^{-1} \left[\frac{1}{\left[\left(1 - \frac{h}{r_e}\right)^2 - 1 \right]^{\frac{1}{2}}} \right]$$

where

W_s = spin rate in rad/sec

$$= \frac{2\pi}{60} W_{\text{RPM}}$$

W_{RPM} = spin rate in rev/min

h = satellite altitude in n. mi. ($100 \leq h \leq 10897$)

r_e = earth radius in n. mi. (3440)

ℓ = distance from earth center to chord of detector path in n. mi.

e.g.

let

$W_{\text{RPM}} = 100$

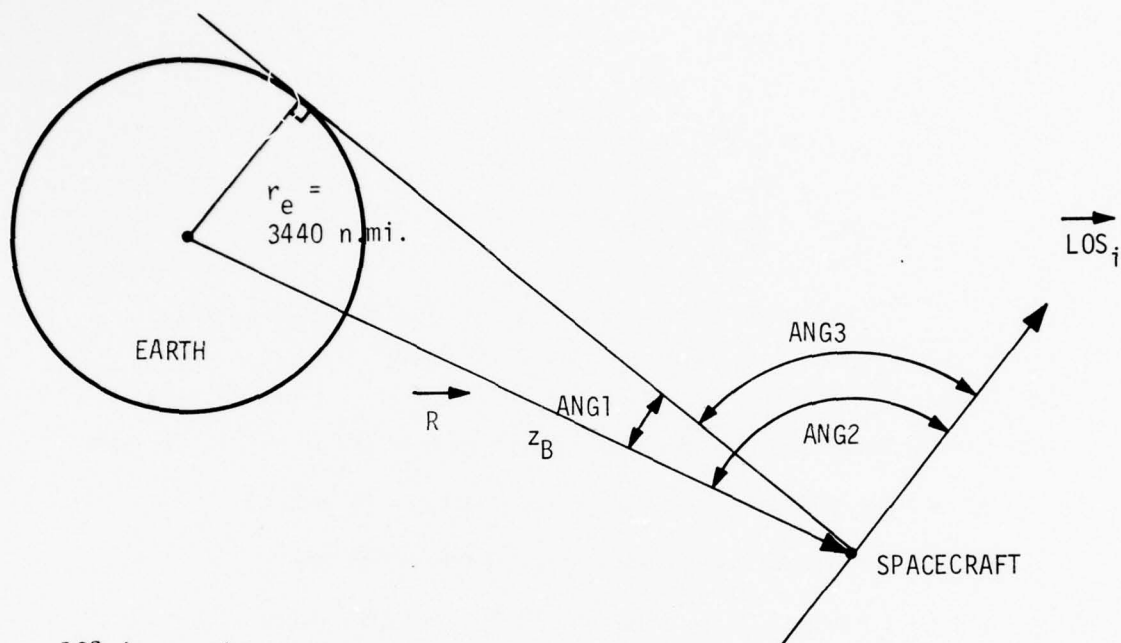
$h = 10897$

$r_e = 3440$

$\ell = 3405.6 = 0.99 r_e$

then $\Delta t \leq 0.00326$ seconds.

o The equations used in the flow diagram are derived below



LOS is a unit vector

$$\frac{|\vec{R} \times \vec{LOS}|}{|\vec{R}|} = \sin (ANG2)$$

$$\frac{\vec{R} \cdot \vec{LOS}}{|\vec{R}|} = -\cos (ANG2)$$

$$ANG2 = \tan^{-1} \frac{\sin (ANG2)}{\cos (ANG2)}$$

$$ANG2 = \tan^{-1} \frac{|\vec{R} \times \vec{LOS}|}{-\vec{R} \cdot \vec{LOS}}$$

$$\begin{aligned}
 \text{ANG1} &= \text{SIN}^{-1} \frac{r_e}{|\vec{R}|} \\
 &= \text{TAN}^{-1} \frac{r_e/|\vec{R}|}{[1 - (r_e/|\vec{R}|)^2]^{\frac{1}{2}}} \\
 &= \text{TAN}^{-1} \frac{r_e}{[|\vec{R}|^2 - r_e^2]^{\frac{1}{2}}}
 \end{aligned}$$

$$\text{ANG3} = \text{ANG2} - \text{ANG1}$$

Note that $3440 + 100 \leq |\vec{R}| \leq 10897 + 3440$ n. mi.
 $13.8^\circ \leq \text{ANG1} \leq 76.4^\circ$.

Characteristics of the two-axis earth sensor model are as follows:

- The sensor output is updated every 1/8 second.
- The sensor model has four states which are:

State 1	Compute Roll 1, Output Pitch 2 if valid
State 2	Compute Pitch 1, Output Roll 1 if valid
State 3	Compute Roll 2, Output Pitch 1 if valid
State 4	Compute Pitch 2, Output Roll 2 if valid

The state is advanced every 1/8 second.

- Each detector area is divided into $1^\circ \times 1^\circ$ squares. The area coverage of each $1^\circ \times 1^\circ$ square by the earth is computed from the distance between center of the earth circle on the focal surface and the center of the square. The orientation of the square is not considered.
- The position of the earth image on the focal surface (B&C) is computed from true attitude. The diameter of the earth image on the focal surface (RE) is computed from satellite altitude. Measurements on the focal surface are in equivalent radians.

- Each detector output is the sum of the coverages of $1^\circ \times 1^\circ$ squares within the detector.
- The sensor output is computed from the detector outputs according to the functions in the electronics.
- Functions of the system programmer to reject spurious or incorrect signals is included.
- Subroutine must be initialized by calling with MODE = 0 prior to operating in two-axis mode.
- The time increment, Δt , should be selected from one of the following to synchronize with the sensor update frequency:

<u>Recommended Δt</u>	<u>Increments per Update</u>	
0.125	1	
0.0625	2	
0.025	5	
0.0125	10	
0.01	12.5	} Synchronization error 0.005 sec. is insignificant
≤ 0.01	≥ 12.5	

EARTH RADIANCE VARIATION

The variation of radiance over earth surface for the $14\text{-}16 \mu \text{CO}_2$ band has been calculated in Figure J-1. Plots of the radiance as function of latitude and time of year for various altitudes is shown in Figure J-2. The model for GPS simulation is deduced from these results. For maximum radiance variation a January situation is considered. The radiance is assumed to be a function of latitude but not longitude. The radiance variation for southern hemisphere is assumed to be that for northern hemisphere six months later. The radiance variation for earth disk is approximated by piecewise linear segments using the values corresponding to 20 Km altitude shown in Figure J-2. The radiance values and the normalized variations are summarized

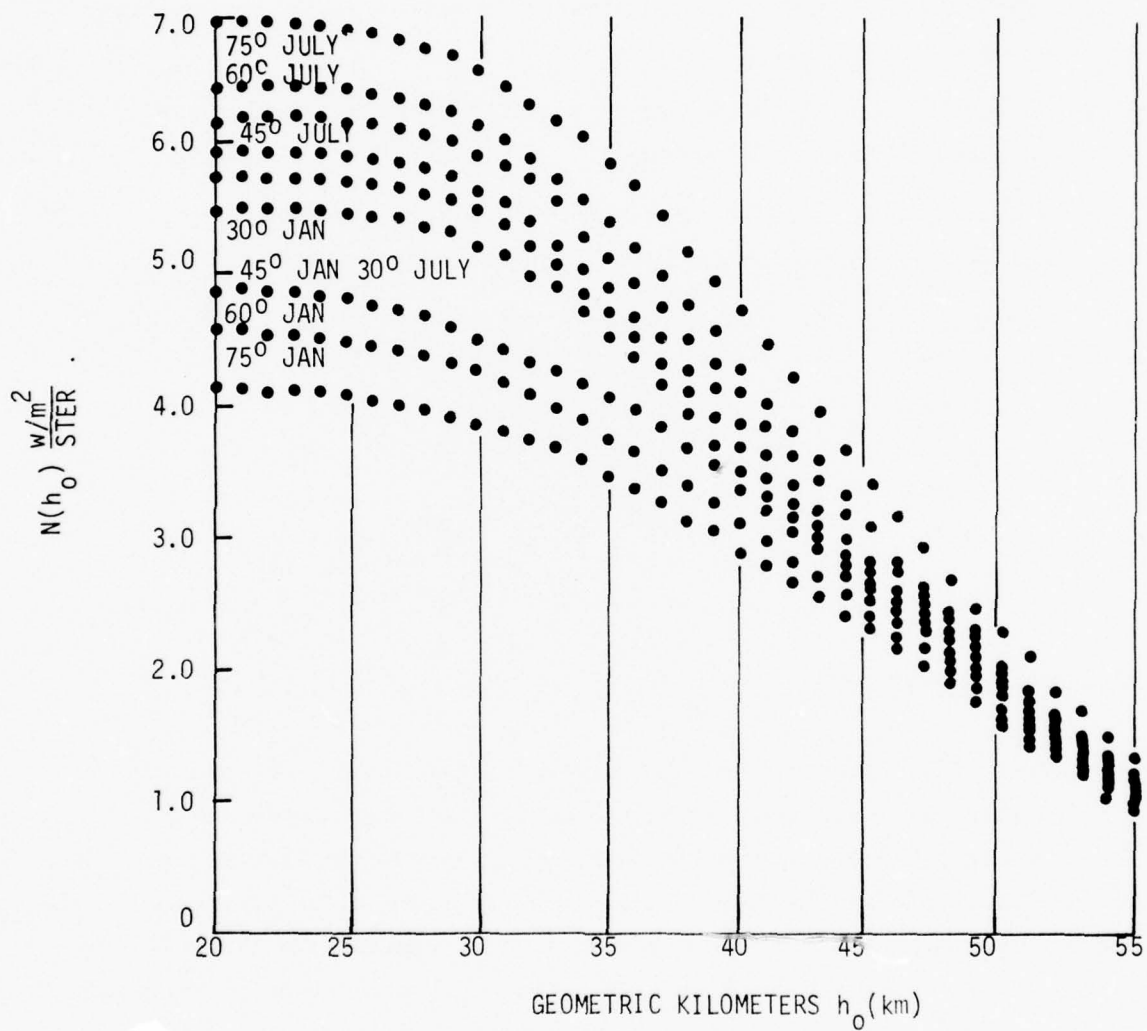


Figure J-1. Radiance CO_2 14-16 μ

$$v = y_1 + L = y_1 + \frac{\beta - x_1}{x_2 - x_1} (y_2 - y_1)$$

$$\frac{L}{y_2 - y_1} = \frac{\beta - x_1}{x_2 - x_1} (y_2 - y_1)$$

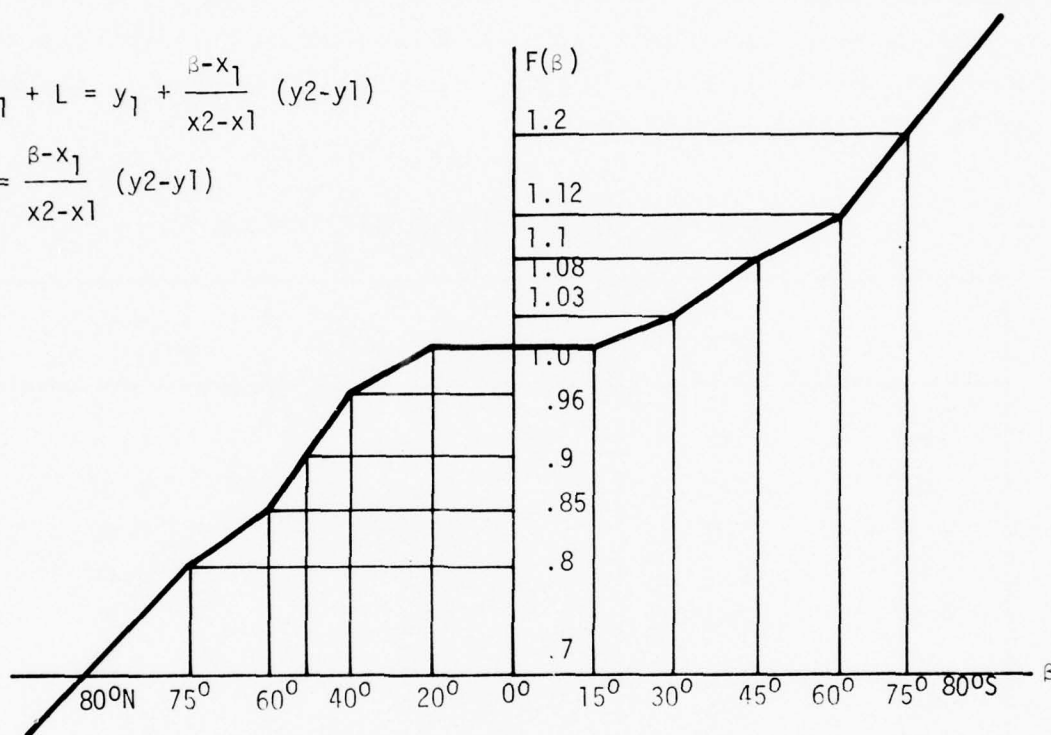


Figure J-2. Normalized Earth Radiance Variation with Latitude at January

in Table J-1. The normalized variation is used to be compatible with the existing earth sensor simulation that does not include the details of sensor optics and filter response. The radiance for the 15° latitude band is taken as that corresponding to a 220°K earth which, in conjunction with the sensor optics and filter response, provides 3.15 μw when the "A" detector FOV is fully illuminated.

TABLE J-1. EARTH RADIANCE VARIATION WITH
LATITUDE AND TIME OF YEAR

LAT.	MON.	RADIANCE $\frac{\text{W/M}^2}{\text{STER}}$	NORMALIZED VARIATION
-75°	JAN	4.13	0.72
-60°	JAN	4.63	0.80
-45°	JAN	4.88	0.85
-30°	JAN	5.5	0.96
$\mp 15^\circ$	JAN/JUL	5.75	1.00
30°	JUL	5.94	1.03
45°	JUL	6.19	1.08
60°	JUL	6.44	1.12
75°	JUL	6.94	1.21

Implementation of the earth radiance variation into the sensor model requires the following computations which are based on the geometry given in Figure J-3.

(a) LOS-vector for detector cell element centered at (X_a, Y_a) :

$$U = \sqrt{X_a^2 + Y_a^2}$$

$$X_s = \frac{X_a \sin U}{U}$$

$$Y_s = \frac{-Y_a \sin U}{U}$$

$$Z_s = \cos U$$

Denote

$$(\bar{L}_a^s) = \begin{bmatrix} X_s \\ Y_s \\ Z_s \end{bmatrix}$$

(b) Look point on earth surface along L_a :

$$(\bar{L}_a^I) = T_{IB}^I T_{SB}^I (\bar{L}_a^s)$$

$$(\bar{R}_a^I) = (\bar{R}_V^I) + S (\bar{L}_a^I)$$

where

(\bar{R}_a^I) = look point on earth surface along L_a .

(\bar{R}_V^I) = vehicle position from center of earth

S = slant range from R_V to R_a

$$= -(\bar{R}_V^I)^T (\bar{L}_a^I) - \{ \gamma_e^2 - (\bar{R}_V^I)^T (\bar{R}_V^I) + [(\bar{R}_V^I)^T (\bar{L}_a^I)]^2 \}^{1/2}$$

γ_e = 3590.95 n. mi.

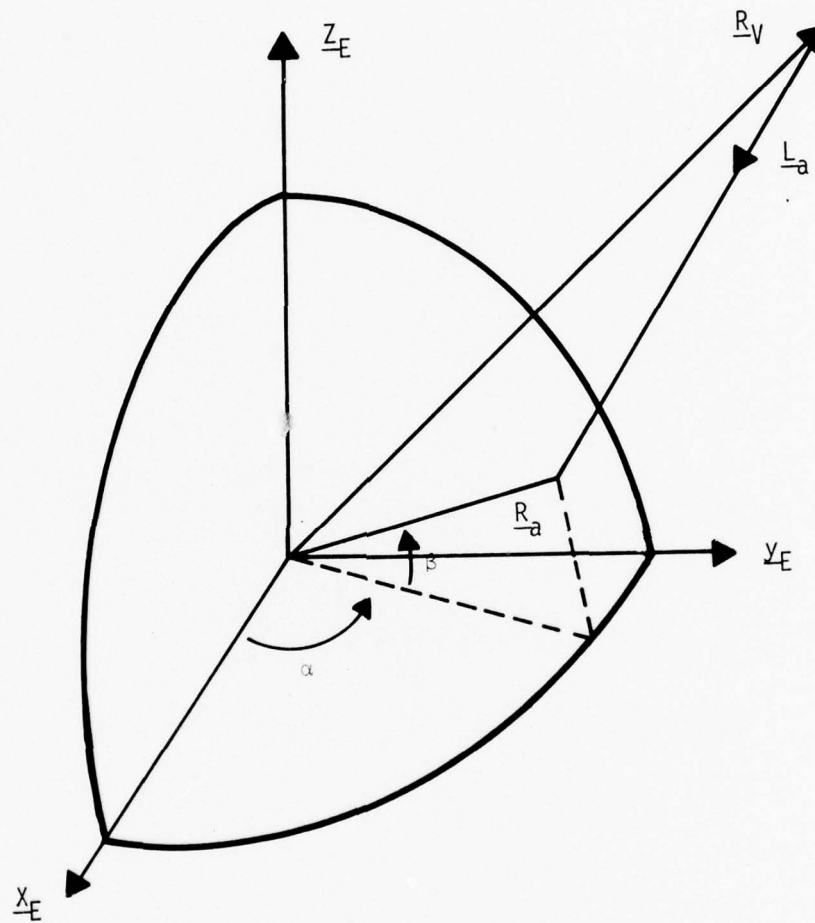


Figure J-3. Sensor Model Geometry

(c) Look point latitude:

$$(\bar{R}_a^{-E}) = T_{EI} (\bar{R}_a^I)$$

Denote

$$(\bar{R}_a^{-E}) = \begin{bmatrix} R_1 \\ R_2 \\ R_3 \end{bmatrix}$$

$$\beta = \sin^{-1} (R_3 / \gamma_e)$$

= look point latitude

(d) Scaling factor for radiance variation:

$$V = F(\beta)$$

where $F(\beta)$ is the piecewise linear function defining the radiance variation with latitude; $F(\beta)$ is plotted in Figure J-1.

(e) The value of AREA is modified from the original value by the scaling factor, i.e.:

$$AREA \leftarrow AREA * V$$

Figure J-4 presents a comparison of the GPS simulation radiance model and a model described in a Barnes Engineering document, "Technical Description Model 13-16901 and Model 13-16903 Synchronous Altitude Static-Sensors", 22 August, 1975. Models agree reasonably well.

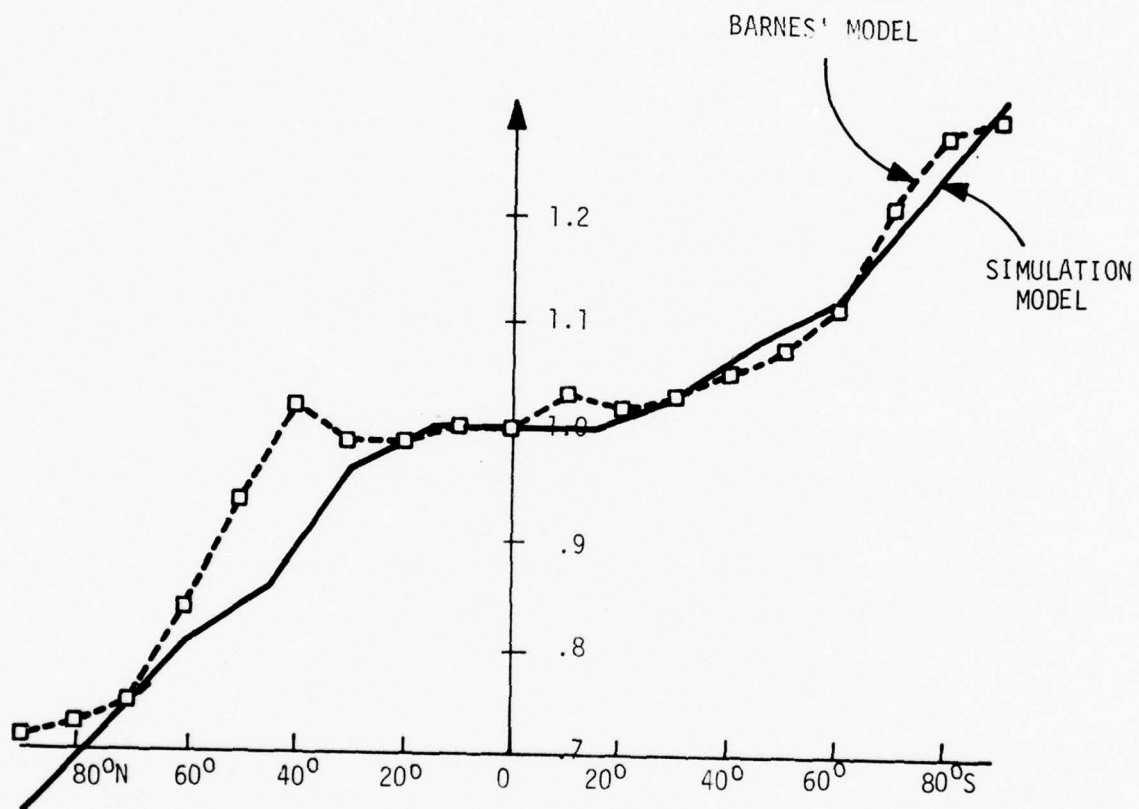


Figure J-4. Comparison of Models

SENSOR ERROR MODELING

The sensor error modeling considered here includes detector and pre-amp noises, electronics parameter shift error, error due to temperature gradient across detector and sensor alignment error. Horizon uncertainty errors, though not a sensor originated error, are also included in the consideration. These are errors that exist in all operational situations.

Errors due to sun or moon in sensor detector field of view and errors resulted from variation of earth disk size due to vehicle orbit eccentricity exist only for a specific operational condition and are not included here. The detector and preamplifier noise has been calculated to be $0.379 \mu\text{V}$ (3σ) for sensor in track mode (A detectors only) and $0.464 \mu\text{V}$ (3σ) for sensor in acquisition mode (A+B detectors) with a detector scale factor of $3.15 \mu\text{V}/\text{deg.}$ and responsivity of 20 V/W. These noises are equivalent to 0.0060 deg. (3σ) and 0.0074 deg. (3σ) respectively. Use the output scale factors of 5 V/deg and 1.25 V/deg for track and acquisition modes respectively. The noise at output then becomes $0.03 \text{ V}(3\sigma)$ and $0.0093 \text{ V}(3\sigma)$. The noise error will be simulated as white noise.

Electronics parameter shift has been analyzed by Barnes, Reference J-2. The values at initial setting and at end of life have been calculated to be 0.0034 deg. (3σ) and 0.0219 deg. (3σ) respectively. These correspond to output errors of 0.017 V (3σ) and 0.1095 V (3σ) for track mode and 0.0043 V (3σ) and 0.0274 V (3σ) for acquisition mode. The error due to electronics parameter shift will be simulated as bias errors.

The temperature gradient considered by Barnes amounts to a temperature difference of 0.00048°F between A and S reference junctions. The corresponding attitude error evaluated for temperature of 70°C is 0.0103° or 0.0515 V

for track mode. For acquisition mode, the temperature change of 0.0028 deg. between detectors is calculated to cause attitude error of 0.0029 deg. which amounts to output error of 0.0035 V. All values quoted above are considered to be for worst case and will be treated as 3σ values. The error due to temperature gradient will be simulated as bias errors.

The achievable static sensor alignment accuracy has been estimated by Barnes to be in the order of 0.015 deg. (3σ). The equivalent output error is 0.075 V (3σ) for track mode and 0.019 V (3σ) for acquisition mode. The effect of alignment error will be simulated as bias errors. The horizon uncertainty error has been treated as an exponentially correlated noise with standard deviation 0.88 Km, correlation time 10 days and correlation distance 2500 N. Mi in Reference J-1, i.e.,

$$E[h(t,s)h(t+T, S+d)] = \sigma_h^2 e^{-T/10} e^{-d/2500}$$

where

$$\sigma_h = 0.88 \text{ Km}$$

$$T = \text{time in days}$$

$$d = \text{distance in n. mi.}$$

The term $e^{-T/10}$ can be approximated by 1 if T is much less than 10 days. Factoring in the GPS orbit altitude of 10897 N. Mi the horizon uncertainty error amounts to 0.0020 deg. of earth disk angle error. In the evaluation of P_1 and R_1 detectors at opposite sides of the earth disk are involved. The separation between the look points of these detectors is:

$$d = \frac{(180^\circ - 14^\circ)X\pi}{180^\circ} \times 3461.6 \text{ N. Mi.}$$

$$= 10029 \text{ N. Mi.}$$

The separation is approximately four times the correlation distance. Hence the effects of horizon uncertainty error at opposing detectors are essentially uncorrelated. The equivalent error in evaluation of P_1 and R_1 is then $0.0020^\circ \times \sqrt{2} = 0.0028^\circ$ (1σ) or 0.0085° (3σ). The output error becomes 0.0424 V for track mode and 0.0106 V for acquisition mode. The same values can be used for P_2 and R_2 . (The distance between look points of every other detector cell is approximately 5383.1 N.Mi. The correlation of horizon uncertainty at points separated by this distance is only 0.12. It is neglected for simplicity of model.) For vehicle points at nadir and spins at a yaw rate of W RPM, the sensor detector scans the earth surface at a rate of 358.87 W N.Mi/sec. The 2500 N. Mi correlation distance would then be equivalent to a correlation time of $6.97/W$ sec.

The sensor output error $e(t)$ due to the horizon uncertainty will be modeled as an exponentially correlated noise as follows:

$$E[e(t) e(t+T)] = \sigma_0^2 e^{-T/T_c}$$

where

$$\begin{aligned}\sigma_0 &= 0.0424 \text{ V for track mode} \\ &= 0.0106 \text{ V for acquisition mode} \\ T_c &= 6.97/W \text{ sec} \\ &= 3.485 \text{ sec for } W = 2 \text{ RPM}\end{aligned}$$

The above model will be used to account for the effect of horizon uncertainty even for cases where vehicle is not quite pointing at the nadir. (The change of correlation time due to the pointing offset from nadir by $\pm 4^\circ$ is expected to be small. For large offset from nadir the effect of detector not seeing the earth disk will be much more significant than the effect of horizon uncertainty.)

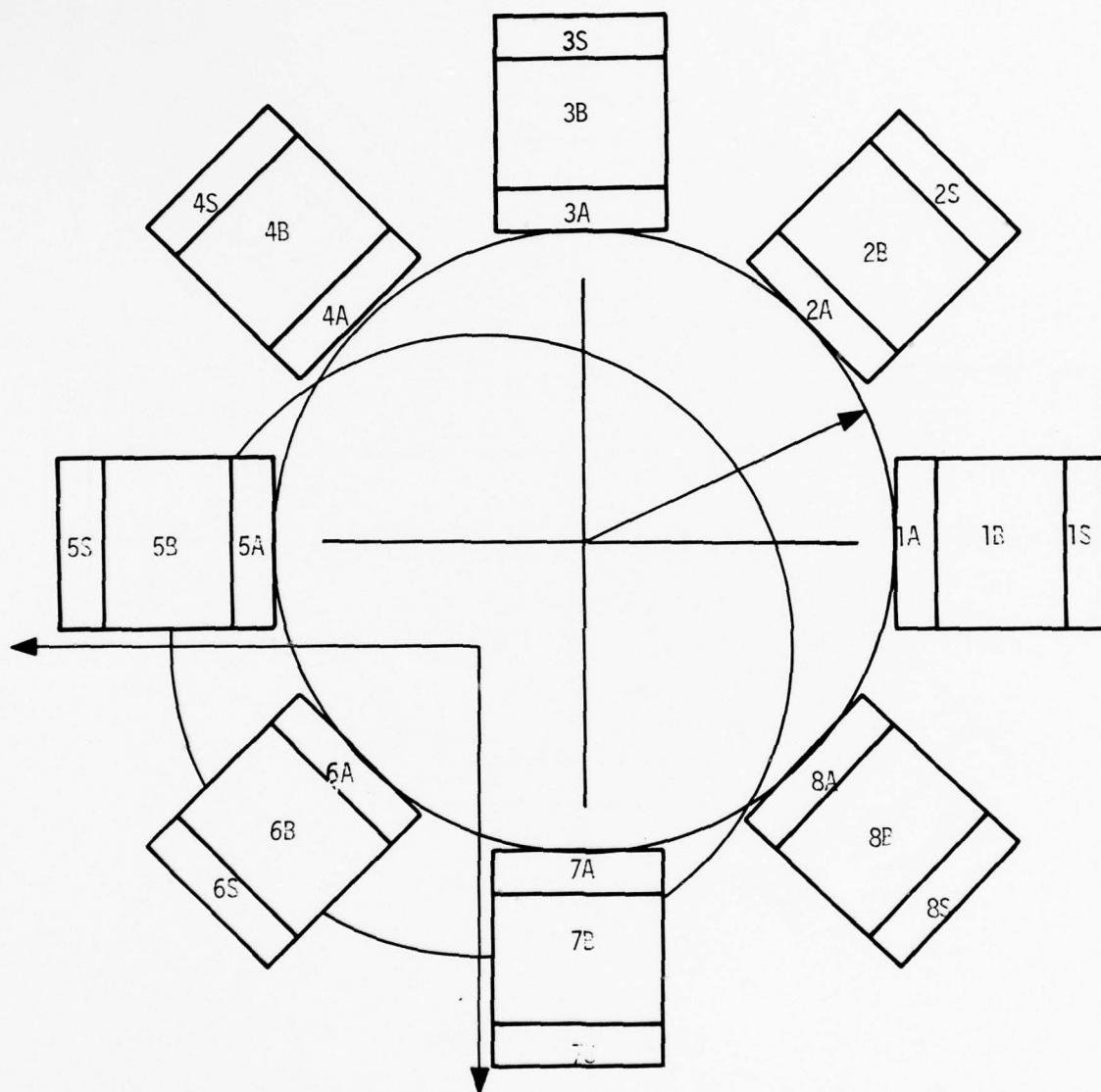
In summary, the sensor error will be simulated as an additive output error consists of a white noise component, a bias component and an exponentially

correlated random noise. The white noise is used to simulate the effect of detector and preamplifier noises. The equivalent attitude error of the white noise is 0.0060° (3σ). The exponentially correlated noise is used to simulate the effect of horizon uncertainty error. The equivalent attitude error is 0.0085° (3σ). The correlation time of this error for the vehicle spin rate of 2 RPM at initiation of earth acquisition is 3.485 sec.

The bias error is introduced to account for the total effects of electronics error, temperature gradient error and sensor alignment error. The equivalent attitude error is 0.0285° (3σ) evaluated as the RSS value of each individual effects.

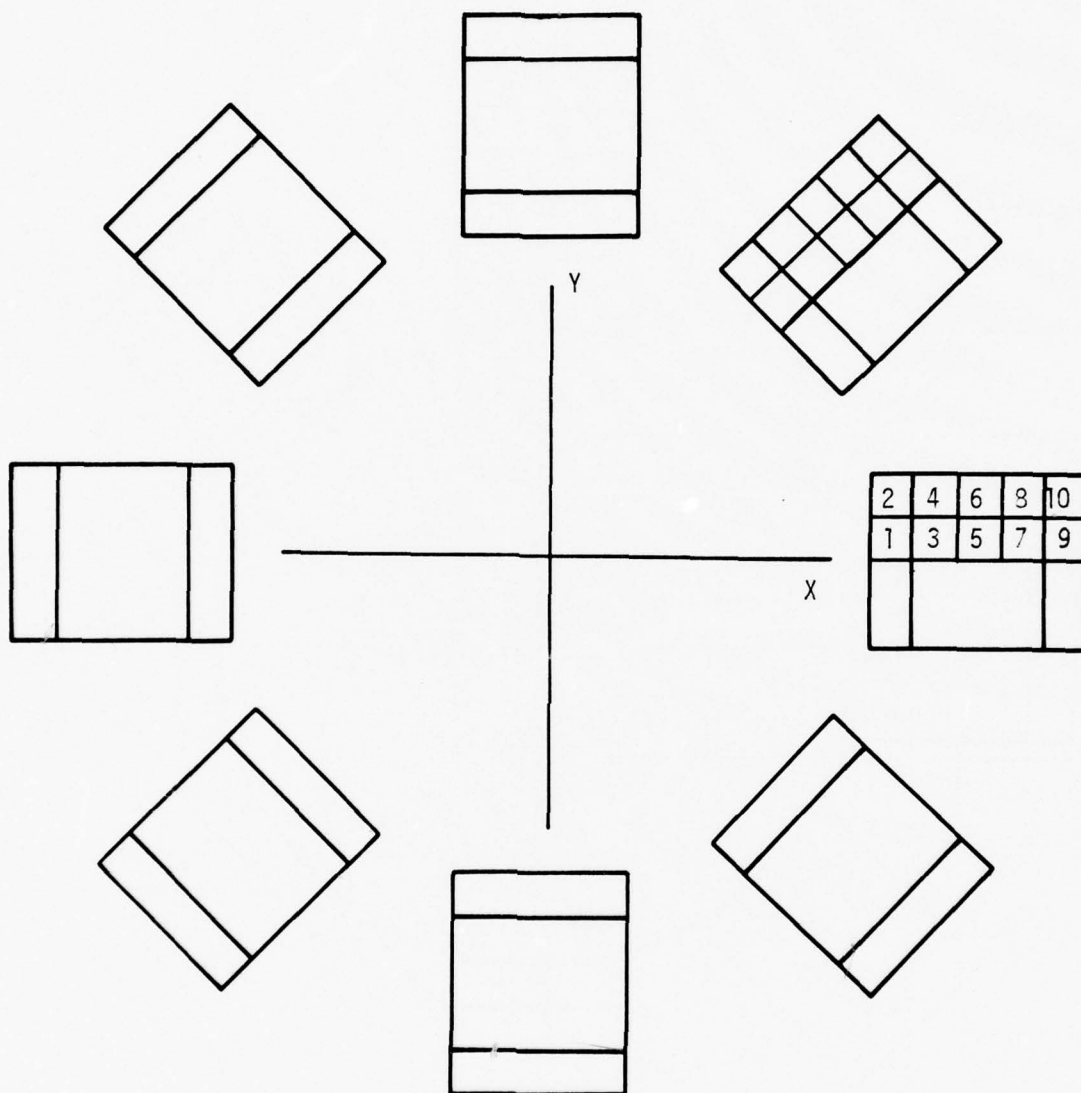
CONCERNS

- o The detector geometry and output computations may not be correct since Barnes has two different designs. The one used here (Figure J-5) is one of their designs. The other has detector pattern rotated $22\frac{1}{2}^{\circ}$ about the line of sight from the one shown here.
- o The output update frequency for GPS is not certain. The one used here is the one proposed by Barnes for DSCS III.
- o Earth image distortion and focus are not modeled. Excluding radiance, the earth image is assumed to be a perfect circle on the focal surface.
- o The detector output approximation using $1^{\circ} \times 1^{\circ}$ squares causes very little error near null (normal operation) and up to 0.15° maximum detector error at extreme attitudes (during acquisition). The extent of the errors near null and the sensor output errors during acquisition has not been analyzed. The approximation errors off null are on the order the errors due to earth radiance variation and earth image quality. Smaller squares may be used to improve accuracy but computer cost will go up.



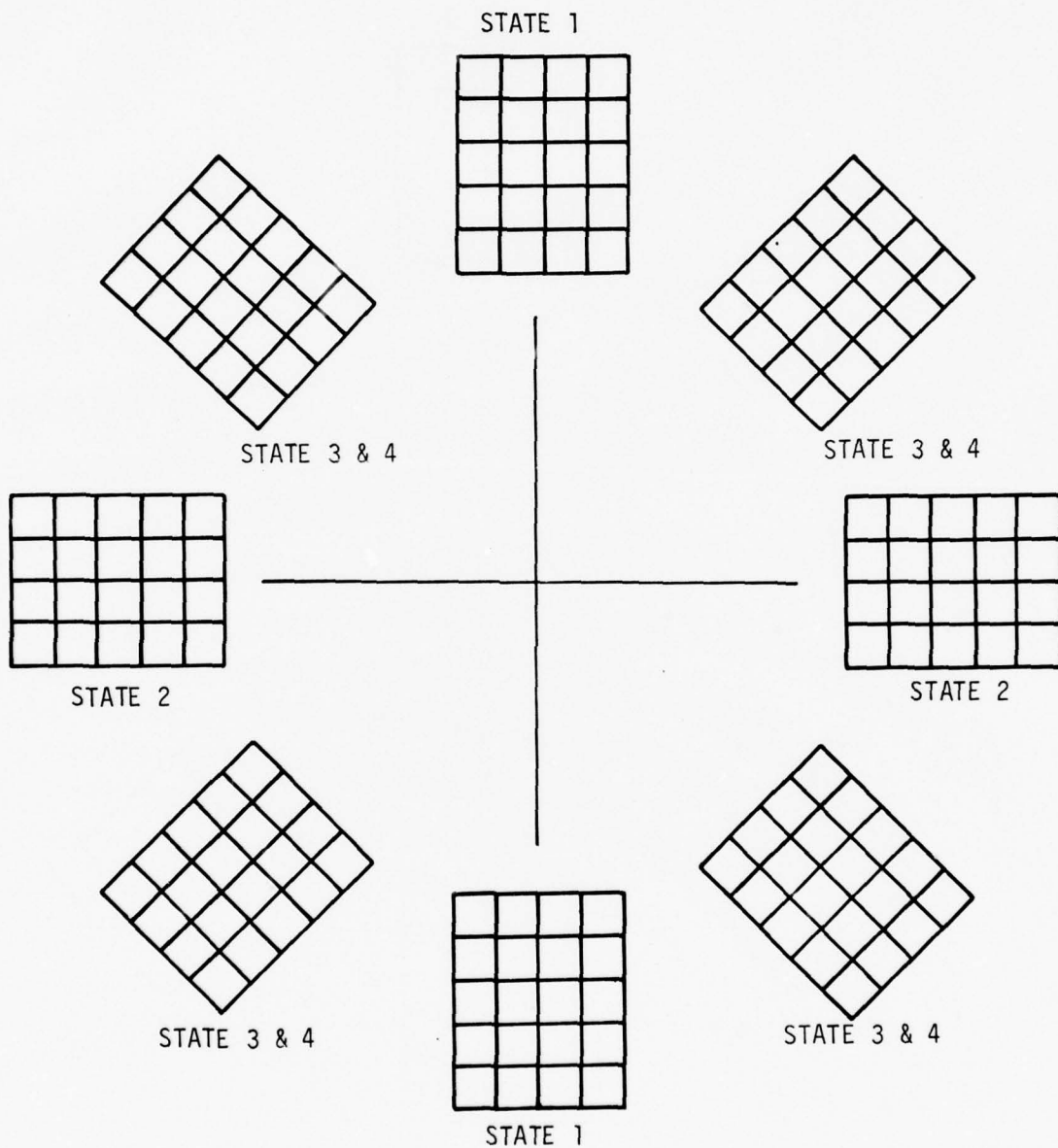
DIRECTOR NUMBERING BY BARNES

Figure J-5. Detector Geometry--2-Axis Earth Sensor



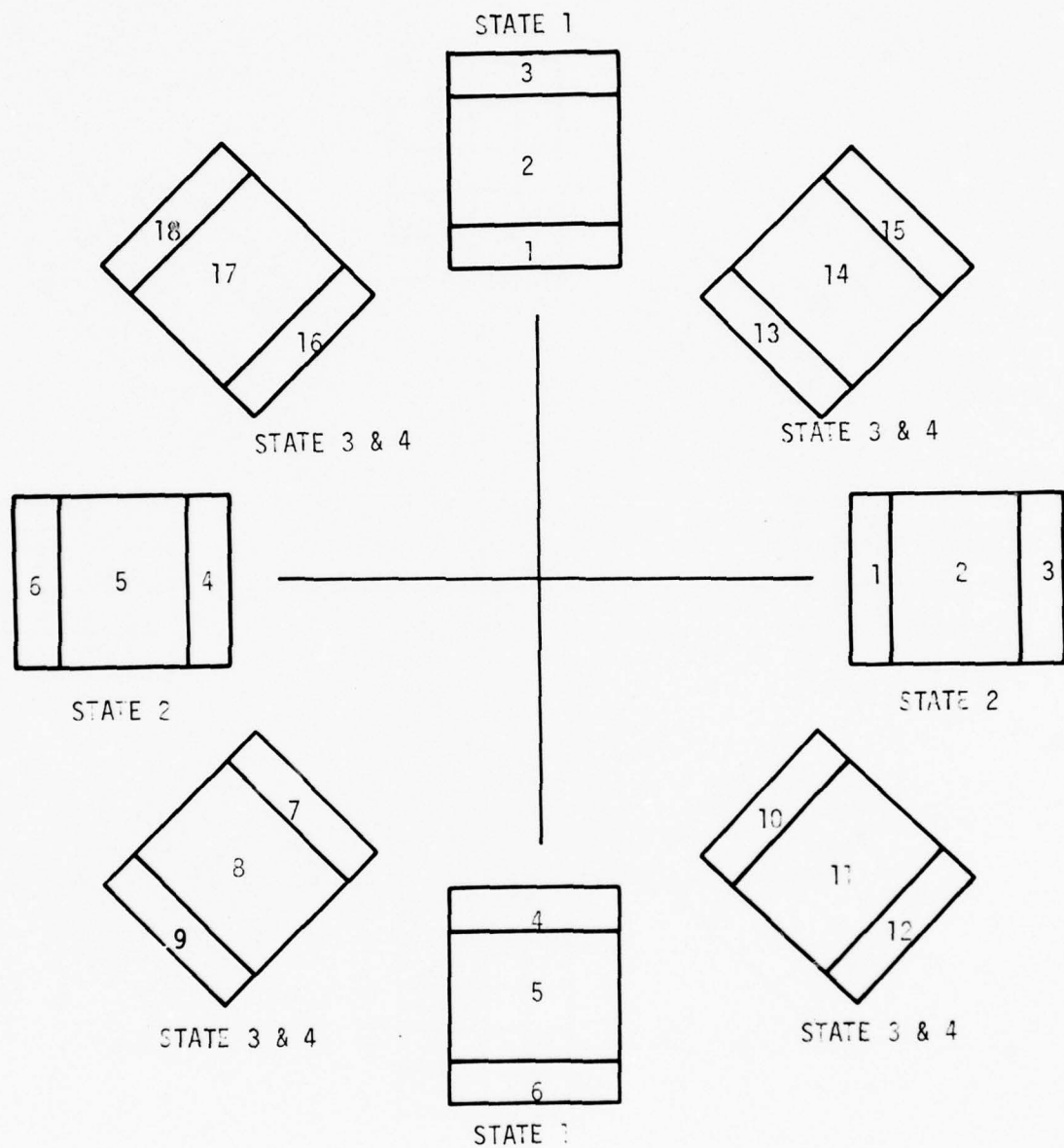
NUMBERING OF X-Y COORDINATES FOR POSITION OF $1^{\circ} \times 1^{\circ}$ SQUARES.
 X-Y COORDINATES OF ALL 160 $1^{\circ} \times 1^{\circ}$ SQUARES ARE OBTAINED FROM
 THESE 20 STORED VALUES

Figure J-5. Detector Geometry--2-Axis Earth Sensor (continued)



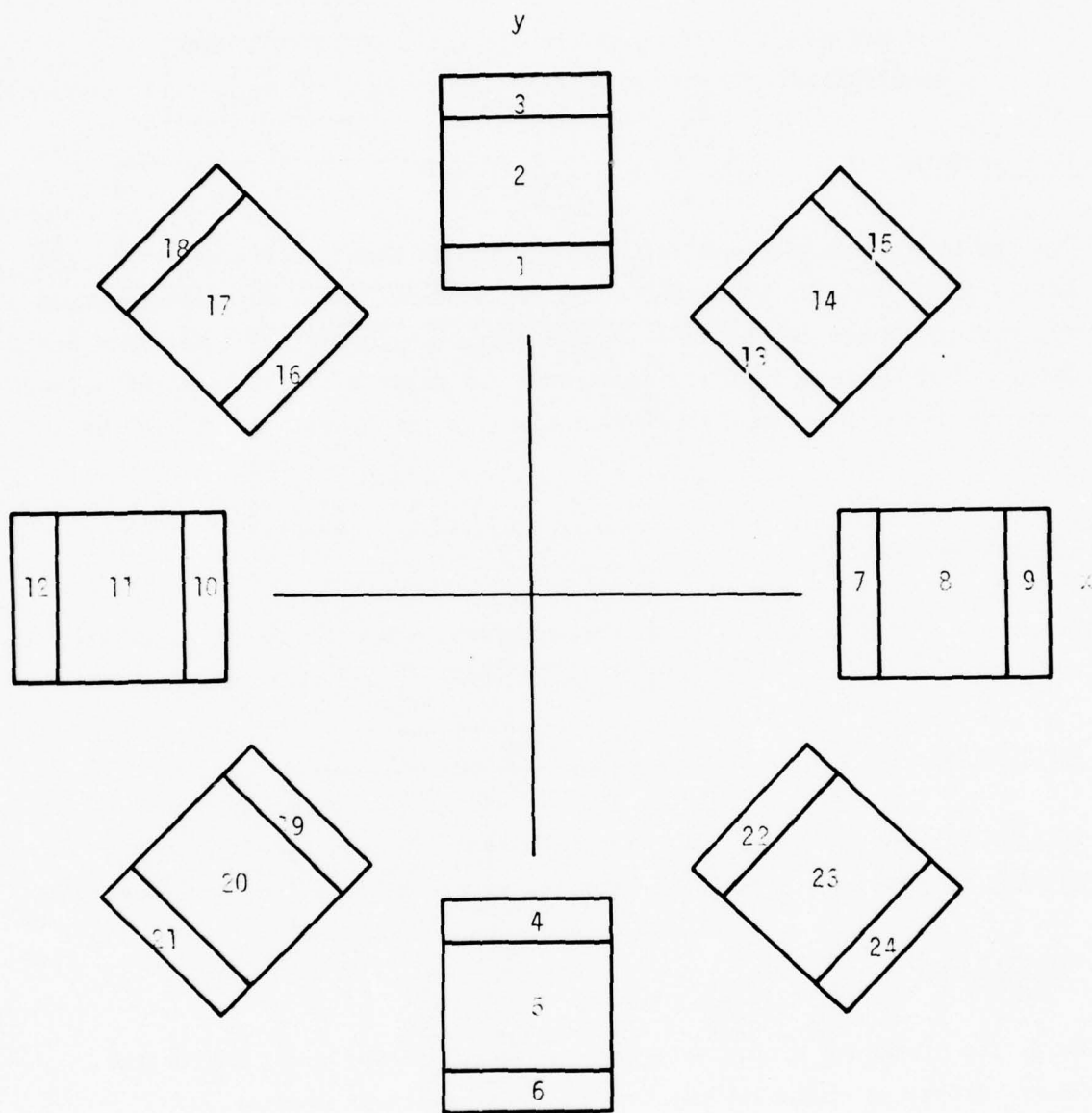
NUMBERING OF A ELEMENTS

Figure J-5. Detector Geometry--2-Axis Earth Sensor (continued)



NUMBERING OF D ELEMENTS

Figure J-5. Detector Geometry--2-Axis Earth Sensor (continued)



NUMBERING OF V AND DSAV ELEMENTS

Figure J-5. Detector Geometry--2-Axis Earth Sensor (concluded)

- o Sun and moon interference are not included in this model description.

FLOW DIAGRAM

The combined earth sensor model flow diagram is shown in Figure J-6. The left arrow (←) within boxes indicates replacement, i.e., the expression on the right replaces the variable on the left. Mathematical subscripts are used. Symbols used in the flow diagram are defined in the sections below. Comments appear outside the boxes to describe the operations within the boxes.

INITIALIZATION DATA

Table J-2 lists the initialization parameters, nominal values, tolerance, and source of data. This data is to be input at the start of each run.

INPUT DATA

Table J-3 lists the input data the earth sensor model expects from the calling program each time the subroutine is executed in the normal mode.

OUTPUT DATA

Table J-4 lists the output data from the earth sensor model subroutine. Other subroutine variables may be outputs if the user desires.

INTERNAL VARIABLES

Internal variables used in the flow diagram are defined in Table J-5.

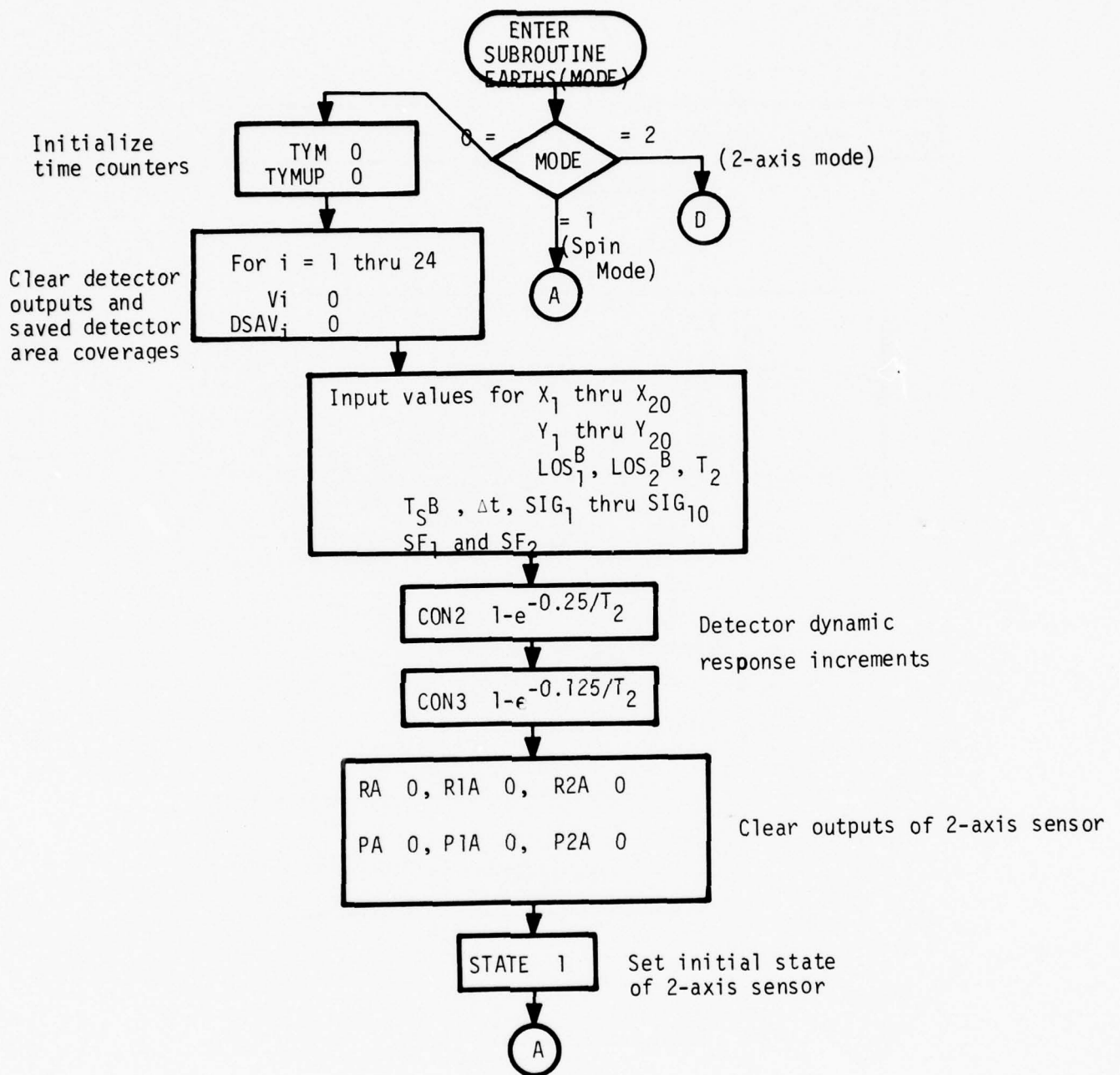


Figure J-6. Earth Sensor Flow Chart

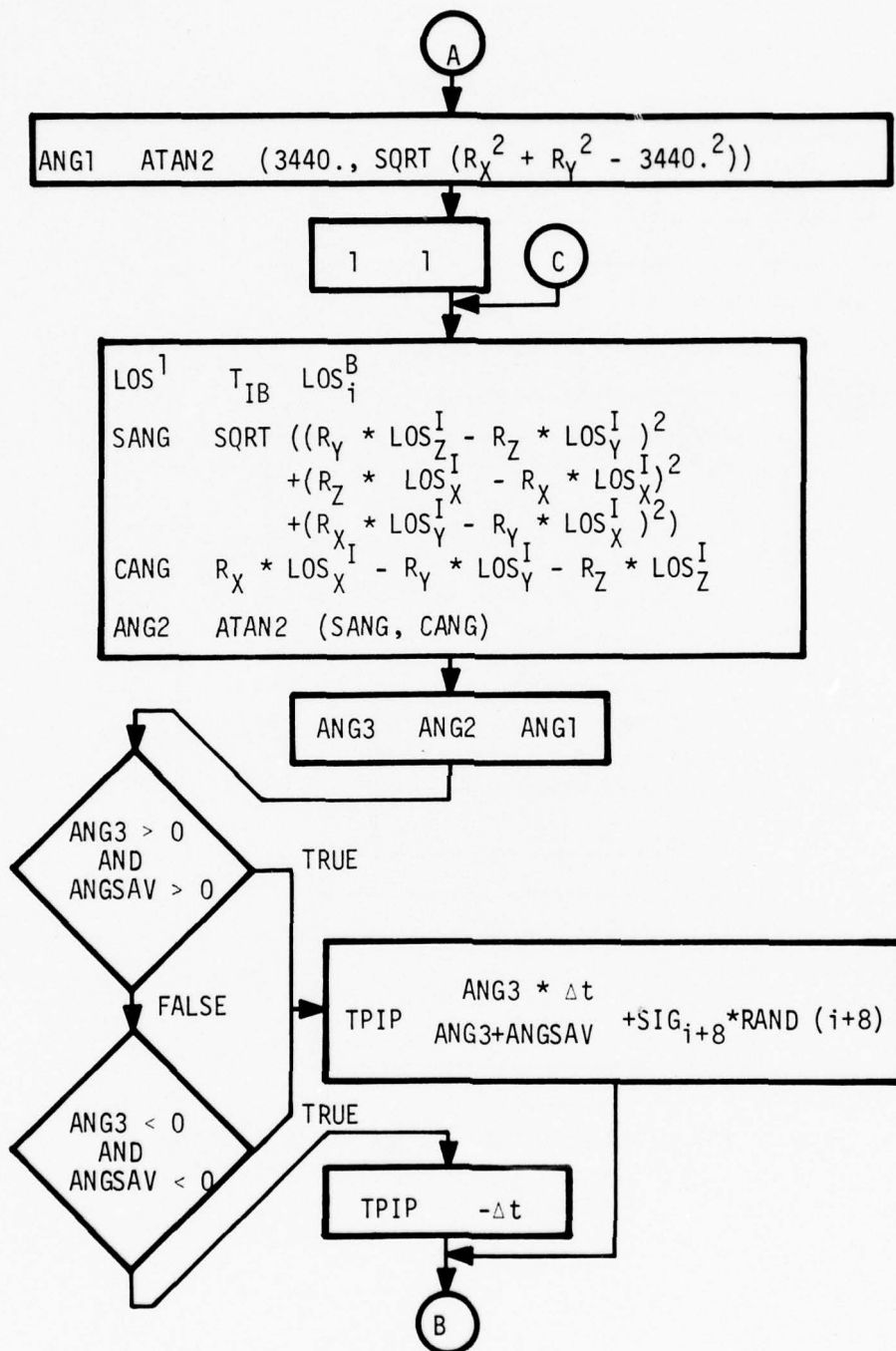


Figure J-6. Earth Sensor Flow Chart (continued)

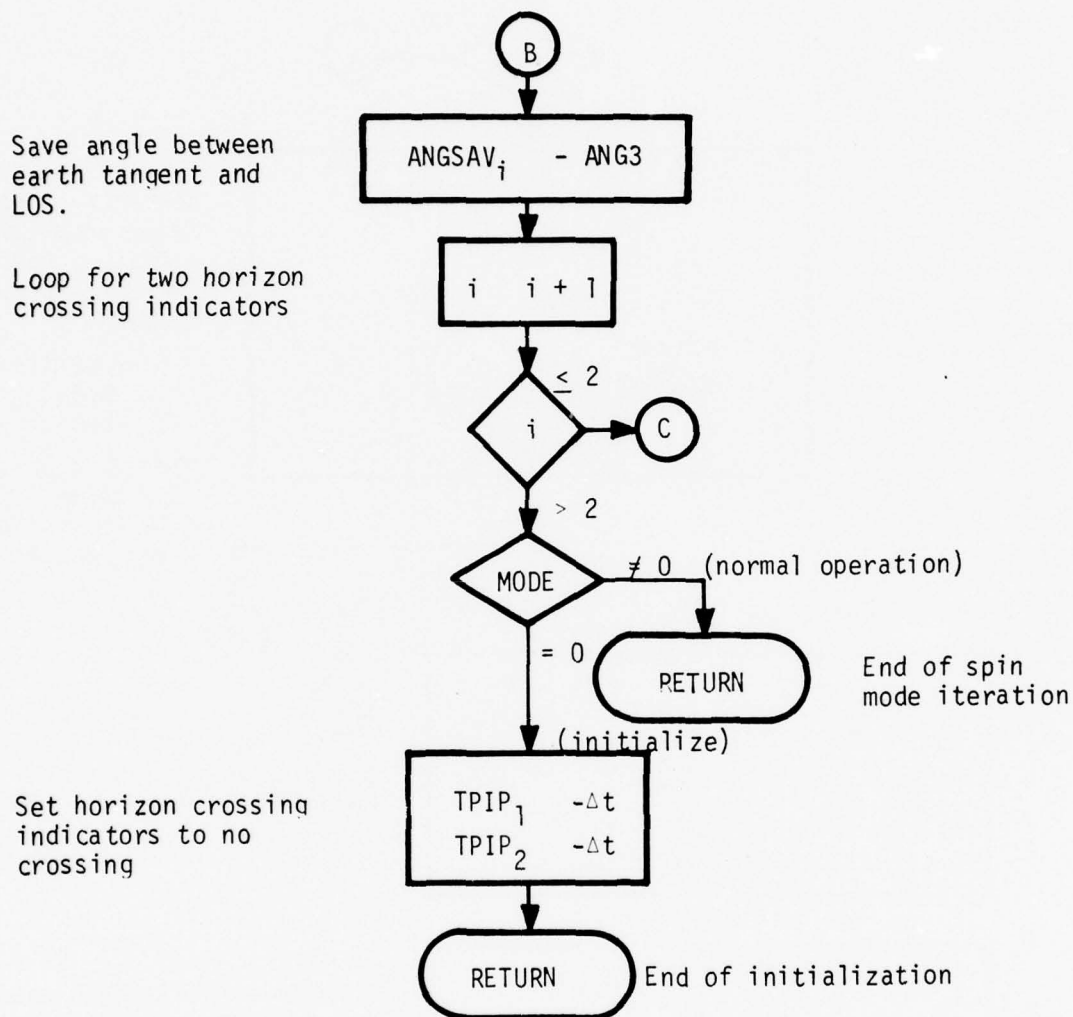


Figure J-6. Earth Sensor Flow Chart (continued)

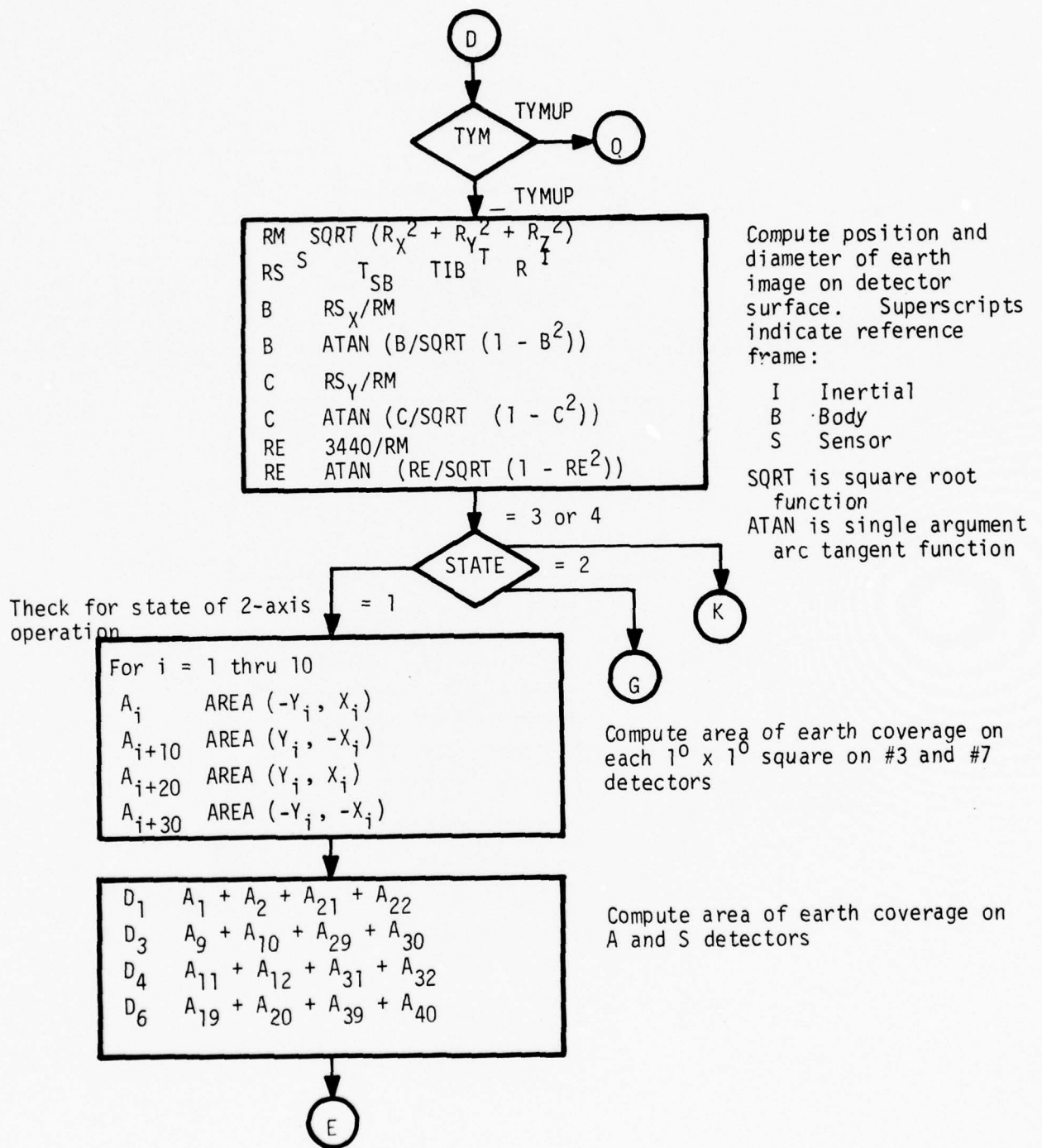


Figure J-6. Earth Sensor Flow Chart (continued)

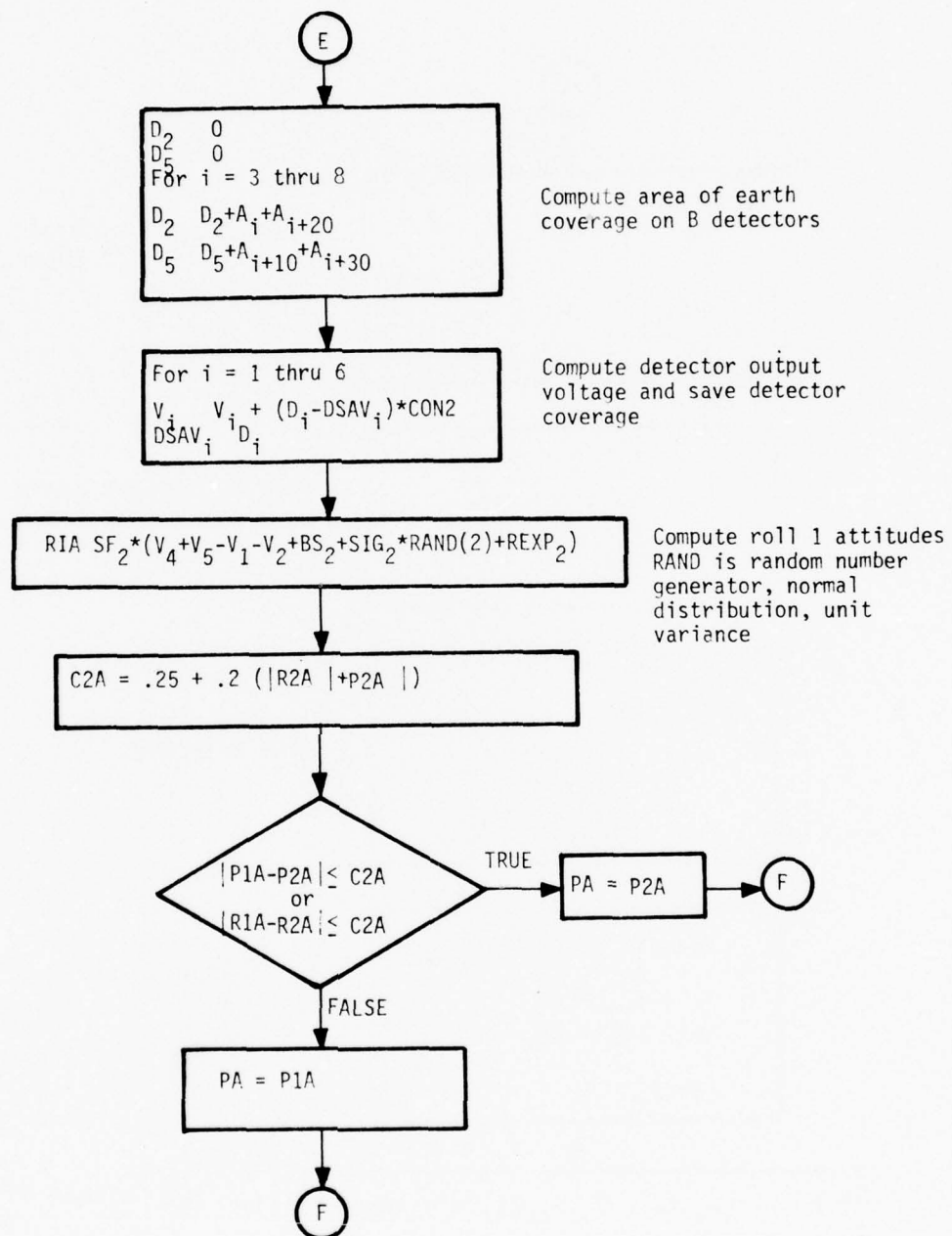
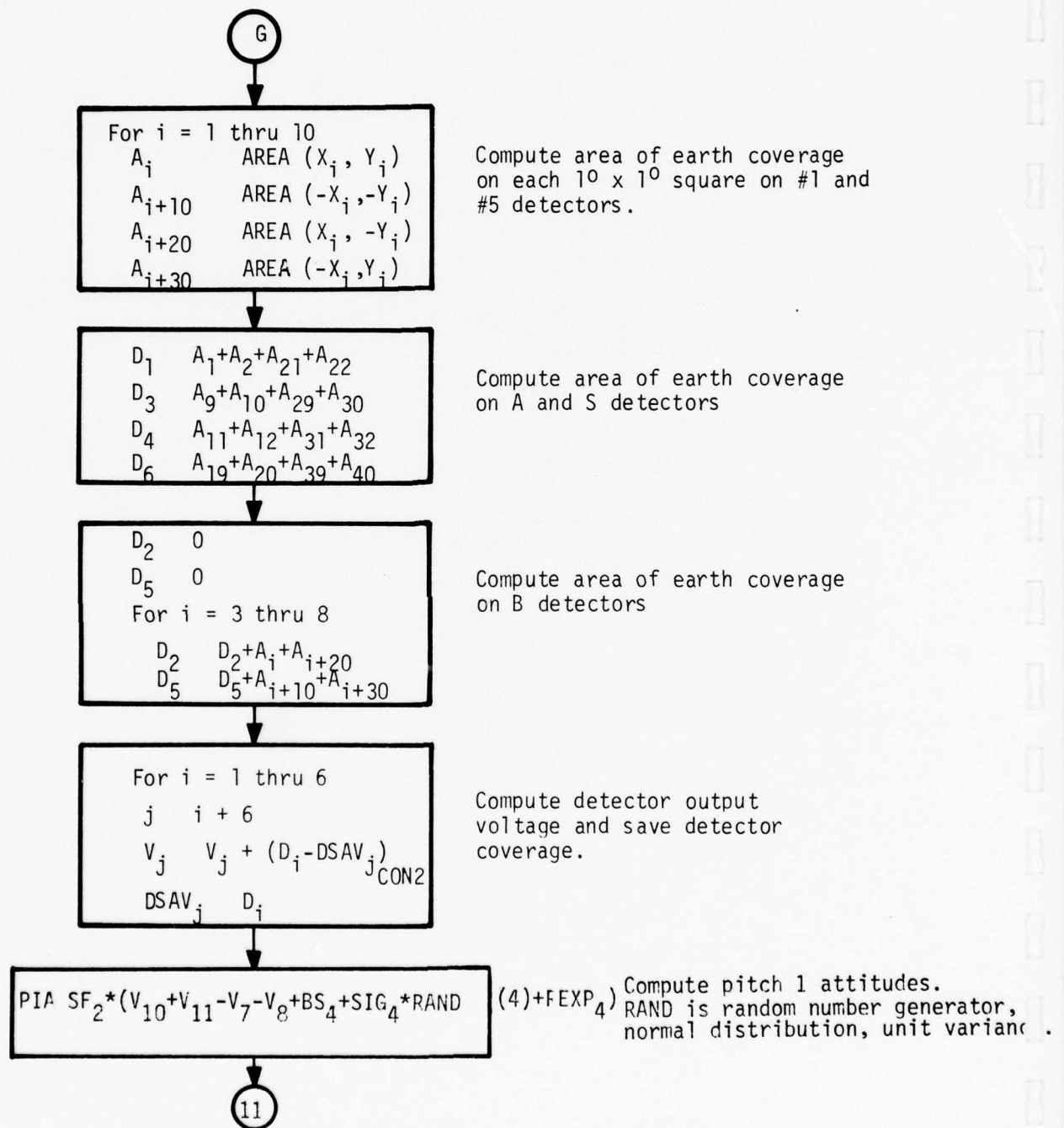


Figure J-6. Earth Sensor Flow Chart (continued)



FigureJ-6. Earth Sensor Flow Chart (continued)

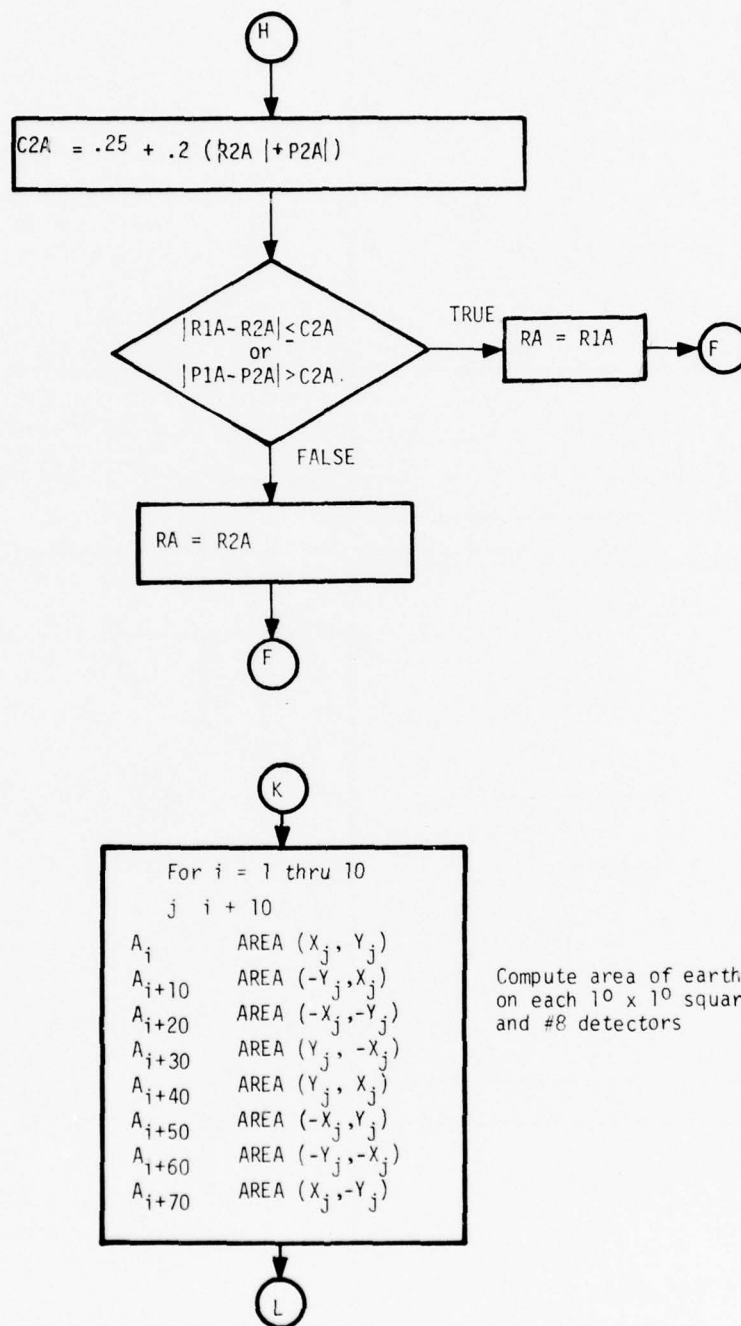


Figure J-6. Earth Sensor Flow Chart (continued)

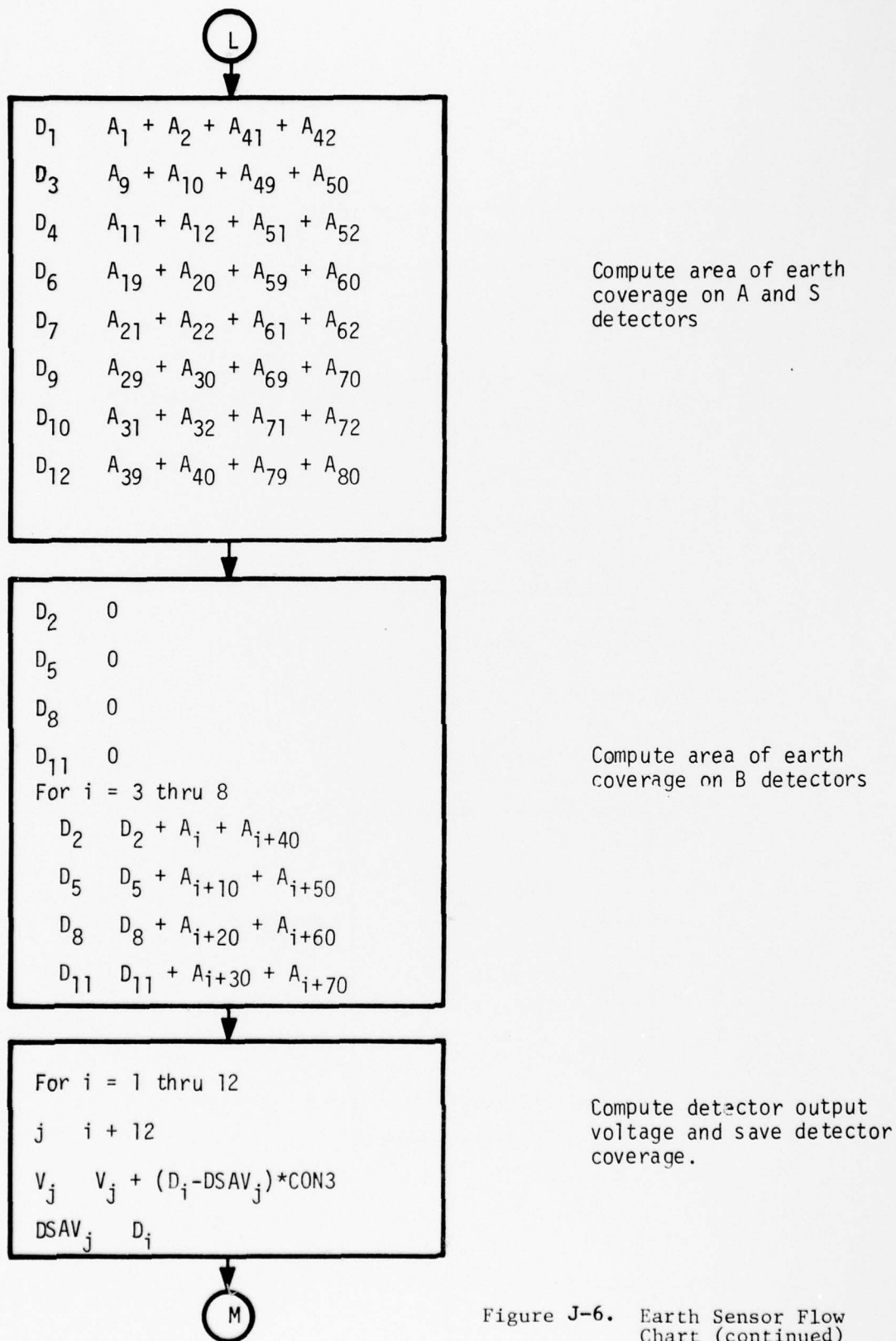


Figure J-6. Earth Sensor Flow Chart (continued)

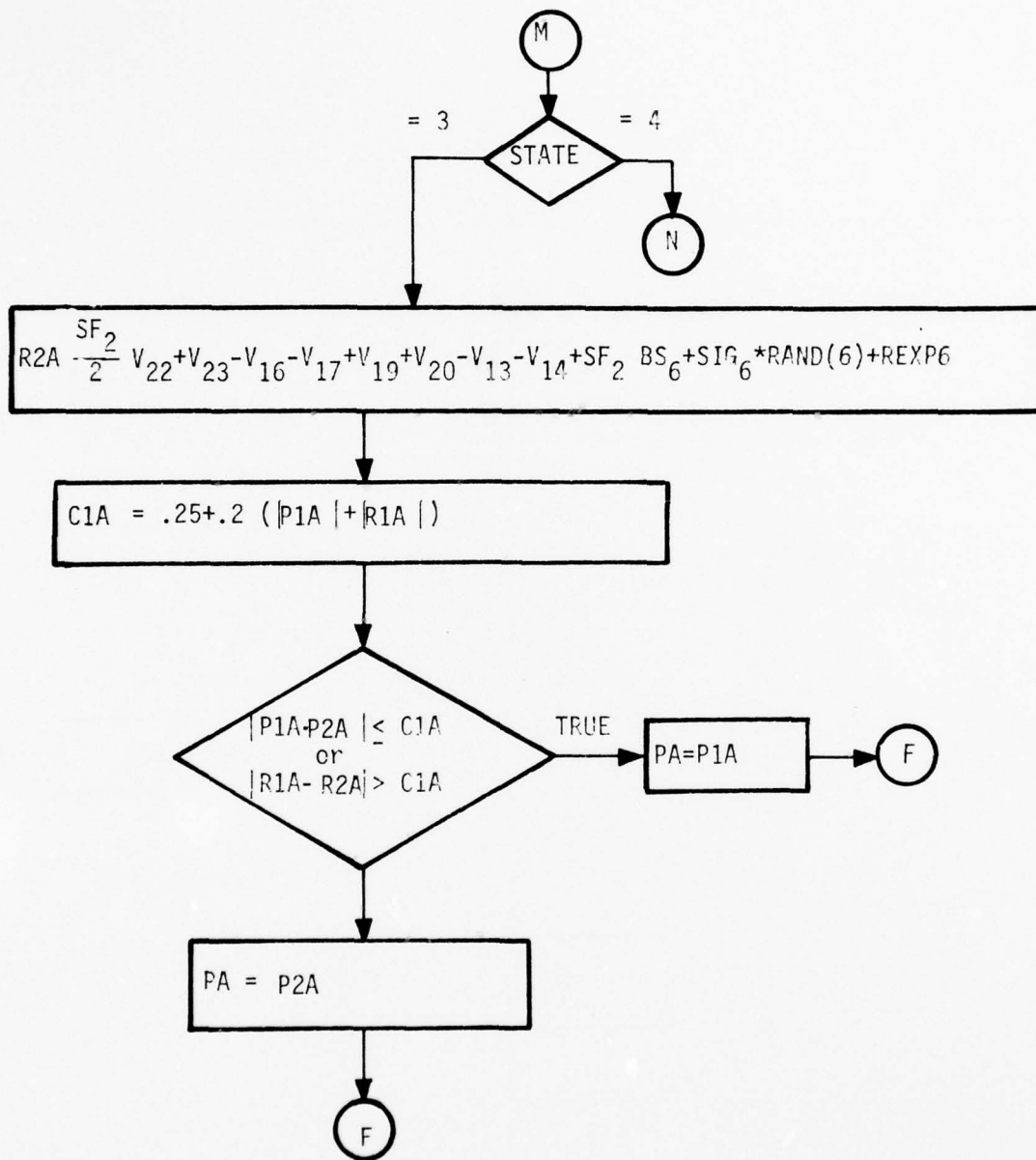


Figure J-6. Earth Sensor Flow Chart (continued)

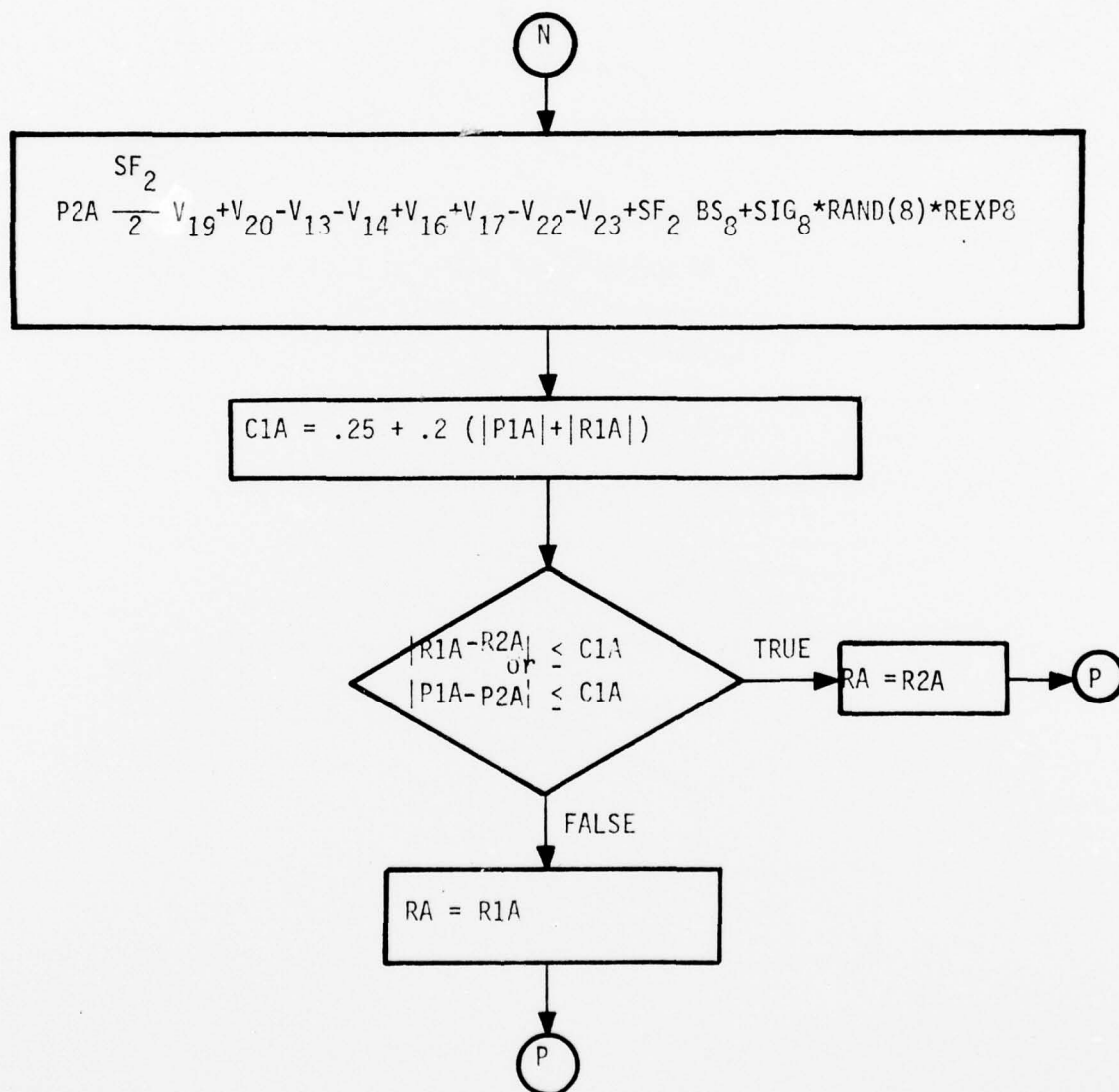


Figure J-6. Earth Sensor Flow Chart (continued)

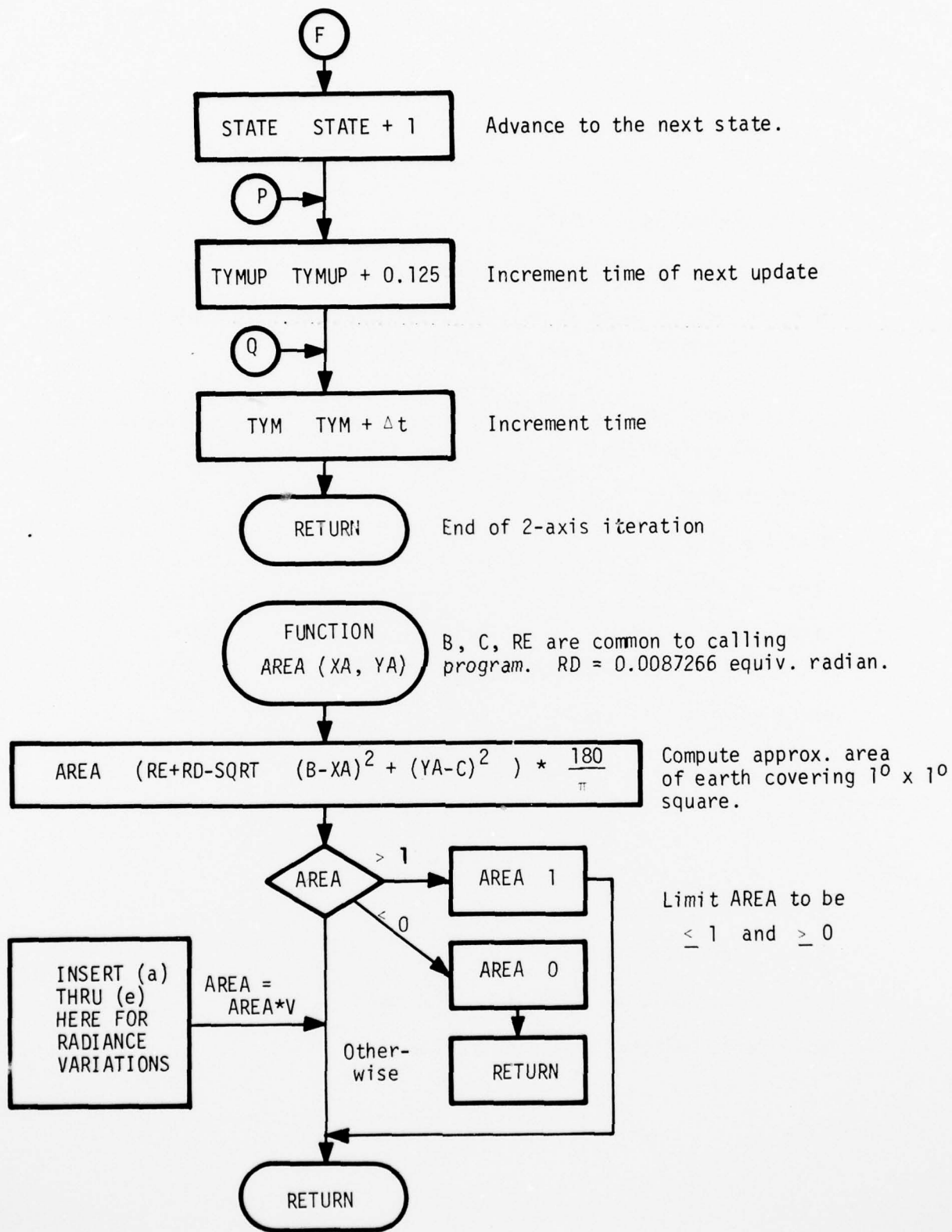


Figure J-6. Earth Sensor Flow Chart (concluded)

Where

$SIG_I = 0.0020$ (deg., 1σ) $I = 1, \dots, 8$

$BS_I =$ Bias error with worst case value 0.0285 (deg., 3σ) $I = 1, \dots, 8$.

$REXP_I =$ Exponentially correlated noise with standard deviation
 0.00283° and correlation time 3.485 sec.

The function $REXP_I$ to be used to generate the exponentially correlated noise is given in the following:

```
FUNCTION REXPI
  REXPIO = REXPI
  BETA = 1./TMCNST
  DREXP = -BETA*REXPIO
          +SQRT (2.*BETA)*RSIGI*RANDI
  REXPI = REXPIO + DREXP
  RETURN
END
```

Where

TMCNST = Correlation Time

RSIGI = Standard Deviation

RANDI = Random number generator with unit variance

REXP_I to be assigned an initial value.

TABLE J-2. INITIALIZATION DATA FOR EARTH SENSOR MODEL

PARAMETER	SUBSCRIPT	UNIT	NOMINAL VALUE	SOURCE	TOLERANCE	SOURCE
Time constant of two axis earth sensor detectors, T_2		Seconds	1.4	Note 1	N/A	None
Line of sight of spin earth sensor field						
LOS^B, LOS_X	1	---	-0.9848	Note 2	N/A	Not specified
	2	---	-0.9848			
LOS_Y	1		0			
	2		0			
LOS_Z	1		0.1736			
	2		-0.1736			
Transformation from body to sensor frame: (TSB)						
Row 1 Col. 1	1	---	1.0	Assumed (nominal)	N/A	None
1 2	2		0			
1 3	3		0			
2 1	4		0			
2 2	5		1.0			
2 3	6		0			
3 1	7		0			
3 2	8		0			
3 3	9		1.0			
Calling time increment, Δt		Seconds	≤ 0.00326 ≤ 0.125	(spin mode) (2 axis)	See text See text	
Center position of incremental detector area:						
X_i	1	Equiv.	0.2530727415	Note 1 & Fig. 3	N/A	None
	2	radian	0.2530727415			
	3		0.2705260341			

TABLE J-2. INITIALIZATION DATA FOR EARTH SENSOR MODEL (continued)

PARAMETER	SUBSCRIPT	UNIT	NOMINAL VALUE	SOURCE	TOLERANCE	SOURCE
γ_i	4	Equiv. radian	0.2705260341		N/A	None
	5		0.2879793266			
	6		0.2879793266			
	7		0.3054326191			
	8		0.3054326191			
	9		0.3228859116			
	10		0.3228859116			
	11		0.1727787808			
	12		0.1604374393			
	13		0.1851201222			
	14		0.1727787807			
	15		0.1974614637			
	16		0.1851201222			
	17		0.2098028052			
	18		0.1974614637			
	19		0.2221441467			
	20		0.2098028052			
	1		0.0087266463			
	2		0.0261799387			
	3		0.0087266463			
	4		0.0261799387			
	5		0.0087266463			
	6		0.0261799387			
	7		0.0087266463			
	8		0.0261799387			
	9		0.0087266463			
	10		0.0261799387			
	11		0.1851201222			
	12		0.1974614637			
	13		0.1974614637			
	14		0.2098028051			
	15		0.2098028051			
	16		0.2221441466			
	17		0.2221441466			
	18		0.2344854881			
	19		0.2344854881			
	20		0.2468268296			

TABLE J-2. INITIALIZATION DATA FOR EARTH SENSOR MODEL (concluded)

PARAMETER	SUBSCRIPT	UNIT	NOMINAL VALUE	SOURCE	TOLERANCE	SOURCE
Noise Standard • • • Deviation						
SIG on:				Note 4	N/A	
R1T	1	Volts	0.167			
R1A	2	Volts	0.0417			
P1T	3	Volts	0.167			
P1A	4	Volts	0.0417			
R2T	5	Volts	0.167			
R2A	6	Volts	0.0417			
P2T	7	Volts	0.167			
P2A	8	Volts	0.0417			
TP1P ₁	9	Sec.	0	Not Specif- ied		Not Specif- ied
TP1P ₂	10	Sec.	0	Not Specif- ied		Not Specif- ied
Two axis output scale factor						
Track, SF	1	Volt/sq. deg.	1.25	Note 3	0.0625	Note 3
Acq., SF	2	Volt/sq. deg.	0.3125		0.025	

NOTES TO TABLE J-2

1. Barnes presentation to Honeywell in St. Petersburg on 3-13-75.
2. Rockwell Spec MC 432-0214, Rev. B., 12-11-74.
3. Computed from data in Rockwell Spec MC432-0214, Rev. B, 12-11-74.

Track scale factor

1 degree attitude = 4 sq. deg. coverage = $5 \pm 0.25V$.

$$\frac{5 \pm 0.25V}{4 \text{ sq. deg.}} = 1.25 \pm 0.0625 \text{ volt/sq. deg.}$$

Acquisition scale factor

4 degree attitude = 16 sq. deg. coverage

$$\frac{1.25 \pm 0.1 V}{4 \text{ sq. deg.}} = 0.3125 = 0.025 \text{ volt/sq. deg.}$$

4. Computed from data in Rockwell Spec MC 432-0214, Rev. B, 12-11-74

Track mode

 $\pm 0.1^\circ$, 3 sigma

$$0.1 \times 5 \text{ volt/deg} \times 1/3 = 0.167 \text{ volt, 1 sigma}$$

Acquisition mode

 $\pm 0.1^\circ$, 3 sigma

$$0.1 \times 1.25 \text{ volt/deg} \times 1/3 = 0.0417 \text{ volt, 1 sigma}$$

TABLE J-3. INPUT DATA FOR EARTH SENSOR MODEL

DEFINITION	FLOW DIAGRAM SYMBOL	DIMENSION	TYPE	UNITS
Mode control flag	MODE		Integer	0 = initialize 1 = spin operation 2 = 2 axis operation
Satellite position vector	$R_x, R_y, R_z; R$	3	Real	N Mi
Transformation from body to inertial frame	TIB	9	Real	

TABLE J-4. OUTPUT DATA FOR EARTH SENSOR MODEL

DEFINITION	FLOW DIAGRAM SYMBOL	DIMENSION	TYPE	UNITS
Spin earth sensor output	TPIP	2	Real	Seconds
Pitch attitude in track mode	PT		Real	Volts
Pitch attitude in acquisition mode	PA		Real	Volts
Roll attitude in track mode	RT		Real	Volts
Roll attitude in acquisition mode	RA		Real	Volts

TABLE J-5. INTERNAL VARIABLES FOR EARTH SENSOR MODEL

DEFINITION	FLOW DIAGRAM SYMBOL	DIMENSION	TYPE	UNITS
Two axis rise/decay increment for 0.25 sec.	CON2		Real	Volts per sq. deg.
Two axis rise/decay increment for 0.125 sec.	CON3		Real	Volts per sq. deg.
Area of incremental detector covered by earth	A	80	Real	Square degree
Time since start of run	TYM		Doub prec	Seconds
Time of next 2-axis update	TYMUP		Doub prec	Seconds
Satellite distance to earth center	RM		Real	N. M.
Satellite position vector in sensor frame	$RS_x, RS_y, RS_z;$ R	3	Real	N. Mi
Radius of earth image on focal surface	RE		Real	Equiv. radian
Position of earth image on focal surface, X component	B		Real	Equiv. radian
Position of earth image on focal surface, Y component	C		Real	Equiv. radian
State of sequential processing within sensor	STATE		Integer	
Area of detector covered by earth	D	12	Real	Square degree
Area of detector coverage from previous cycle	DSAV	24	Real	Square degree
Dynamic Detector output	V	24	Real	Square Degree

TABLE J-5. INTERNAL VARIABLES FOR EARTH SENSOR MODEL (concluded)

DEFINITION	FLOW DIAGRAM SYMBOL	DIMENSION	TYPE	UNITS
Pitch 1 track attitude	P1T		Real	Volts
Pitch 2 track attitude	P2T		Real	Volts
Roll 1 track attitude	R1T		Real	Volts
Roll 2 track attitude	R2T		Real	Volts
Pitch 1 acquisition attitude	P1A		Real	Volts
Pitch 2 acquisition attitude	P2A		Real	Volts
Roll 1 acquisition attitude	R1A		Real	Volts
Roll 2 acquisition attitude	R2A		Real V	Volts
Index	i	3	Integer	
Index	j		Integer	
Line of sight of spin sensor field in inertial frame	LOS ^I		Real	
Normalized cross product magnitude of R and LOS	SANG	2	Real	
Normalized dot product of R and LOS	CANG		Real	
Angle between -R and tangent to earth	ANG1		Real	Radian
Angle between -R and LOS	ANG2		Real	Radian
Angle between LOS and earth tangent	ANG3		Real	Radian
Saved angle between earth tangent and LOS	ANGSAV		Real	Radian
Half dimension of 1° x 1° square	RD		Real	Equiv radian. (a constant preset to 0.0087266)
Area of earth covering 1° x 1° square	AREA		Real Function	Square Degree

REFERENCES

- J-1 McArthur, W.G., "Horizon Sensor Navigation Errors Resulted from Statistical Variations in the CO₂ 14-16 Micron Radiation Band," Ninth Symposium on Ballistic Missile and Space Technology, San Diego, California, August 1964.
- J-2 "Performance Analysis of Static Sensor," Barnes Engineering Company, 4 August, 1975.

APPENDIX K

WHEEL-MOMENTUM COUPLING

APPENDIX K

WHEEL-MOMENTUM COUPLING

To examine the effects of wheel-momentum coupling, we begin with the rotational equations of motion, i. e.,

$$T = I\dot{\omega} + \omega \times (I\omega + \dot{H}_W) + \dot{H}_W = T_J + T_d \quad (K-1)$$

where

I = inertia tensor

H_W = wheel momentum

T_J = jet control torque

T_d = disturbance torque

Linearizing about the nominal orbit rate $\omega = \omega_o + \delta\omega$ gives

$$I\delta\dot{\omega} = -\omega_o \times (I\omega_o + H_W) - \delta\omega \times (I\omega_o + H_W) - \omega_o \times I\delta\omega + T_J + T_W + T_d \quad (K-2)$$

where

$T_W = -\dot{H}_W$ = wheel reaction torque

Solving for $\delta\dot{\omega}$ and substituting for

$$\omega_o^T = (0 \quad -\omega_e \quad 0)$$

$$I = \begin{bmatrix} I_x & 0 & 0 \\ 0 & I_y & 0 \\ 0 & 0 & I_z \end{bmatrix} \quad (K-3)$$

yields

$$\delta\dot{\omega} = \begin{bmatrix} 0 & -H_{Wz}/I_x & [H_{Wy} + (I_z - I_y)\omega_e]/I_x \\ H_{Wz}/I_y & 0 & -H_{Wx}/I_y \\ -[H_{Wy} + (I_x - I_y)\omega_e]/I_z & H_{Wx}/I_z & 0 \end{bmatrix} \delta\omega$$

AD-A056 812

HONEYWELL INC MINNEAPOLIS MINN SYSTEMS AND RESEARCH --ETC F/G 17/7
INDEPENDENT STABILITY AND CONTROL ANALYSIS OF NAVIGATION DEVELO--ETC(U)
JAN 78 R E POPE, M D WARD, M F BARRETT F04701-75-C-0135

UNCLASSIFIED

78SRC10-VOL-2

SAMSO-TR-78-74-VOL-2

NL

3 OF 3
AD
A056812



END
DATE
FILMED

9-78

DDC

$$+ \begin{bmatrix} H_{Wz}/I_x \\ 0 \\ -H_{Wx}/I_z \end{bmatrix} \omega_e + \begin{bmatrix} 1/I_x & 0 & 0 \\ 0 & 1/I_y & 0 \\ 0 & 0 & 1/I_z \end{bmatrix} (T_J + T_W + T_d) \quad (K-4)$$

where

ω_e = earth rate

We have two effects to examine--one static and the other dynamic. The static effect is that wheel momentum induces wheel momentum coupling torques in the roll and yaw axes. If necessary, this error source can be compensated for by using tachometer feedback to generate wheel commands in the cross axis, i.e.,

$$T_{Wc} = -I_W \begin{bmatrix} \hat{\Omega}_{Wz} \\ 0 \\ -\hat{\Omega}_{Wx} \end{bmatrix} \omega_e \quad (K-5)$$

where

I_W = wheel inertia

$\hat{\Omega}_W$ = wheel-speed estimate from tachometer

Assuming that wheel speed is known to within one percent of its true value, the effective disturbance due to wheel-momentum coupling is reduced, i.e.,

$$\begin{aligned} T_{dWMC} &= \begin{bmatrix} H_{Wz} \\ 0 \\ -H_{Wx} \end{bmatrix} \omega_e - I_W \begin{bmatrix} \hat{\Omega}_{Wz} \\ 0 \\ -\hat{\Omega}_{Wx} \end{bmatrix} \omega_e \\ &= I_W \begin{bmatrix} \tilde{\Omega}_{Wz} \\ 0 \\ -\tilde{\Omega}_{Wx} \end{bmatrix} \omega_e \end{aligned} \quad (K-6)$$

$$\leq H_{Wmax} (\tilde{\Omega}_W / \Omega_{Wmax})$$

where

$$\tilde{\Omega}_W = \Omega_W - \hat{\Omega}_W = \text{true minus estimated wheel speed}$$

The other effect of wheel-momentum coupling is a dynamic one. It introduces nutation coupling between all axes. The maximum frequency of this nutation coupling is given by

$$\Omega_{xz} = [H_{W\max} + (I_x - I_y)\omega_e]/I_z$$

$$\Omega_{xy} = H_{W\max}/\sqrt{I_x I_y} \quad (K-7)$$

$$\Omega_{yz} = H_{W\max}/\sqrt{I_z I_y}$$

The effect of this nutation coupling on control loops which are designed to be independent should cause no problem, provided that these nutation frequencies are well below the crossover frequency of the wheel loop.